C1916

Repair of Distortion-Induced Fatigue Damage in Bridge No. 135-87 (043SB and 044NB) Using Newly-Developed Strengthening Schemes

By

Kathleen S. McElrath
Adolfo Matamoros
Caroline Bennett
Jian Li
Stan Rolfe

A Report on Research Sponsored by

The Kansas Department of Transportation

Structural Engineering and Engineering Materials
SM Report No. 112

September 2015

THE UNIVERSITY OF KANSAS CENTER FOR RESEARCH, INC.
2385 Irving Hill Road – Campus West, Lawrence, Kansas 66045

Executive Summary

A steel girder twin bridge structure located near Park City, Kansas has experienced extensive distortion-induced fatigue cracking in its web gap regions. Due to the bridge's skewed, staggered configuration, the majority of these cracks have occurred in the bottom web gap region. The bridge was previously the subject of a series of detailed finite element analyses that investigated the effectiveness of several types of retrofits in repairing its distortion-induced fatigue cracks. One of these retrofits, the "angles-with-plate" retrofit, was developed and tested at the University of Kansas as a new retrofitting technique aimed at providing a more economical and easy-to-install distortion-induced fatigue cracking repair. The retrofit is made up of a pair of angles and a backing plate that connect the cross frame connection plate and girder web in order to stiffen the web gap region. Results from the finite element analyses determined that the angles-with-plate retrofit was the most effective and economical choice for repairs in the bridge, and plans were made for its installation.

To investigate the performance of the angles-with-plate retrofit, two field tests were performed that monitored behavior of the bridge both before and after the retrofit was installed. Results from these field tests were compared with results from complementary finite element analyses to determine the overall effectiveness of the retrofit. In the bottom web gap region, where cracking is most prevalent in the bridge, the angles-with-plate retrofit was successful at lowering stress demands that would lead to crack propagation. The same conclusion could not clearly be made for all cases in the bridge's less problematic top web gap region, so a secondary set of finite element analyses was performed to gain a better understanding of what was happening in that region. Further analyses of the two common types of distortion-induced fatigue cracking determined that, while not always large, the angles-with-plate retrofit was successful in reducing stress demands in the top web gap region.

Therefore, it was concluded that the angles-with-plate retrofit was an effective repair for the problematic bottom web gap regions of the bridge, and if needed, can be used effectively in the less demanding top web gap region.

Acknowledgements

The authors of this report would like to gratefully acknowledge the Kansas Department of Transportation (KDOT) that supported the work performed under this project, as well as the knowledgeable guidance and input provided by Mr. Loren Risch, Mr. John Jones, Mr. Calvin Reed, and Mr. Paul Kulseth throughout the project activities.

The authors would also like to thank the University of Kansas Transportation Research Institute (KU TRI) and the KU School of Engineering for their support of this project.

Finally, the authors are grateful to the many graduate and undergraduate students who have contributed their talents to this project, especially: Dr. Amanda Hartman, Mr. Temple Richardson, Ms. Alisha Elmore, Mr. Say Hak Bun, Mr. Riley Piles, Mr. Zach Olson, Ms. Patrícia Aguiar, Mr. Nick Crain, and Mr. Cody Gibbens. The authors would also like to thank technicians Mr. Matt Maksimowicz, Mr. David Woody, and Mr. Eric Nicholson for their invaluable assistance in the laboratory.

Table of Contents

List of Figures

Appendix B: Kansas Bridge 135-087 (043/044) Plans

Appendix C: Filtered Field Test Data

Appendix D: Field Test and Finite Element Analyses Results

List of Tables

Appendix A: Calibration Constants

1. Introduction

Before implementation of the 1983 American Association of State Highway and Transportation Officials (AASHTO) Bridge Specifications, steel bridge girders in the United States were often designed with a detail, a "web gap," that was highly susceptible to distortion-induced fatigue cracking. To avoid creating a fatigue-vulnerable detail by welding transverse connection plates to girder flanges, the connection plates were often cut short and left unattached to the girder flanges (Grondin, Fraser and D'Andrea 2002). Since no connection was provided between the elements, the web gap region located between the transverse connection plate and the girder flange was left unstiffened. This unstiffened web gap region has since been found to be highly susceptible to out-of-plane distortion, the culprit for significant fatigue cracking in steel bridges in the United States.

In order to repair distortion-induced fatigue cracking in active bridges, retrofits that relieve stress demands in the web gap regions must be installed. Current retrofits in use today have either performance or constructability issues. Recent research at the University of Kansas has been aimed at developing a retrofit that simplifies the installation process but still effectively stiffens the web gap region. This retrofit, termed the "angles-with-plate" retrofit, has been the subject of numerous investigations at the University of Kansas. Based on successful performance of the retrofit in those investigations, the angles-with-plate retrofit was recommended to the Kansas Department of Transportation as a means to repair prevalent distortion-induced fatigue cracking in a steel girder bridge located near Park City, Kansas, Kansas Bridge 135-87(043/044). Investigators at the University of Kansas monitored Kansas Bridge 135-87(043/044) under live loading both before and after the angles-with-plate retrofit was installed to gage the effectiveness of the retrofit in relieving stress demands in the web gap regions in a full-scale, active bridge.

2. Background

Out-of-plane distortion of the web gap occurs when adjacent girders experience differential deflections under live loads. The differential deflection causes the cross frames to rotate and impose out-of-plane forces on the transverse connection plates. The girders to which the connection plates are welded can experience significant out-of-plane stresses in the flexible web gap region, made more severe by the presence of geometric stress concentrations. The

combination of high-magnitude stresses and the small number of cycles needed to induce distortion-induced fatigue cracking have led to large numbers of cracks appearing in the web gaps of steel girder bridges constructed before the mid-1980s (Fisher 1984).

Depending on bridge layout, fatigue cracking can occur in either the top or bottom web gap regions. The literature shows that the majority of distortion-induced fatigue cracking occurs in top web gap regions. The top girder flange is restrained by the concrete deck, which inhibits its lateral displacement. The girder's bottom flange has more freedom to deform laterally. Therefore, distortion tends to occur in the restrained, relatively flexible top web gap region. However, in the case of skewed brides with staggered cross frames, fatigue cracking has been shown to be more prevalent in the bottom web gap (Hartman, Hassel, et al. 2010). Staggered cross frames in skewed bridges are placed at different stations along the girder, which tends to increase differential displacements (Grondin, Fraser and D'Andrea 2002). In addition to this, Hartman et al. (2010) found that staggered cross frame layouts caused the bottom girder flange to laterally displace in reverse curvature, while the top girder flange was restrained from doing so by the concrete deck. Thus, it was hypothesized that the increased differential deflections and reverse curvature response of the bottom girder flange led to maximum stress demands and fatigue cracking occurring in the bottom web gaps of skewed bridges with staggered cross frames.

Detailing changes that have been implemented since the 1983 AASHTO specification, which was the first AASHTO bridge design specification to mandate a positive connection between a connection plate and the adjacent flange, addressed the issue of out-of-plane displacements at web gap regions in new designs, but many steel bridges designed prior to 1983 and still in service are susceptible to distortion-induced fatigue and have experienced cracking. To prevent distortion-induced fatigue cracks from propagating further into the girder web, which could cause severe structural damage, the cracks need to be properly repaired. Two popular techniques currently used to address distortion-induced fatigue damage include drilling holes at crack tips to arrest crack growth and using angles at the connection plate to stiffen the web gap region.

Crack-arrest holes are drilled at the tip of the crack and may be effective in stopping crack propagation in low stress regions, but cracking is likely to recur depending upon the crack type and location of occurrence or if the stress range increases (Liu 2015). They are also only effective in arresting existing cracks and not in preventing new cracks. However, crack arrest holes are easy

to install and are generally considered useful when used in conjunction with other retrofitting techniques. Bolting back-to-back angles to each side of the connection plate and to the girder flange is a popular method for stiffening the web gap region. While this technique is effective, it is inconvenient and costly when applied to the top web gap, as the concrete deck has to be disturbed for the bolts to be installed in the steel girder flange (Roddis and Zhao 2001).

2.1. Development of the Angles-With-Plate Retrofit

Recent research performed at the University of Kansas has investigated a new retrofit technique, which is referred to as the angles-with-plate retrofit. The retrofit consists of a pair of angles and a backing plate applied on opposite sides of the girder web at the web gap regions. One leg of each angle is bolted back-to-back through the transverse connection plate, while the other leg of each angle is bolted to the backing plate through the girder web. Application of the angles-with-plate retrofit provides an alternate load path that redistributes the concentrated force in the web gap region to a larger area of the girder web. The retrofit does not require deck removal when applied in the top web gap, since there is no attachment to the girder flange. This simplifies retrofit application and allows for the retrofit to be installed without removing traffic lanes, providing a more cost effective solution for mitigating distortion-induced fatigue cracks in steel bridge girders.

Alemdar et al. (2013a) performed physical tests to investigate the effectiveness of the angle-with-plate retrofit. The investigations were performed using 2.8 m (9.3 ft.) girder-cross frame subassemblies. The set-up used for these tests can be seen in Figure 1. In a steel girder bridge, the top flange of a girder is laterally restrained by the bridge deck. In order to replicate this in the laboratory, the girder-cross frame subassemblies were tested upside down to restrain the girder's top flange using the laboratory strong floor. This set-up eliminated in-plane bending stresses that would occur in bridges due to dead and live gravity loads and left only out-of-plane stress demands on the girder. The out-of-plane stress demands were implemented by applying cyclic loads at the free end of the cross frame. Initiation and propagation of fatigue cracks were monitored through eight test trials to determine the effectiveness of the angles-with-plate retrofit.

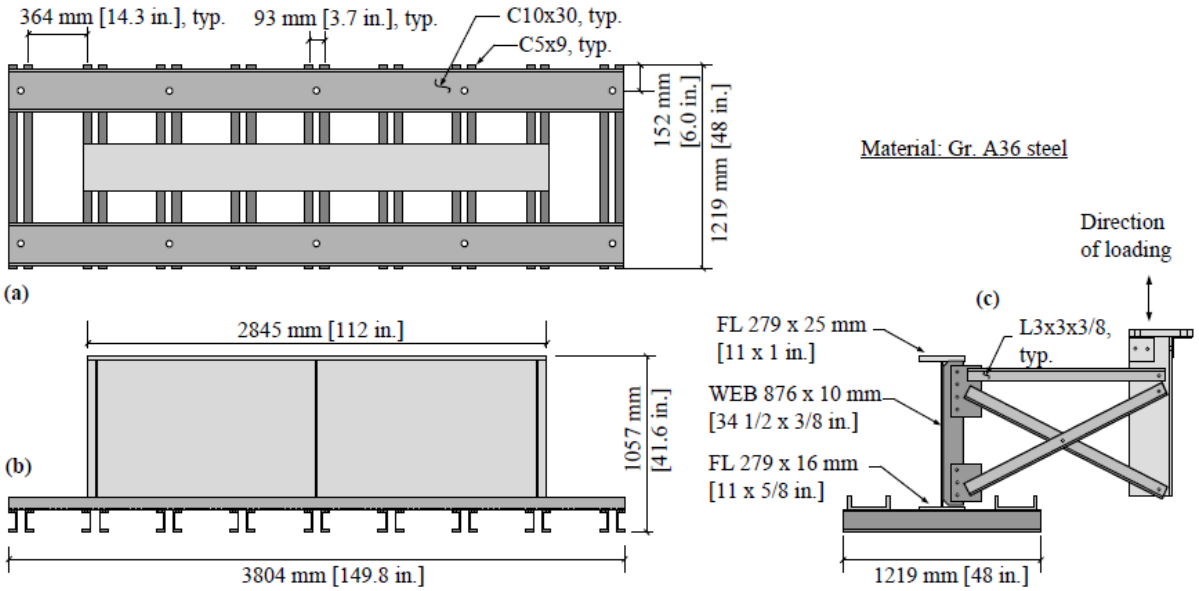

Figure 1: Test set-up for 2.8 m (9.3 ft.) girder subassembly test (Alemdar, Overman, et al. 2013a).

Alemdar et al. (2013b) presents a parallel analytical investigation. Computer simulations of the girder-cross frame subassemblies were created to verify that the stress field of the laboratory set-up was similar to those seen in girders located in a full bridge system. Results from the analytical investigation showed that the stress fields in the web gap and points of fatigue crack initiation in the 2.8 m (9.3 ft.) subassembly were similar to those found in full bridge system simulations performed by Hassel et al. (Hassel, et al. 2013).

Results from the physical and parallel analytical tests by Alemdar et al. (2013a, 2013b) showed that the two primary types of cracks that occur in the web gap region are horseshoe-shaped cracks along the toe of the transverse connection plate-to-girder web weld (referred to hereafter as connection plate-to-web weld cracks) and longitudinal cracks along the girder flange-to-web (referred to hereafter as flange-to-web weld cracks). The tests showed that the angles-with-plate retrofit was successful in mitigating propagation of these cracks. In comparison with unretrofitted specimens, web gap stresses were reduced and crack growth was negligible in the retrofitted specimens. Thus, under pure out-of-plane fatigue loading, the angles-with-plate retrofit proved to be highly effective.

A physical test that captured both in-plane and out-of-plane effects (Hartman 2013) investigated the angles-with-plate retrofit using a 9.1 m (30 ft.) three-girder test bridge with a composite concrete deck (Figure 2). X-type cross-frames were located at mid-span and at the two

end support locations. Regularly-spaced high strength bolts were used to attach the concrete deck to the top flanges of the girders to achieve composite action. The bolts were grouted in place after they were installed.

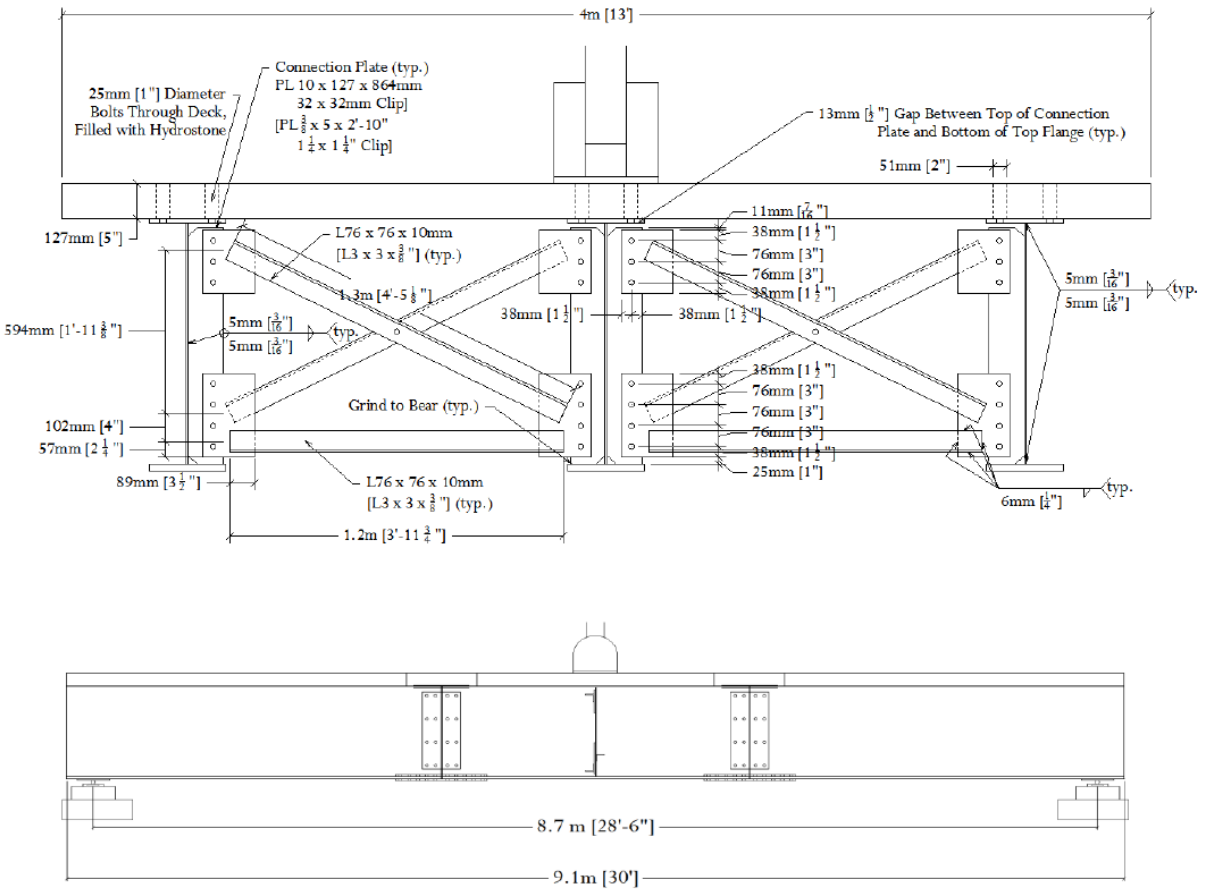

Figure 2: Test set-up for 9.1 m (30 ft.) three girder test bridge (Hartman 2013).

Twelve fatigue test trials were performed at varying load ranges, applied at the center of the bridge deck using a servo-controlled hydraulic actuator. This fatigue loading resulted in distortion-induced fatigue cracks in the top web gap regions of the two exterior girders, which were subsequently repaired using the angles-with-plate retrofit. Once the angles-with-plate retrofit was applied, crack growth, girder deflections, cross frame strains, and web gap region strains were monitored throughout the test trials to determine the effectiveness of the angles-with-plate retrofit.

Physical test results reported by Hartman (2013) showed that application of the angles-with-plate retrofit lowered distortion-induced fatigue crack propensity in the web gap region and web gap rotations were greatly reduced. Growth of existing sharp cracks was shown to

significantly slow after application of the angles-with-plate retrofit. When applied over web gap regions with crack tips that were modified by small crack-arrest holes, crack growth was halted under realistic fatigue bridge loadings.

Hartman (2013) also performed an analytical investigation of the 9.1 m (30 ft.) test bridge. The objective of this investigation was to complement the physical laboratory tests, to examine the influence of crack type and crack length, and to compare the angles-with-plate retrofit with other existing retrofit techniques. Varying lengths of connection plate-to-web weld cracks and flange-to-web weld cracks were modeled in unretrofitted and retrofitted versions of computational models to determine the effectiveness of different types of retrofits in mitigating distortion-induced fatigue crack growth. In addition to the angles-with-plate technique, two other retrofits were modeled. One of these was the existing retrofit technique in which two angles are place back-to-back and bolted to the connection stiffener and girder flange. The other retrofit tested was a back-up stiffener technique in which a full depth secondary stiffener is placed on the opposite side of the girder web at the connection plate in an effort to stiffen the web gap region.

Stress demands in the web gap region were reduced under all retrofit techniques in the simulations performed by Hartman (2013); however, the full depth back-up stiffener technique provided little stress relief and was not an especially effective retrofit. While the angles-with-plate retrofit provided the most reduction in stress demand for the connection plate-to-web weld cracks, the angles-to-top girder flange technique provided the most reduction in stress demand for the flange-to-web weld cracks. However, the angles-with-plate technique still provided a significant reduction in stress demand for the flange-to-web weld crack.

Overall, the tests and simulations performed using the 2.8 m (9.3 ft.) girder cross frame subassembly and 9.1 m (30 ft.) test bridge showed that the angles-with-plate retrofit can be an effective method for repairing distortion-induced fatigue web gap region cracks. Though the simulation results indicated that the angles-with-plate technique did not perform better than the existing retrofit technique of bolting back-to-back angles to the connection plate and top flange in all instances, the angles-with-plate retrofit still showed good performance in mitigating fatigue crack growth and reducing web gap region stress demand in these cases. When ease of application is considered, the angles-with-plate retrofit provides major benefits over the angles-to-top flange technique. Since it does not require attachment to the top flange, there is no need for deck removal. This aspect greatly reduces the cost of retrofit installation and reduces traffic disruption, providing

an effective and more economical retrofit technique (Alemdar, Overman, et al. 2013a, 2013b, Hartman 2013).

2.2. History of Kansas Bridge 135-87(043/044)

Kansas Bridge 135-87(043/044) is an active twin bridge structure located near Park City, KS in Sedgwick County over Chisolm Creek. The bridge system has an average daily traffic of 14,400, which is comprised 16% by trucks. Each welded steel plate girder bridge carries two lanes of traffic, with Bridge 043 carrying traffic in the southbound direction and Bridge 044 carrying traffic in the northbound direction. The bridge system was designed in 1964 and constructed in 1970, and it has unstiffened web gap regions that are prone to distortion-induced fatigue cracking. Prevalent cracking has been reported in the bridge system, with the majority of cracking appearing in the bottom web gaps. However, some cracking was also reported in top web gap regions.

The bridges each have two 23 m (76 ft.) end spans and a 29 m (95 ft.) middle span, and are skewed at an angle of 21°. Both bridges are comprised of five composite steel girders spaced at 2.7 m (9 ft.) with 1220x8 mm (48x5/16 in.) webs and 305x29 mm (12x1-1/8 in.) flanges that taper to a width of 457 mm (18 in.) over the center supports. These girders are labeled A through E, with A being the west girder. The 191 mm (7-1/2 in.) thick reinforced concrete deck was resurfaced in 2004 and provides a roadway width of 12 m (40 ft.). Lateral support is provided by cross frames that are oriented staggered and perpendicular to the girders in all locations except at the interior bolster supports, where they are back-to-back and parallel to the skew. Half sections of the bridge, which show views at the cross frames near mid-span and at the interior supports, are shown in Figure 3. Additional plans and details can be referenced in the original structural drawings of the bridge found in Appendix F.

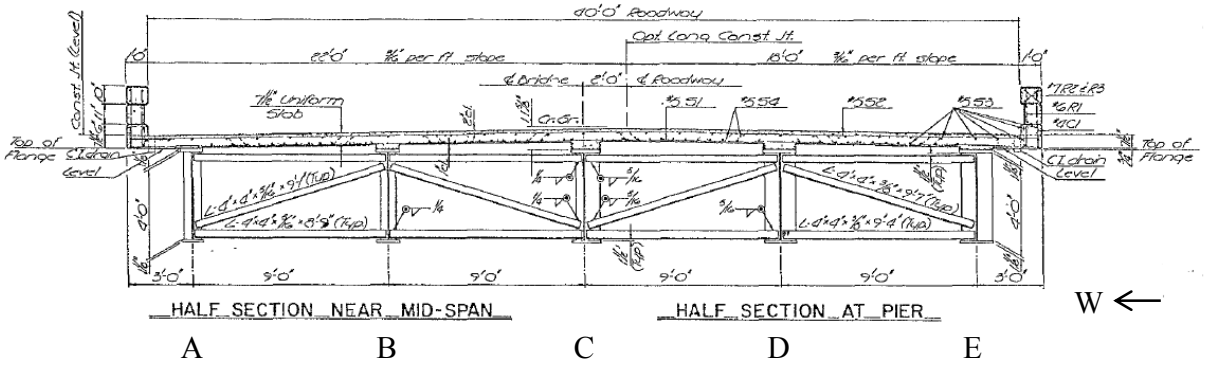

Figure 3: Cross-section of Kansas Bridge 135-87(043/044).

As previously mentioned, skewed bridges with staggered cross frames are likely to have more extensive distortion-induced fatigue cracks in the bottom web gaps due to high differential deflections and reverse curvature deformations of the bottom girder flange (Hartman, Hassel, et al. 2010). This is the case with Kansas Bridge 135-87(043/044), which has a 21° skew and staggered cross frames. According to a 2010 routine snooper inspection, the majority of fatigue cracks are located in the bottom web gaps. Figure 4 shows a plan of the bridge with locations of cracking indicated.

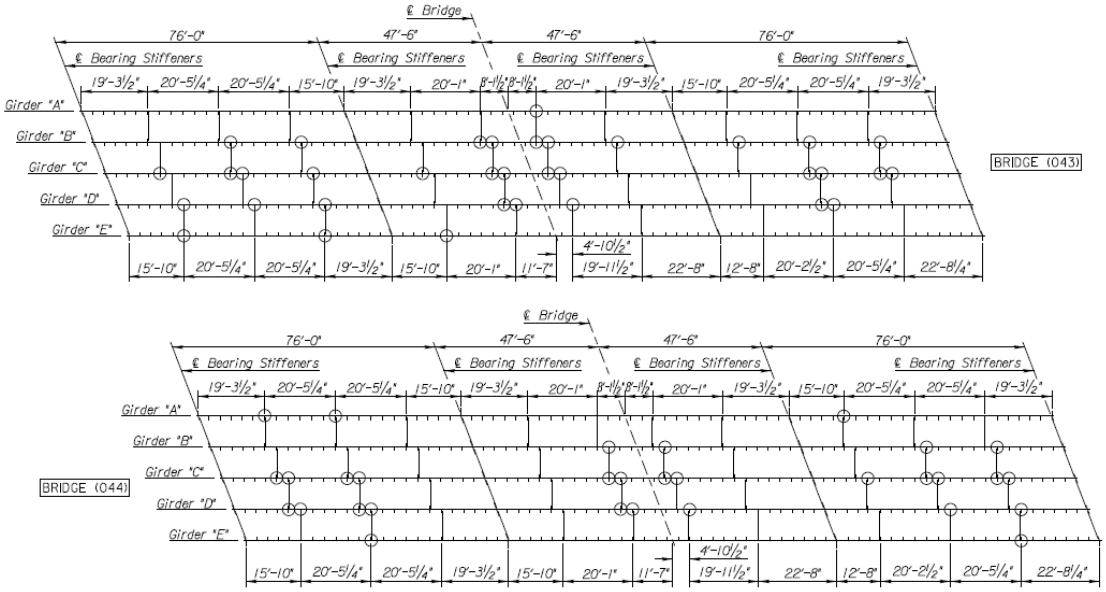

Figure 4: Plan of Kansas Bridge 135-87(043/044); circled areas indicate locations where cracks have been reported.

Crack types A, B, C, and D (Figure 5) have all been reported on Kansas Bridge 135-87(043/044). Type A cracks occur horizontally at the connection plate-to-web weld. Type B cracks occur vertically along the connection plate-to-web weld. Type C cracks propagate away from the connection plate-to-web weld into the base metal of the girder web, and Type D cracks occur along the flange-to-web weld. Drilled crack-arrest holes were implemented in past repairs, but no additional retrofits have previously been applied to the bridge.

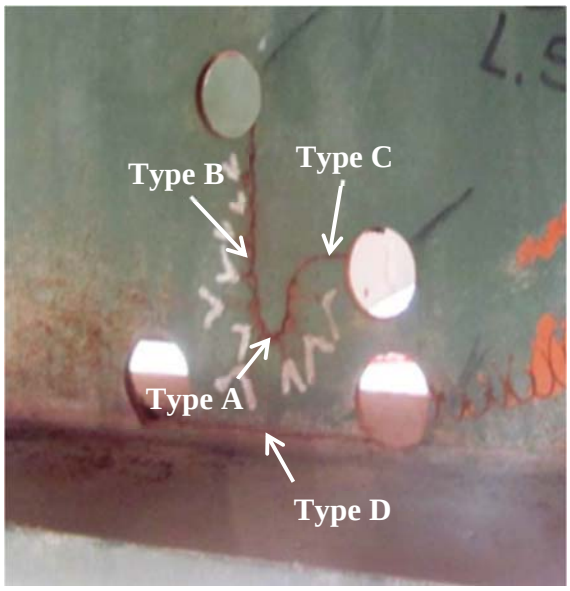

Figure 5: Types of cracks occurring in Kansas Bridge 135-87(043/044).

2.3. Retrofit Recommendation for Kansas Bridge 135-87(043/044)

As part of an investigation performed for the Kansas Department of Transportation (KDOT), a series of finite element analyses of Kansas Bridge 135-87(043/044) were completed. As previously mentioned, the bridge has a history of distortion-induced fatigue cracks in its web gap regions. The purpose of the finite element analysis was to recommend a retrofit to prevent further initiation and propagation of the cracks based on reduction of web gap stresses and ease of retrofit application. In addition to different variations of the angles-with-plate retrofit, three other retrofit techniques were included in the study. The second retrofit was similar to the angles-with-plate retrofit, except that the backing plate was replaced by a backing angle that was bolted to the flange. The other two retrofit techniques included the established retrofit technique of connecting back-to-back angles between the girder flange and transverse connection plate, and a KDOT-proposed retrofit. In the KDOT-proposed retrofit, angles were placed at each corner of the cross frame as a means to stiffen all web gap regions. In each retrofit, 19 mm (¾ in.) diameter pre-tensioned bolts were modeled (Richardson 2012).

A detailed three-dimensional finite element (FE) model of Kansas Bridge 135-87 (043/044) was built and loaded with its self-weight. A 9.3 kN/m (0.64 k/ft.) lane load was applied along the full length of the bridge over the top flange width of Girder C. Cracks were modeled at the top and bottom web gaps of the third cross-frame of span two in Girder C. These cracks included a

25 mm (1 in.) connection plate-to-web weld crack and a 51 mm (2 in.) flange-to-web weld crack. Models of the bridge both with and without retrofits were assessed to determine the percentage of stress reduction provided by each type of retrofit (Richardson 2012).

The angles-with-plate retrofit was studied parametrically in the FE models to determine which combination of angle/plate thicknesses and lengths was most effective. It was found that varying the thickness of the backing plate had a greater effect on the performance of the retrofit than varying the thickness of the angles. The retrofit with a 25 mm (1 in.) backing plate and 13 mm (0.5 in.) angles decreased the stress demand almost as much as when both the angles and backing plate had equal thicknesses of larger values. Length of the angles was shown to have little effect on stress reduction in the web gap regions (Richardson 2012).

The angles-with-plate retrofit was applied in both the bottom and top web gap regions. In the bottom web gap region, the angles-with-plate retrofit was shown to reduce the connection plate-to-web weld crack stress demand by 80% and the flange-to-web weld crack stress demand by 82%. In the top web gap region, the angles-with-plate retrofit was shown to reduce these stresses by 34% and 28%, respectively. While this was less than the bottom web gap stress reductions, it should be noted that stresses in the top web gap region were small in comparison to those found in the bottom web gap region, which is expected in a bridge with skewed, staggered geometry (Richardson 2012).

The other three retrofits were only modeled in the bottom web gaps. The angles-with-backing plate retrofit performed better in this region than all but the retrofit that replaced the backing plate with a backing angle attached to the girder flange. However, the difference in performance was only 1-2%. The extra labor and material required to apply the backing angle to the girder flange would not be warranted with only this slight increase in stress reduction. Additionally, connection of the backing angle to the top flange would require bridge deck removal (Richardson 2012).

While the remaining two retrofit techniques studied were also successful in significantly reducing stress demand in the bottom web gap region, they were not as effective as the angles-with-backing plate technique. They also present significant installation obstacles. As mentioned previously, the existing retrofit technique of bolting back-to-back angles to the connection plate and girder flange requires bridge deck removal when applied at the top flange.

Also, Kansas Bridge 135-87 (043/044) has cross frames with two horizontal cross frame members framing directly into the connection stiffener at the top and bottom web gaps, as shown in Figure 6.

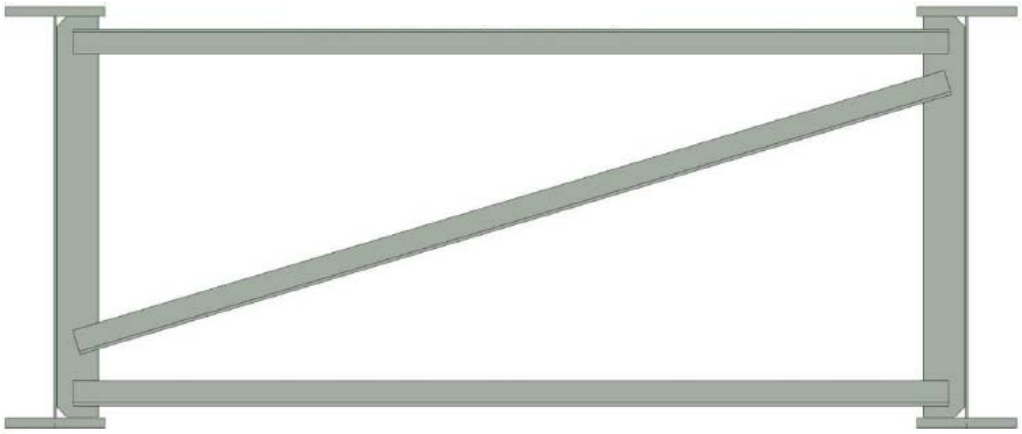

Figure 6: Cross frame geometry of Kansas Bridge 135-87(043/044) (Richardson 2012).

In bridges with cross frame geometry such as this, application of the existing retrofit technique would first require removal of at least the horizontal cross frame members. Similarly, the KDOT-proposed retrofit technique of applying angles at each corner of the cross frame would also require cross frame members to have to be first removed before application (Richardson 2012).

Richardson (2012) concluded that the angles-with-plate retrofit was effective in reducing stresses in the web gap regions and would be the most cost effective and convenient repair technique. Since this retrofit technique does not require attachment to the girder flange, field implementation would be simplified in both web gap regions. In the top web gap, bridge deck removal would not be required. In both web gap regions, cross frame removal would be unnecessary, because the angles-with-plate retrofit could be bolted through the horizontal cross frame members while avoiding their outstanding legs. These benefits would reduce labor costs and allow for maintaining daily traffic. Therefore, it was recommended to KDOT that they use the angles-with-plate retrofit on Kansas Bridge 135-87(043/044) to repair distortion-induced fatigue cracking in the susceptible web gap regions. Based on the parametric results of the angles-

with-plate retrofit, recommended dimensions for the angles and backing plate were L152x152x25 mm (L6x6x1 in.) and L457x145x25 mm (PL18x5-11/16x1 in.), as shown in Figure 7.

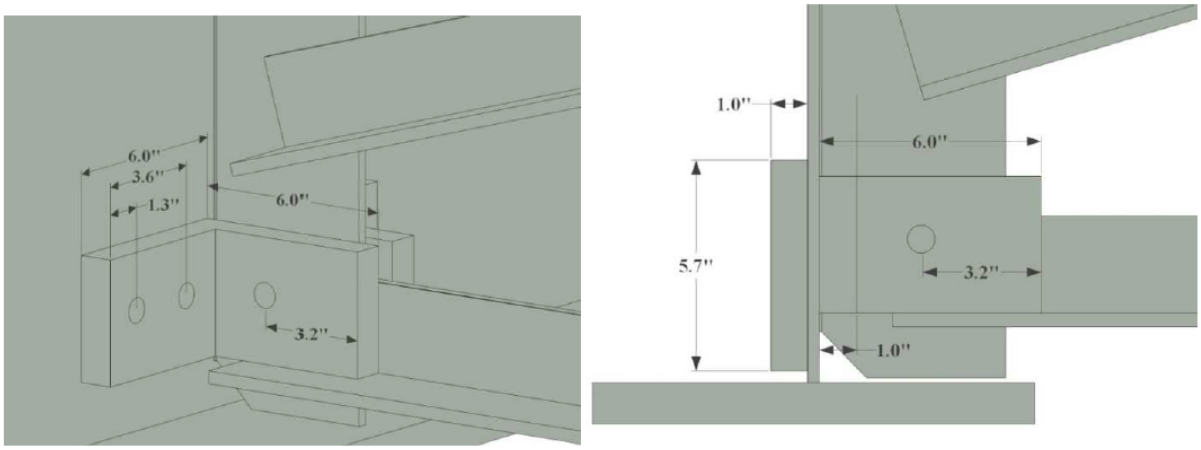

Figure 7: Angles-with-plate retrofit recommended to KDOT for repair of Kansas Bridge 135-87(043/044) (Richardson 2012).

3. Objective

In the spring of 2013, KDOT installed the angles-with-plate retrofit on Kansas Bridge 135-87(043/044). The objective of this study was to assess the performance of the angles-with-plate retrofit in its field application and determine its effects on the stress demand in the web gap regions of the bridge. This was done by performing field testing on the bridge both before and after the retrofit was installed and comparing the results of those tests to a refined finite element analysis of the bridge.

4. Field Tests

The first field test was performed at the bridge site in March 2013 before KDOT installed the angles-with-plate retrofit. After KDOT installed the retrofit, the second field test was performed in July 2013. In both tests, a KDOT loaded dump truck of known weight, approximately 222 kN (50 kips), was driven over the bridge with no other traffic on the structure. Data was recorded six separate times for each field test, as the dump truck traveled at 8-16 kph (5-10 mph) and 105-121 kph (65-75 mph) down the east lane, the west lane, and the center of the bridge.

Field testing was performed on the northbound bridge, Bridge 044. This bridge was selected for testing because KDOT installed the angles-with-plate retrofit in both its top and bottom web gaps, as opposed to only in the bottom web gap for the southbound bridge (Bridge 043). KDOT chose to do this so that the cracking behavior in the southbound bridge could be compared with that in the northbound bridge in the future to examine the repair's effectiveness. Figure 8 shows details of the retrofit that was installed. Member sizes and bolt-hole spacings were slightly different from those recommended by the University of Kansas due to member availability, edge distance requirements, and installation clearances.

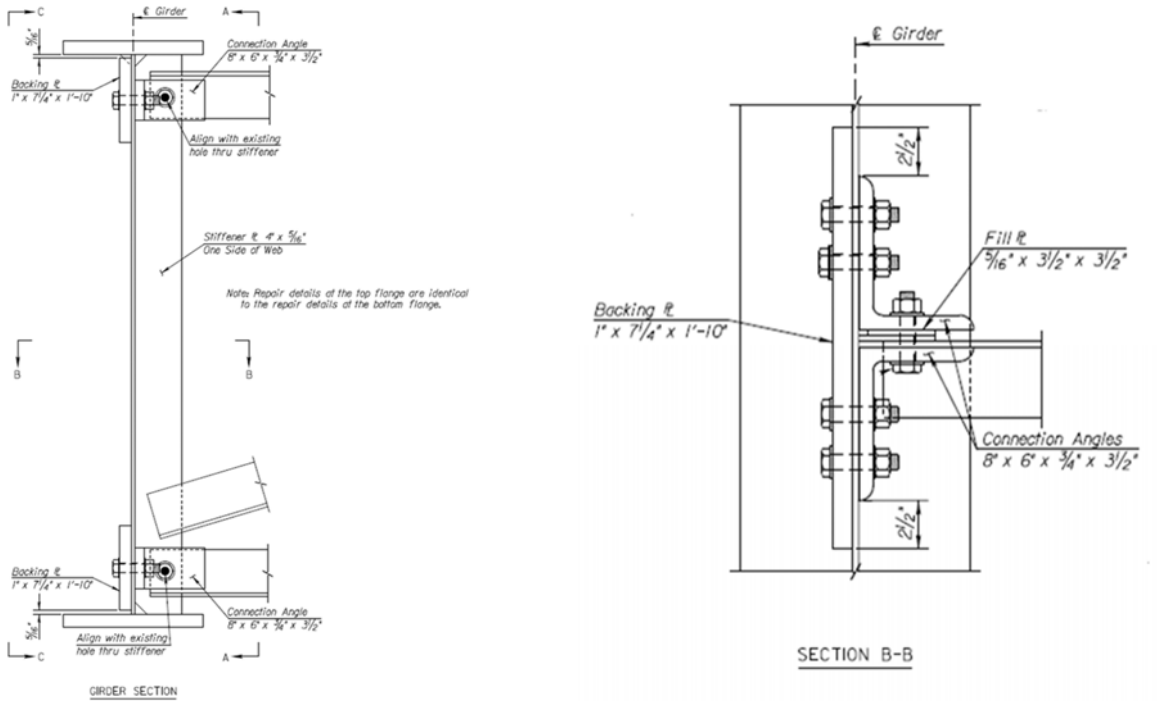

Figure 8: Details of retrofit applied to the bridges.

4.1. Instrumentation

The selected location for testing on the bridge was chosen based on the types of fatigue cracks reported in the web gaps and ease of access for placing instrumentation. The selected location for instrumentation was Girder C of the northbound bridge at cross frame 1-2, which was the second cross frame from the south end of the bridge. This location had Types A, B, C, and D cracks. Types B, C, and D cracks were located in the bottom web gap region and crack-arrest holes had been previously drilled. The top web gap had one 19 mm (3/4 in.) Type A crack that had not

been previously repaired. Figure 9 shows a photograph of the bottom web gap at the location where the majority of the instrumentation was placed.

(a) **(b)**

Figure 9: Cracking at the instrumentation location on the (a) stiffener side (b) non-stiffener side.

Instrumentation used for the field tests included 16 bondable strain gages, 11 Bridge Diagnostics Inc. (BDI) strain transducers, one string potentiometer, two inclinometers, and one linear variable differential transformer (LVDT). The bondable strain gages were used to record strain readings at the web gap regions to quantify stress demand in the web gap areas. The BDI strain transducers were used to record strains for the girder flanges and for the cross frame members between Girders C and D. The string potentiometer was used to measure deflection of Girder C at the transverse connection plate, and the inclinometers and LVDT were used to record out-of-plane rotation and displacement of the top web gap relative to the top girder flange.

The bondable strain gages were Micro-Measurements WK-06-250BG-350 gages and were powered directly through a NI-9236 module in a quarter bridge configuration using an excitation voltage of 3.3V. The strain gages were placed on the girder web near both the bottom and top flanges, and were placed on both sides of the girder web. The side on which the cross frame was attached to the connection plate is referred to as the *stiffener side*, while the opposing side is referred to as the *non-stiffener side*. The strain gages were placed at the same locations in the top and bottom web gaps. The goal was to keep the strain gages in the same locations for the first test and the second test. In some cases, strain gages were moved or not applied in the second test because the footprint of the retrofit covered the strain gage locations from the first test. Figure 10 shows the strain gage locations for both tests for the stiffener and non-stiffener sides of the girder

web. Strain gages were purposely located far away from crack tips so that they would not be placed in regions of severe strain gradient. This was done so that a less placement-sensitive strain could be read by the gage, resulting in more accurate comparisons for the pre-retrofit and post-retrofit field tests. Additionally, application of the retrofit would have covered any strain gages in the immediate region of the web gap, making a comparison of results between tests impossible.

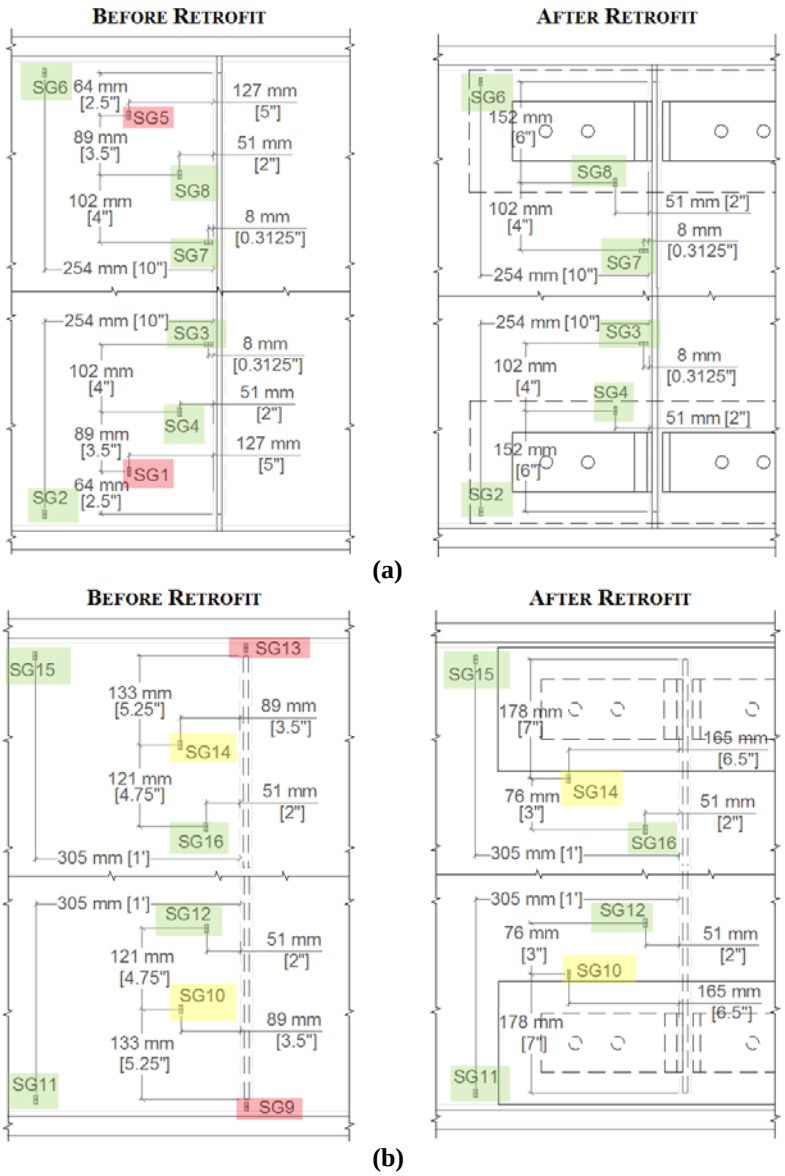

Figure 10: Strain gage locations for both tests on the (a) stiffener side (b) non-stiffener side. Green highlighting indicates that the strain gage was placed in the same location for the second test, yellow highlighting indicates that the strain gage was moved for the second test, and red highlighting indicates that the strain gage was not applied for the second test.

The BDI strain transducers were powered with 5V and connected to a NI-9205 module for data recording. The BDI strain transducers were placed on the bottom flange of each girder, on the top flange of Girder C, and on the cross frame members between Girders C and D. The BDIs on Girder C were placed five feet to the north of the cross frame, while the BDI strain transducers on the remaining girders were placed so that they followed the skew of the bridge. Figure 11 shows the locations of the BDIs in both section and plan view.

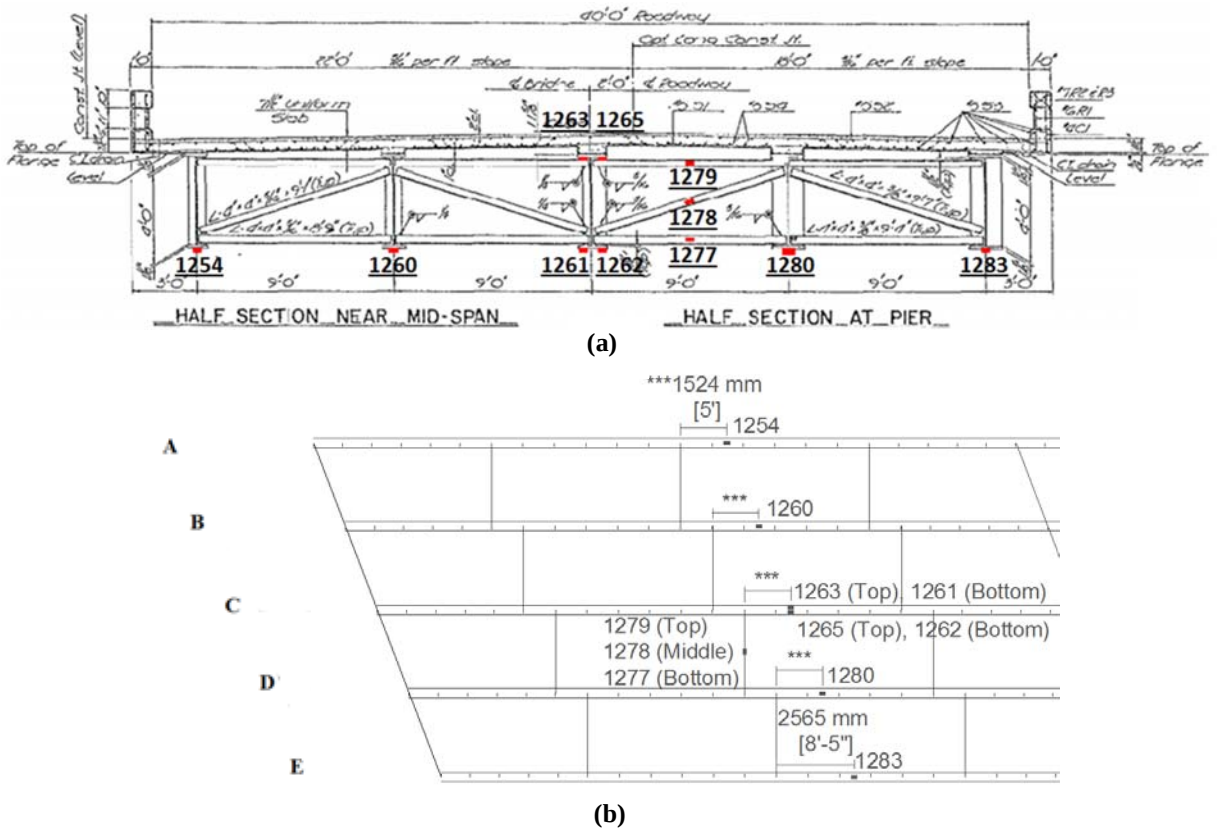

Figure 11: BDI strain transducer locations for both tests in (a) section view (b) plan view.

The string potentiometer was placed under Girder C. It was attached to the middle of the bottom flange, directly under where the connection plate connected to the girder web. Inclinometers were placed at the connection plate on Girder C. One inclinometer was placed at the vertical midpoint of the connection plate while the other was attached to the bottom flange of Girder C. The LVDT was attached to the underside of the top flange of Girder C and positioned near the top of the connection plate, similar to the setup shown in Figure 12. The string potentiometer and LVDT were powered using 15V and were connected to a NI-9223 module for

data recording, while the inclinometers were powered using 5V and were connected to a NI-9205 module for data recording.

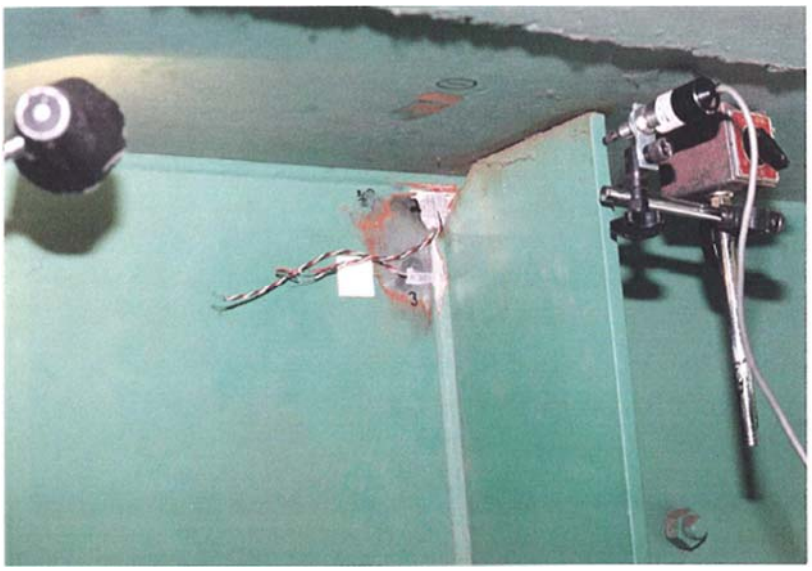

Figure 12: Photograph of LVDT placement similar to that used in the first and second field test.

All data was recorded using a National Instruments data acquisition system. This system was comprised of a single NI cDAQ 9188 chassis that housed each of the NI modules. The NI software, Labview (2011), was used to write a protocol that read and recorded the data into a text file. The data was recorded using a sampling rate of approximately 800 samples per second. Calibration factors were applied in the Labview software so that data was recorded into the text file with proper units.

Unforeseen electrical noise and connection grounding issues were encountered during the first field test. This resulted in very noisy data and also prevented viable readings from the BDI strain transducers. Measures were taken during the second field test to overcome these challenges. A PS Power Plant Premier was used to regulate the line voltage from the generator, which provided cleaner power for the instrumentation and reduced electrical noise. A 2.4 m (8 ft.) copper-bonded grounding rod was installed in the ground and connected to the generator with 14 gauge wire. Additionally, the NI-9205 module that read data from the BDIs was changed to a differential measurement configuration. These measures reduced the electrical noise and adequately solved the connection grounding issues, resulting in cleaner data and viable results for the BDI strain transducers during the second field test.

4.2. Loading

The loaded weight of the truck for the first test was 217 kN (48.8 kip) while for the second test, the loaded weight was 250 kN (56.3 kip). KDOT enforced traffic control, allowing the loaded dump truck to pass over the bridge alone over the east lane, west lane, and center of the bridge. Each of these runs was completed twice at 8-16 kph (5-10 mph) and 105-121 kph (65-75 mph), for a total of six truck tests each for the pre-retrofit and post-retrofit field tests. Data was recorded separately via the data acquisition system for each truck test. Since the loads were different, data from the second test was normalized to the loading of the first test so as to make clear comparisons between the first and second field tests.

5. Finite Element Models

To accurately reflect field testing conditions, a second series of full-scale finite element models of Kansas Bridge 135-87(043/044) were created using Abaqus version 6.12-3. In these models, focus was shifted from the third cross frame of span two of Girder C to the second cross frame of span one of Girder C, since this was where measurements were recorded during field tests. Additionally, crack conditions at the testing location, truck loadings, and the as-installed retrofit were modeled as faithfully as possible to coincide with field conditions. Models were analyzed with cracks in both the unretrofitted and retrofitted conditions. Screenshots from the FE models are shown in Figure 13.

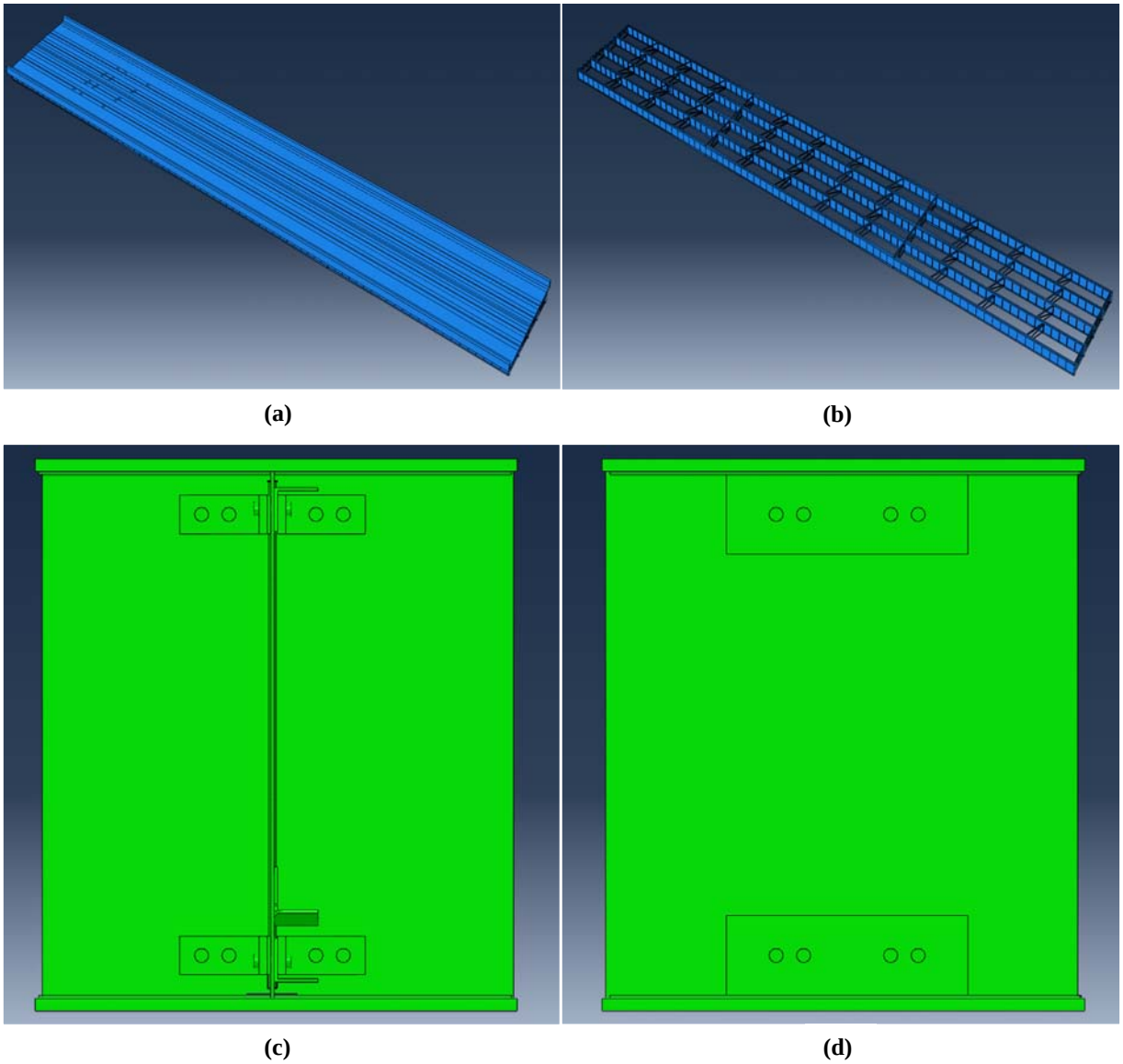

Figure 13: (a) Full scale model with concrete deck (b) Full scale model without concrete deck (c) stiffener side of Girder C with angles-with-plate retrofit (d) non-stiffener side of Girder C with angles-with-plate retrofit.

All materials were modeled as linear elastic. Concrete was modeled with a modulus of elasticity of 25,000 MPa (3,605 ksi) and a Poisson's ratio of 0.2, while steel was modeled with a modulus of elasticity of 200,000 MPa (29,000 ksi) and a Poisson's ratio of 0.3. All structural elements were modeled and assembled in Abaqus version 6.12-3 using three-dimensional solid elements to match as closely as possible the original and repair structural plans, included in Appendix F. The end supports of the bridge are rockers, while the two interior supports are bolsters. These support conditions were modeled as rollers and pins, respectively.

The concrete deck was sloped as in the structural plans and modeled as one part with the two side barriers. The concrete haunches were created in five parts, each being sized and sloped according to their position to the bottom of the bridge deck on each girder. The concrete deck, barriers, and haunches were meshed using structured hexahedral elements (C3D8R) with a mesh size of 127 mm (5 in.). The deck was attached to the haunches and the haunches to the steel girder's top flanges using tie constraints.

The steel girders were modeled in three parts-the web, top flange, and bottom flange. The top flange and bottom flange were connected to the web using 8 mm (5/16 in.) fillet welds. The fillet welds were modeled as right triangles and connected to the flanges and girders using tie constraints. Intermediate stiffeners were modeled and attached directly to the girder webs with tie constraints. Stiffeners serving as cross frame connection plates were modeled and connected to the girder webs with 4.8 mm (3/16 in.) fillet welds using tie constraints. With the exception of the Girder C web, these steel elements were meshed using structured hexahedral elements (C3D8R) with a mesh size of 25mm (1 in.). A dense mesh was applied to the web gap regions at the second cross frame of span one in Girder C (the focus area of the analyses). At these locations, structured hexahedral elements (C3D8R) with a mesh size of 25 mm (0.1 in.) were used over an area that measured 305x1016 mm (12x40 in.) symmetrically about the connection stiffener in the top and bottom web gap regions. Transition regions were modeled using swept hexahedral elements (C3D8R).

The retrofit was modeled to match that installed in the field, which included two angles, a backing plate, and a fill plate between the angle and connection plate on the side without a cross frame element. Retrofit elements were modeled with structured and swept hexahedral elements (C3D8R) and a mesh size of 6 mm (0.25 in.). Bolts and bolt holes were modeled with 19 mm (3/4 in.) diameters to match those used by KDOT. Bolt heads and nuts were connected directly to the elements they were in contact with using tie constraints. The angles, backing plates, and fill plates were modeled with hard contact interactions with a friction coefficient of 0.35. Bolts were modeled with a pre-tension bolt load of 125 kN (28 kip), which was applied to each bolt shank using Abaqus' bolt load function. A pre-tension bolt load model step was created to activate the bolt loads.

Cracks were modeled using Abaqus' Extended Finite Element Method (XFEM), which allows cracks to be modeled at any location in an element. Cracks were modeled as three-

dimensional extruded shell elements and given depths equal to the girder web thickness. The lengths of the cracks were modeled as closely as possible to those observed in the field at the testing location, as shown in Figure 14. The crack pattern in the bottom web gap included a 116 mm (4-9/16 in.) Type D crack, a 117 mm (4-5/8 in.) Type B crack on the north side of the connection plate, and a 51 mm (2 in.) Type B crack that spidered out into a 33 mm (1-5/16 in.) Type C crack on the south side of the connection plate. The crack pattern in the top web gap included a 19 mm (¾ in.) Type A crack.

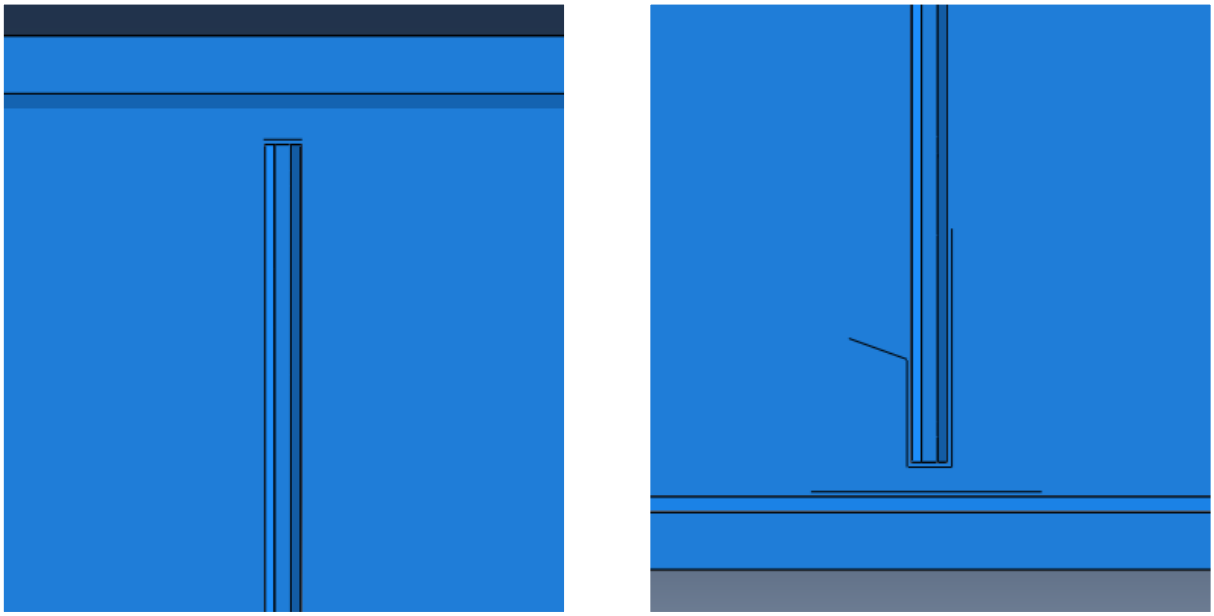

(a) **(b)**

Figure 14: Crack patterns modeled at (a) top web gap (b) bottom web gap.

Since the goal of the field testing was to determine the change in stresses under the action of live loads due to the application of the retrofit, no dead loads were applied. In the field, stresses from the dead loads were already essentially applied to the bridge, so instrumentation only measured what took place in response to traffic live loads. Thus, only the loading from the truck was applied in the finite element models. The loads from the truck were modeled as tire contact areas on the concrete deck. The tire contact areas were modeled with widths of 508 mm (20 in.) and lengths of 254 mm (10in.). These dimensions were taken from AASHTO LRFD Bridge Design Specifications Section 3.6.1.2.5 for wheels consisting of one or two tires. The lengths between tire contact areas were kept the same as the axle distances measured on the trucks used in

the field tests, which were 4 m (13.2 ft.) between the first and second axle, and 1.3 m (4.4 ft.) between the second and third axle. The width between tire contact areas was kept the same as the axle width measured on the trucks used in the field tests, which was 1.8 m (6.1 ft.). A sketch of the truck tire contact area dimensions is shown in Figure 15.

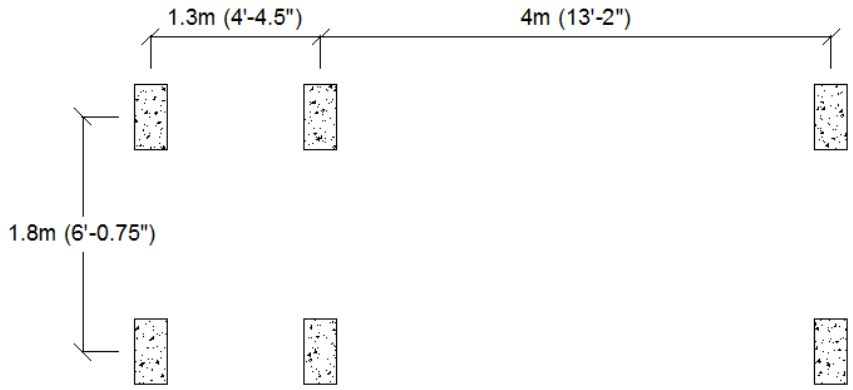

Figure 15: Truck tire contact area dimensions and placements, as measured in the field.

The truck load from the first test, 217 kN (48.8 kip), was used in the models, since the field test results were normalized to this load. Distribution of the truck load was based on AASHTO's Design Truck, which has a front axle load of 36 kN (8 kip) and two rear axle loads of 142 kN (32 kip) each. This correlated to a front axle load in the model of 24 kN (5.4 kip) and rear axle loads of 96 kN (21.7 kip). Each of these axle loads were halved and applied over their respective tire contact areas as pressure loads, which resulted in front tire contact area loads of 93 kPa (13.5 psi) and rear tire contact area loads of 374 MPa (54.25 ksi). The truck load was modeled in the west and east lanes and over the center of the bridge. Screenshots of these model loads can be seen in Figure 16.

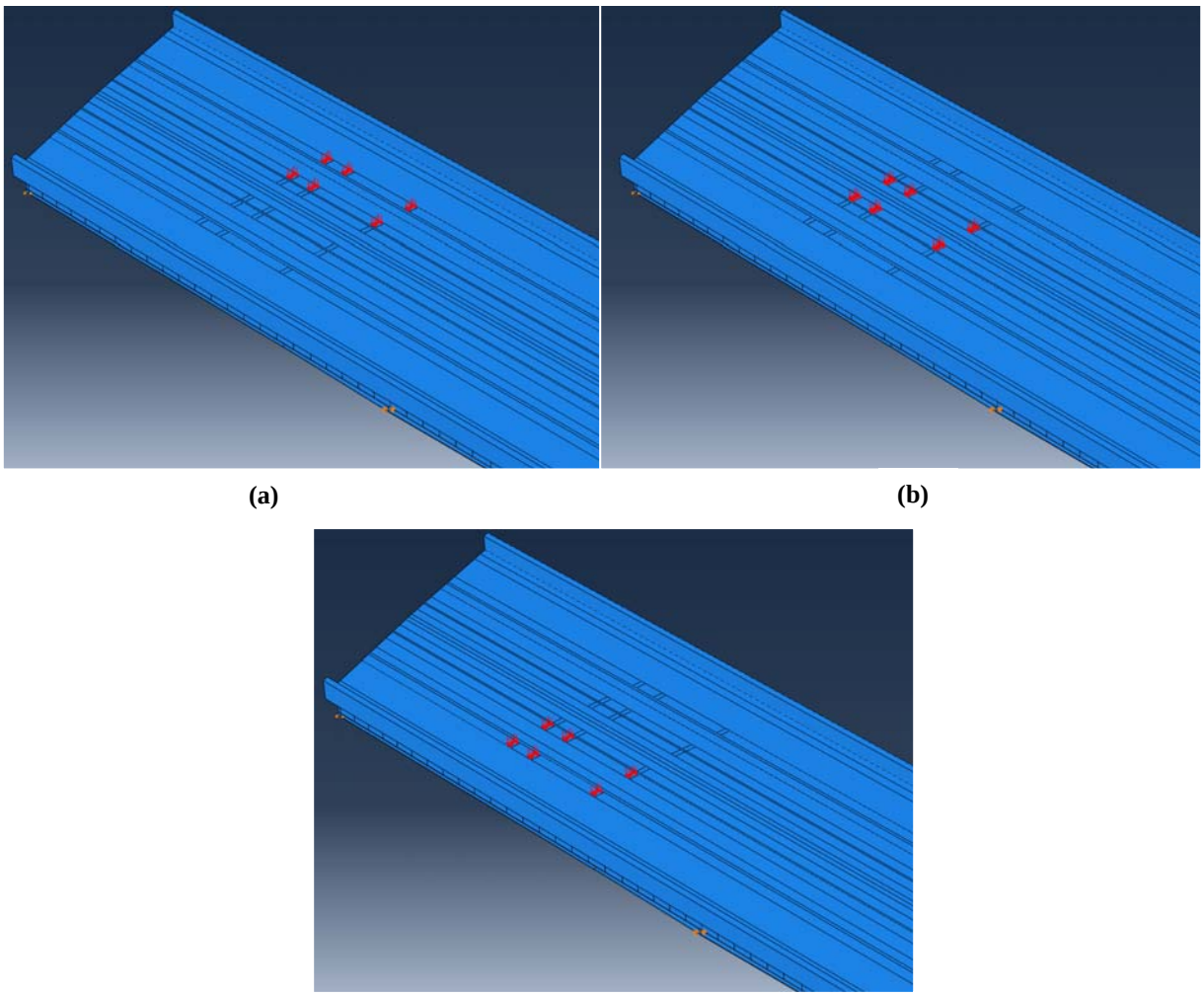

Figure 16: Truck load modeled in (a) west lane (b) bridge center (c) east lane.

To compare results of the finite element model with field test results, the truck location that produced the maximum stress demands needed to be determined. This was accomplished by executing a suite of models in the unretrofitted state in which the truck was "moved" along the bridge in 610 mm (24 in.) increments. A total of seventy-five models, twenty-five for each truck lane position, were run and analyzed. Stresses were extracted from locations that corresponded to the bondable strain gage locations from the field tests, and then results from each model were compiled into stress curves. The highest stresses from the curves were found to correlate to a truck located a distance of 13.7 m (45 ft.) from the southwest corner of the bridge to the furthest rear axle of the truck. Once this truck position was established, six models were analyzed with this loading and results from these models were compared with the two field test results. Three models

were analyzed in the unretrofitted condition with the truck load in the east lane, west lane, and bridge center, and three models were analyzed in the retrofitted condition with the truck load in the east lane, west lane, and bridge center.

6. Top Web Gap Comparison

Separate finite element analyses that focused on the top web gap region were also performed. In these analyses, the cracking pattern in the top web gap was changed to determine what effect this had on stresses in the top web gap region. Crack patterns in the bottom web gap remained the same as those modeled from the field test conditions. The top web gap was modeled with both a 25 mm (1 in.) crack at the connection plate-to-web weld and a 51 mm (2 in.) crack at the flange-to-web weld. Models were also created that included each of these cracks occurring separately in the top web gap. Models of the bridge with these crack conditions were analyzed in both the unretrofitted and retrofitted conditions under the established east lane, west lane, and bridge center truck load positions detailed in the previous section, which led to a total of nine finite element models.

The Hot Spot Stress (HSS) technique was used to compare stresses in the top web gap region between the unretrofitted and retrofitted conditions. Using this technique, maximum principal stresses were taken from nodes along a path located half the thickness of the girder web away from the cracks. Previous studies by Richardson (2012) and Hartman (2013) have shown that distortion-induced fatigue crack growth closely follows maximum principal stress paths. The HSS paths in this study were taken along the length and around the tips of the connection plate-to-web weld and flange-to-web weld cracks to capture the high stresses present in these regions. Figure 17 shows these stress paths for each crack type. HSS 1 refers to the path taken around the connection plate-to-web weld crack, while HSS 2 refers to the path taken around the flange-to-web weld crack.

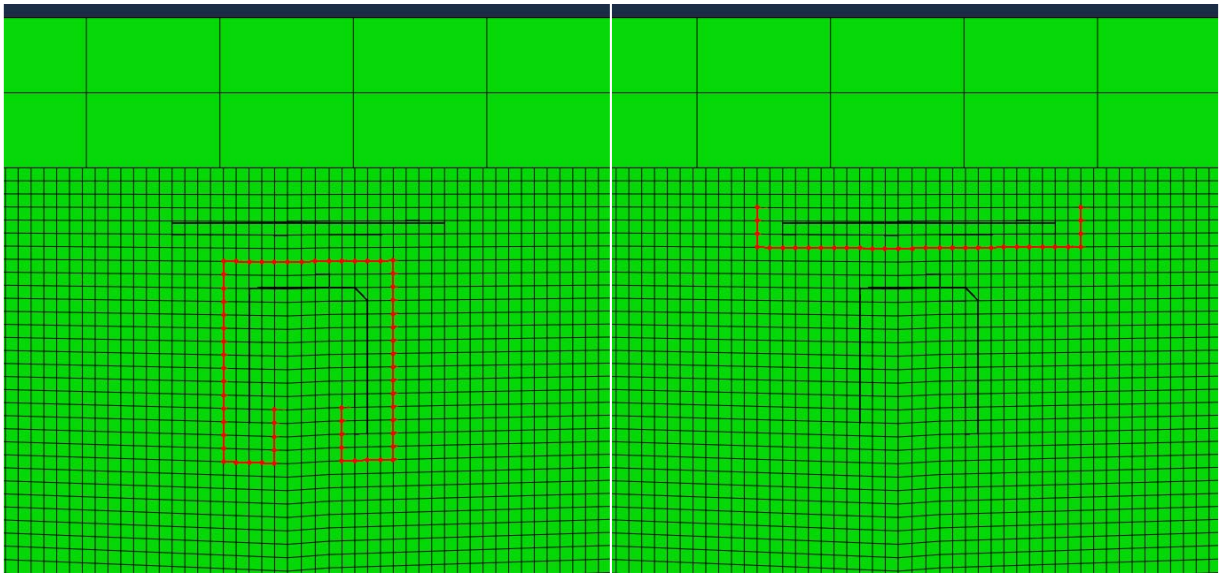

(a) (b)

Figure 17: Maximum principal stress paths (a) HSS 1 (b) HSS 2.

7. Results and Discussion

To reduce noise in the field test data, a low-pass filter was created and applied in Matlab to create a smoothing effect on the data. The data output from each instrument was passed through the filter, which had a passband frequency of 10 Hz and a stopband frequency of 50 Hz. Data curves from each instrument for each field test run can be found in Appendix G. Strain readings were converted into stresses and compared with results from finite element analyses of the bridge. Peak strain values were taken from the field test data curves, converted into stresses, and compared with values from the FEM analyses of the bridge.

7.1. Global Behavior – Field and FEM Investigations

Figures 18 and 19 show the maximum stresses for the BDI strain transducers for the west lane, east lane, and center truck loadings for the second field test. As previously mentioned, electrical noise and connection grounding issues prevented the BDI strain transducers from producing viable data during the first field test. In these figures, the field test data overlays the FE analyses results; field test values are presented with callout boxes to indicate instrument location. The stress values shown in Figures 18 and 19 show that maximum stresses in the girders and cross frames coincided with the respective truck position. For instance, as the truck traveled over the

west lane, the highest stress was recorded for the BDI strain transducers located on the girders under that lane. This was the same relationship for each truck loading location and corresponding girder BDI. The BDI strain transducers placed on the cross frame show that the bridge center and east lane loadings had the most effect on the cross frame members. Center loading produced the highest tensile stress in the diagonal cross frame member, while the east lane loading produced the highest tensile stresses in the top and bottom horizontal cross frame members. The BDI instrument results made sense intuitively and corresponded to the expected global behavior of the bridge girders. Additionally, the values from the field test corresponded to those from the FE analyses, indicating that the FE models provided a good comparison to the actual bridge and its behavior.

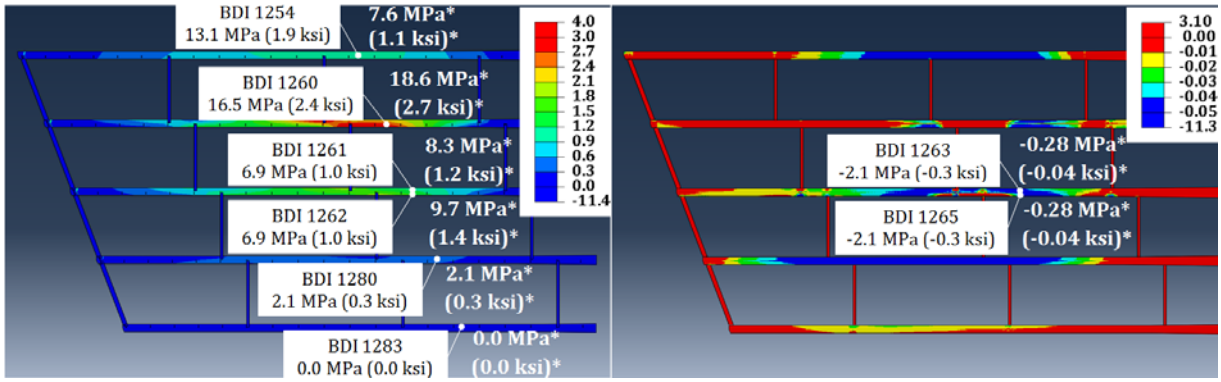

(a)

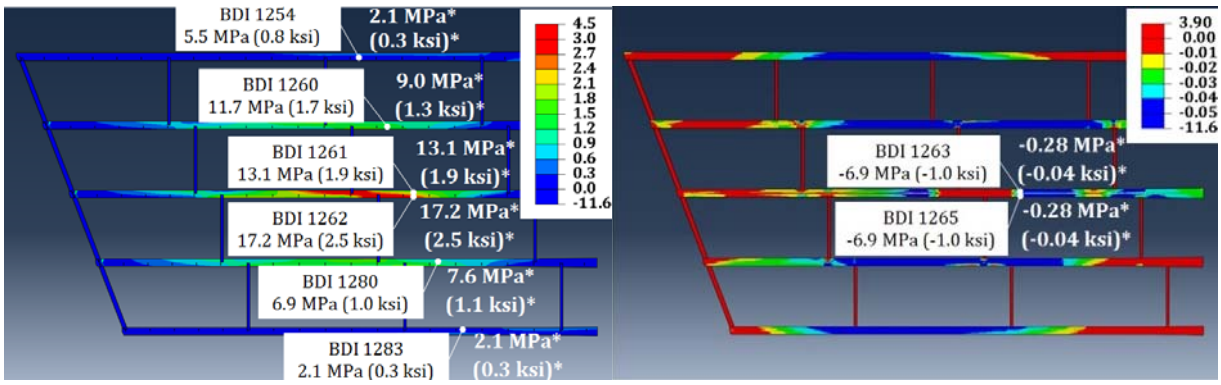

(b)

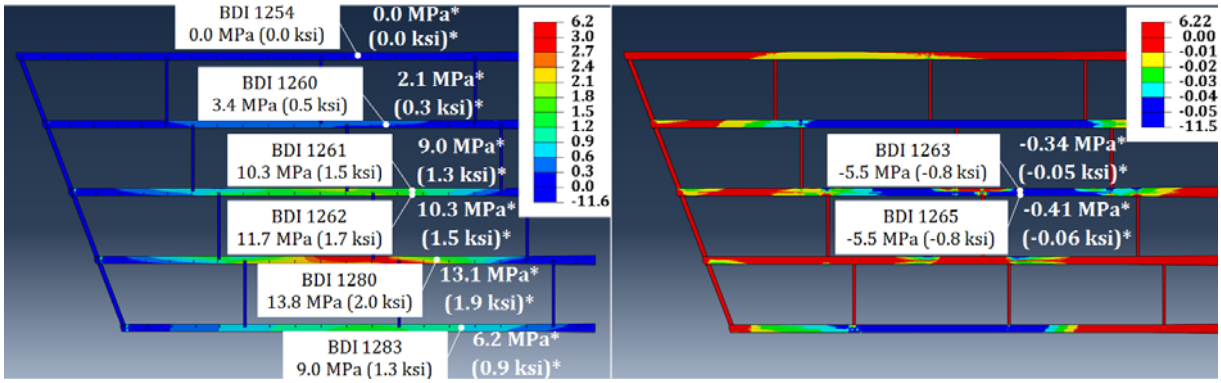

(c)

Figure 18: Girder flange BDI results from field tests and FE analyses for (a) west truck load placement (b) center truck load placement (c) east truck load placement. Bottom flange BDIs are shown on the left side of the figure, while top flange BDIs are shown on the right. Legend stresses are in ksi. *FE analyses values.

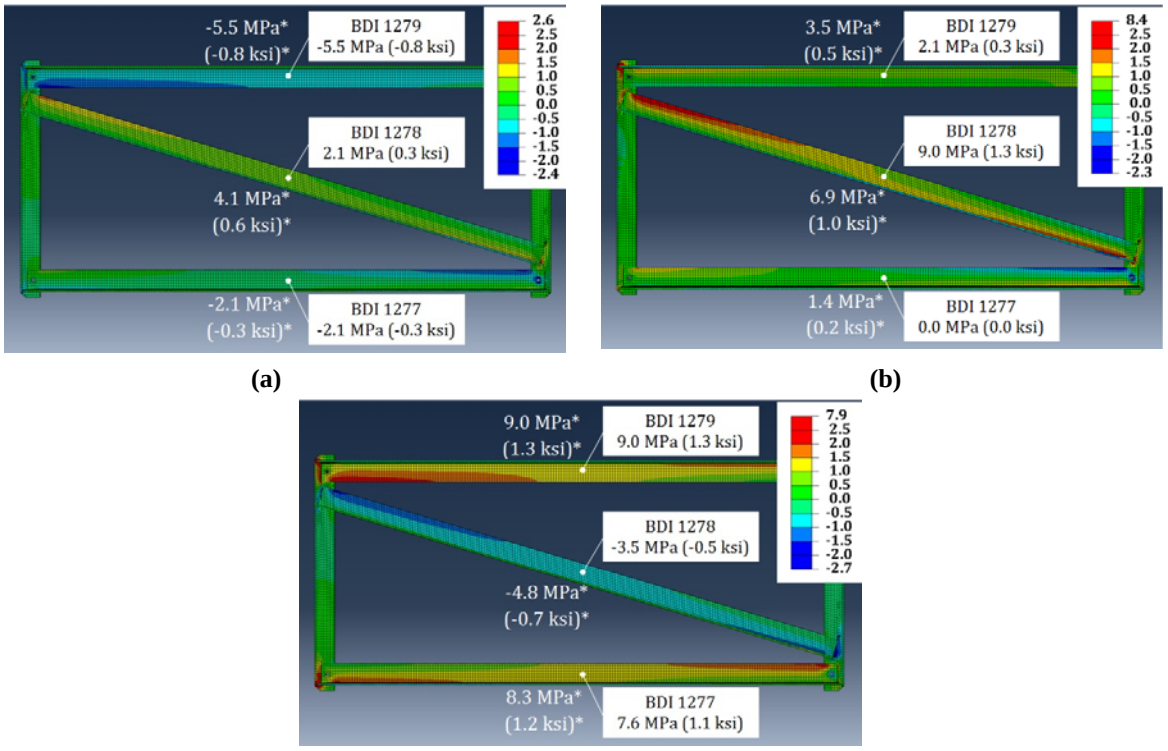

Figure 19: Cross frame BDI results from field tests and FE analyses for (a) west truck load placement (b) center truck load placement (c) east truck load placement. Legend stresses are in ksi. *FE analyses values.

The string potentiometer results for west lane, east lane, and bridge center truck loadings are shown in Figure 20. Maximum vertical deflection of girder C at the connection plate occurred when the truck traveled over the center of the bridge. There was no change in deflection between the first test and the second test, indicating that application of the retrofit did not have an impact on vertical deflection, which was the expected result. As with the BDI results, the values from the field test corresponded to those of the FE analyses, indicating that the FE models provided a good comparison to the actual bridge and its behavior.

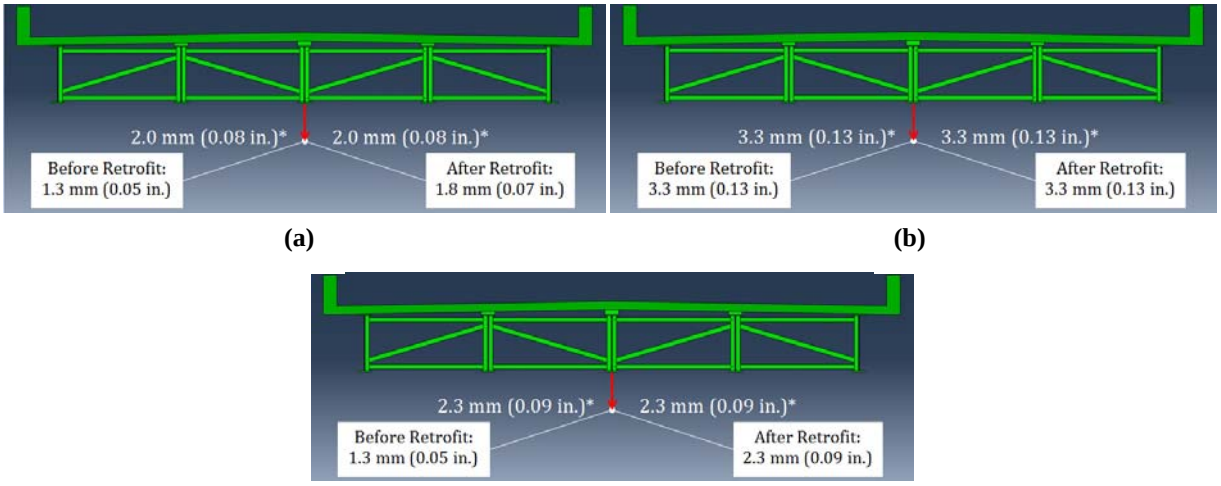

(a) **(b)**

(c)

Figure 20: String potentiometer results from field tests and FE analyses for (a) west truck load placement (b) center truck load placement (c) east truck load placement. *FE analyses values.

7.2. Local Behavior - Field and FEM Investigations

Bondable strain gages were used to provide localized results at the top and bottom girder web gap regions. The strain gages were placed in the same locations for the top and bottom web gaps. Strain gage results are presented herein for the field tests, and computed results from identical locations in the finite element analyses are also reported. Results are shown in terms of both maximum principal stresses and directional stresses. Directional stresses are used to make a direct comparison between field test strain gage readings and FE analyses results. Strain gages in the field were placed either vertically or horizontally, and are compared accordingly with the appropriate directional stresses from the finite element models. Maximum principal stresses, while not comparable directly with what was measured in the field, capture both in-plane and out-of-plane stresses and are shown to illustrate the overall behavior of the web gap regions before and after the retrofit was applied. All results are shown for the stiffener and non-stiffener sides of Girder C, both before and after retrofit application.

Figures 21, 22, 23, and 24 show results and comparisons of strain gage results between the unretrofitted and retrofitted states. Corresponding strain gage measurements and FE results generally show that the stress demand at the bottom web gap was at least 20% higher than that of the top web gap for tests before the retrofit was applied. Since the majority of fatigue cracks found on the bridge have occurred in the bottom web gap, this was expected. It also supports the findings

of previous research that has concluded that skewed bridges with staggered cross frames see maximum stress demands and fatigue cracking occurring in the bottom web gaps.

For all loading scenarios, field test and FE results show that peak stresses in the bottom web gap were significantly reduced after application of the angles-with-plate retrofit. Reduction of stresses in this area is very favorable because, as previously mentioned, the bottom web gap is the region of Kansas Bridge 135-87(043/044) in which the highest web gap out-of-plane stress demands are experienced. Therefore, the reduction of stresses in the bottom web gap region shows that the angles-with-plate retrofit should be successful in greatly slowing or halting crack propagation for the most problematic areas on the bridge.

For stresses nearest the top flange, peak stresses showed favorable reduction and behavior after application of the angles-with-plate retrofit for the center truck loading test. However, for the east and west lane truck loadings, low levels of stress decrease, and in a few cases, stress increase, in the top web gap region were observed. Although the top web gap region was found to experience lower stress demands before the retrofit than the bottom web gap, this is still a result that warranted further investigation. For this reason, an additional analytical investigation was performed that focused on the top web gap region of the bridge.

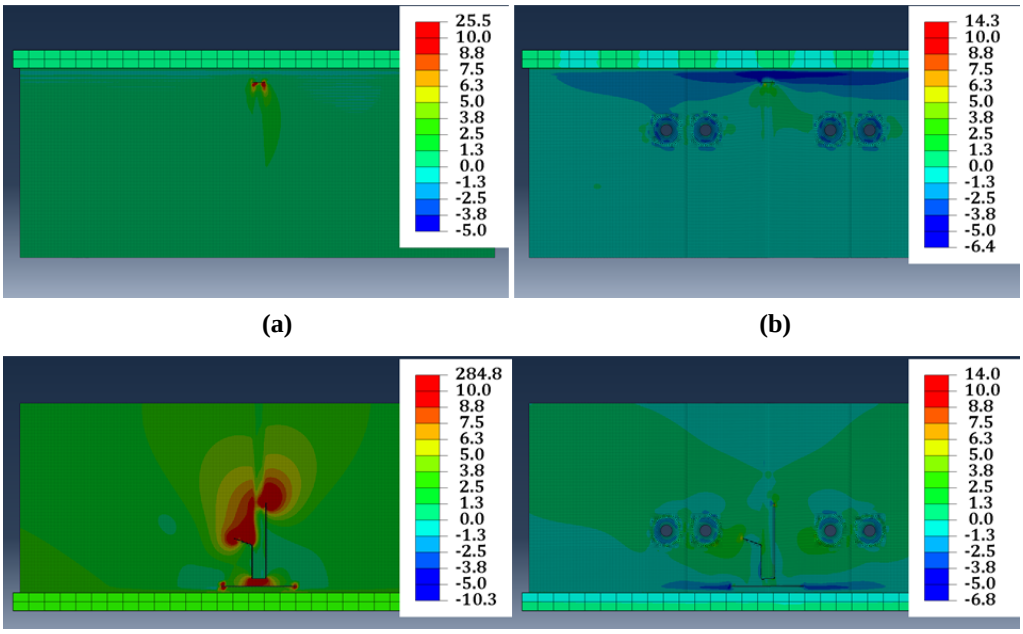

Figure 21: Maximum principal stresses for center load truck placement at (a) top web gap, before retrofit (b) top web gap, after retrofit (c) bottom web gap, before retrofit (d) bottom web gap, after retrofit. Legend stresses are in ksi.

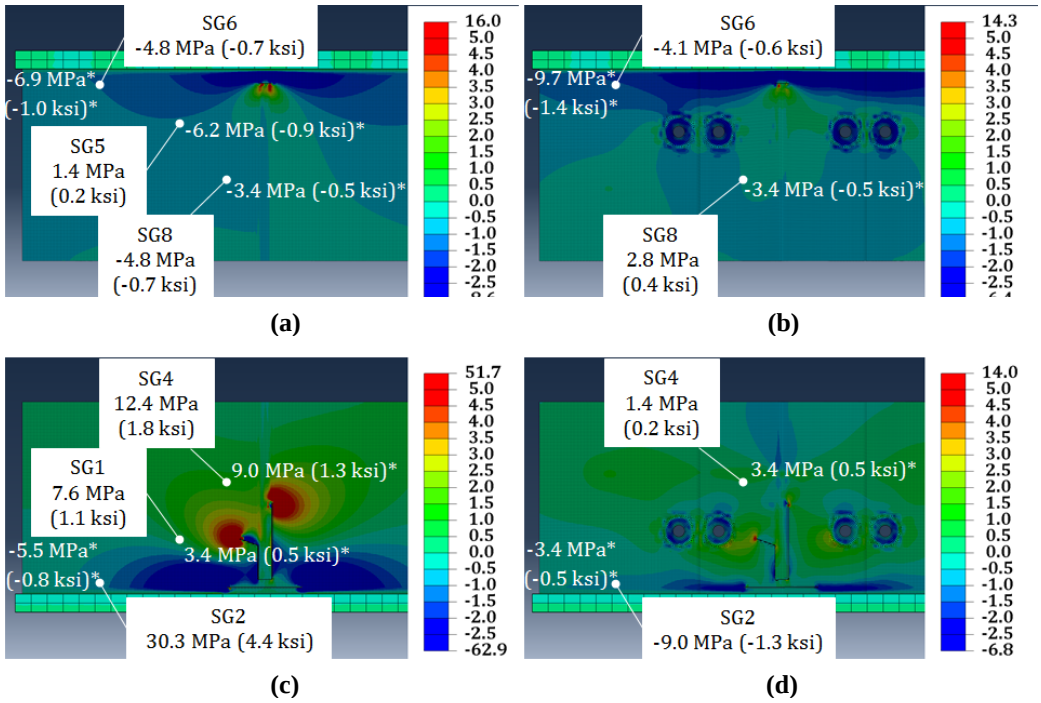

Figure 22: Directional stresses for center load truck placement at (a) top web gap, before retrofit (b) top web gap, after retrofit (c) bottom web gap, before retrofit (d) bottom web gap, after retrofit. Legend stresses are in ksi. *FE analyses values.

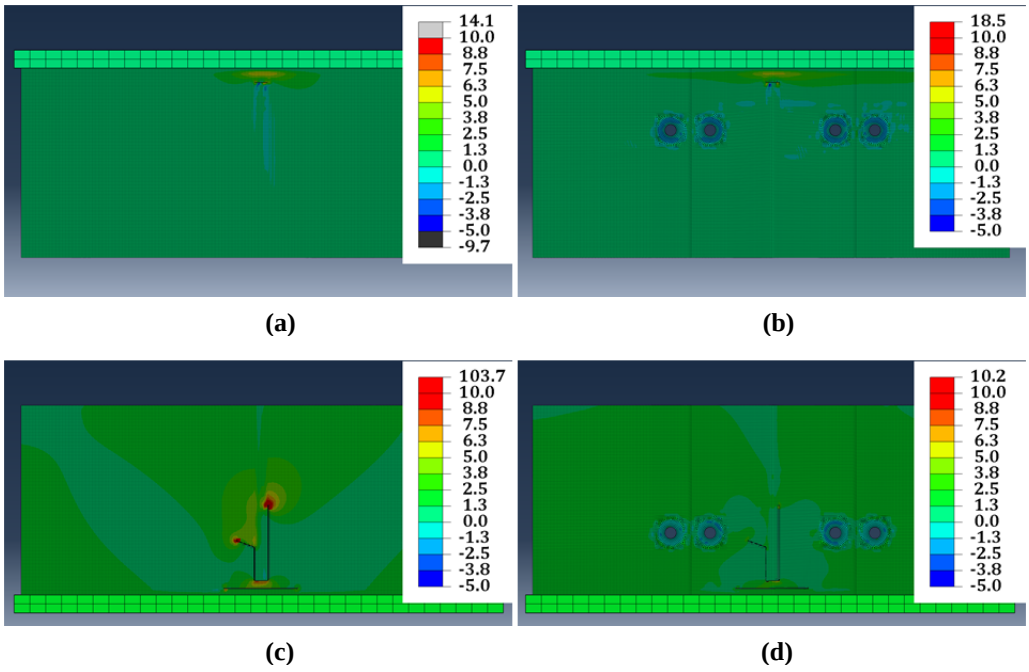

Figure 23: Maximum principal stresses for west load truck placement at (a) top web gap, before retrofit (b) top web gap, after retrofit (c) bottom web gap, before retrofit (d) bottom web gap, after retrofit. Legend stresses are in ksi.

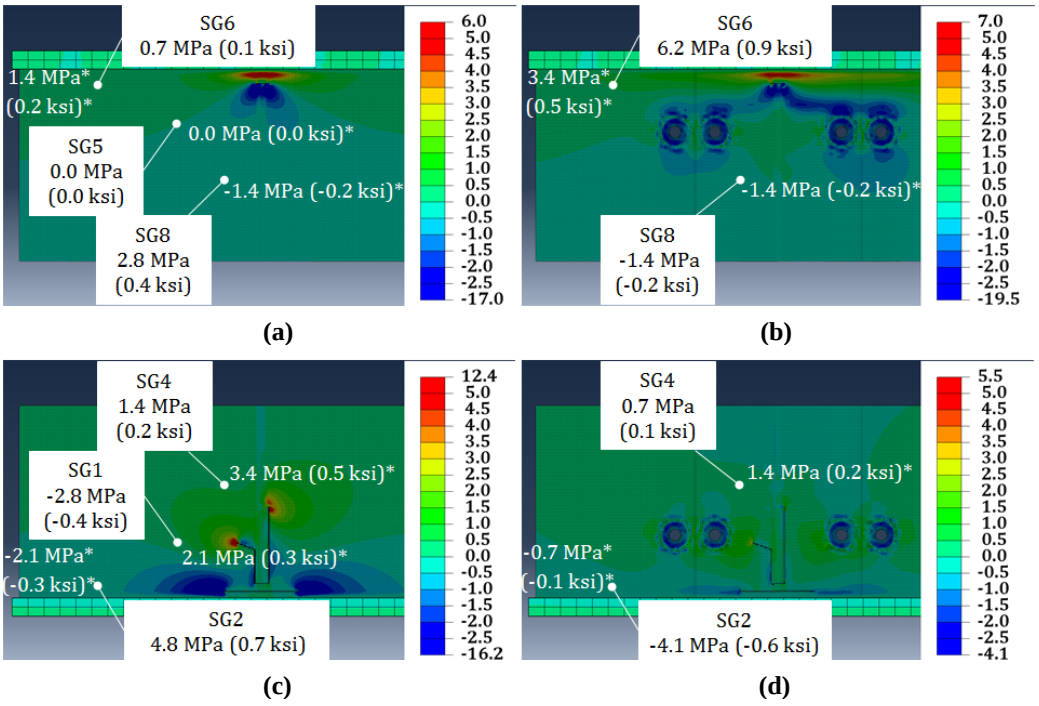

Figure 24: Directional stresses for west load truck placement at (a) top web gap, before retrofit (b) top web gap, after retrofit (c) bottom web gap, before retrofit (d) bottom web gap, after retrofit. Legend stresses are in ksi. *FE analyses values.

7.3. Top Web Gap Behavior - FEM Investigation

Hartman's (2013) study of a non-skewed, 9.1 m (30 ft.) test bridge showed that stress demand in the top web gap region decreases as crack length increases. This phenomenon is most apparent when cracks are at their smallest lengths. It should be noted again that the crack in the top web gap at the testing location of Kansas Bridge 135-87(043/044) was a 19 mm (3/4 in.) crack at the connection plate-to- web weld. Typical behavior of this type of crack upon growth is propagation around the toe of the connection plate weld.

Based on the findings by Hartman (2013), it was hypothesized in this study that if the 19 mm (3/4 in.) top web gap crack in the FE model of Kansas Bridge 135-87(043/044) was lengthened into a 25 mm (1 in.) horseshoe-shaped crack, unretrofitted stress demands would decrease and the retrofit would essentially become more effective in the top web gap of Kansas Bridge 135-87(043/044). Investigators in this study also wanted to investigate behavior of the top web gap if a longitudinal top flange-to-web weld crack was introduced in the FE model of Kansas Bridge 135-87(043/044). From KDOT inspection reports, the most severe crack of this type was 51 mm (2 in.), so this was the longitudinal crack length selected for the FE analyses. The inspection reports also indicated that the connection plate-to-web weld cracks and flange-to-web weld cracks occurred both separately and together in the top web gap region, so all three scenarios were investigated in the finite element models.

Using the HSS technique, stress demands around both cracks were compared using the stress paths previously shown in Figure 17. HSS 1 stresses were higher on the stiffener side for both the bridge center and east lane truck loadings, while for the west lane truck loading HSS 1 stresses were higher on the non-stiffener side. The opposite was true for the HSS 2 stress path. Stresses along this path were highest on the non-stiffener side for both the bridge center and east lane truck loadings and on the stiffener side for the west lane truck loading.

Figures 25, 26, and 27 show maximum principal stresses when both the connection plate-to-web weld and flange-to-web weld cracks were present for all three truck location loadings, both before and after retrofit application. Under bridge center truck loading, the retrofit reduced HSS 1 and HSS 2 stress demands by 66% and 35%, respectively. Under west lane truck loading, HSS 1 stress was reduced by 27% and HSS 2 stress was reduced by 26%. Under east lane truck loading, HSS1 and HSS 2 stresses were reduced by 53% and 23%, respectively.

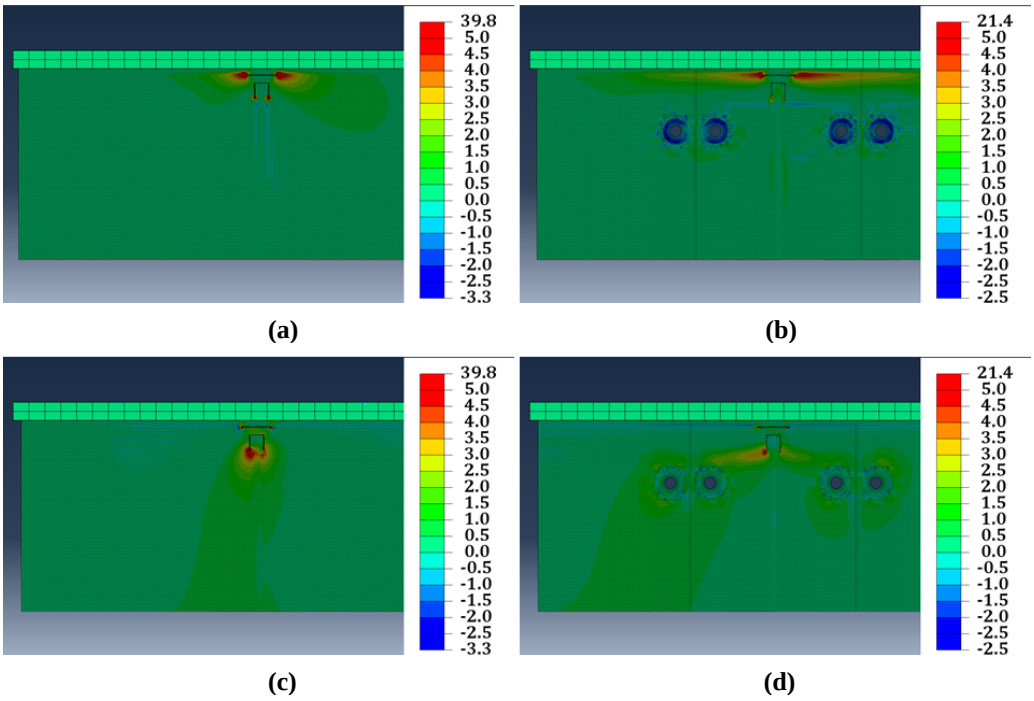

Figure 25: Maximum principal stresses at top web gap for west load truck placement when both the connection plate-to-web and flange-to-web weld cracks are present for (a) stiffener side, before retrofit (b) stiffener side, after retrofit (c) non-stiffener side, before retrofit (d) non-stiffener side, after retrofit. Legend stresses are in ksi.

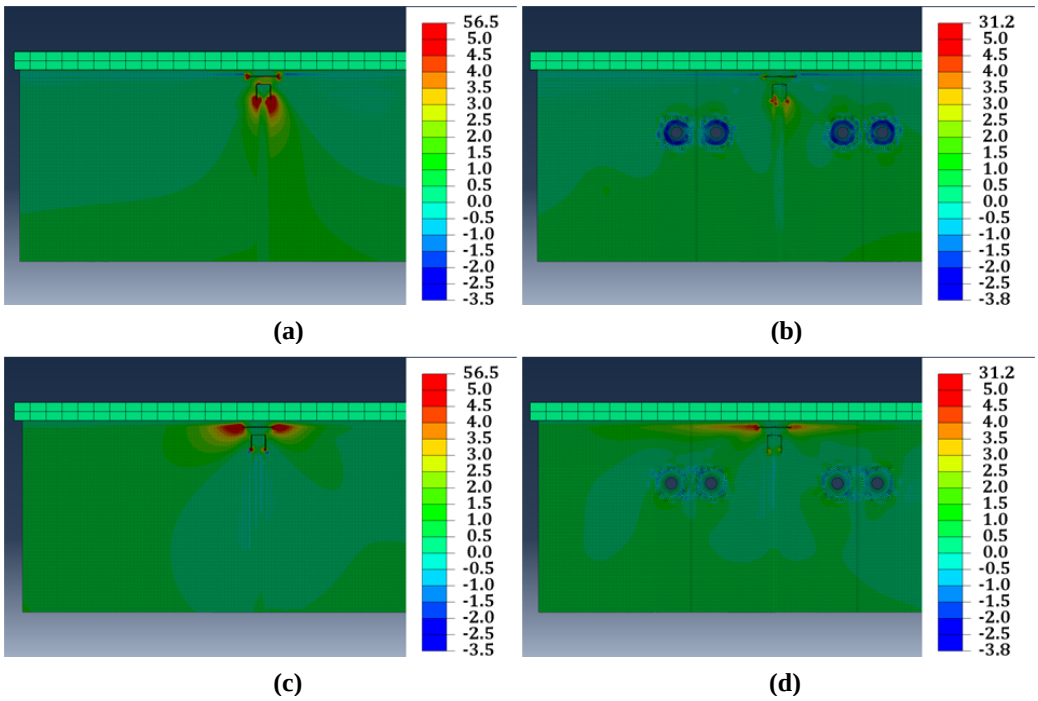

Figure 26: Maximum principal stresses at top web gap for center load truck placement when both the connection plate-to-web and flange-to-web weld cracks are present for (a) stiffener side, before retrofit (b)

stiffener side, after retrofit (c) non-stiffener side, before retrofit (d) non-stiffener side, after retrofit. Legend stresses are in ksi.

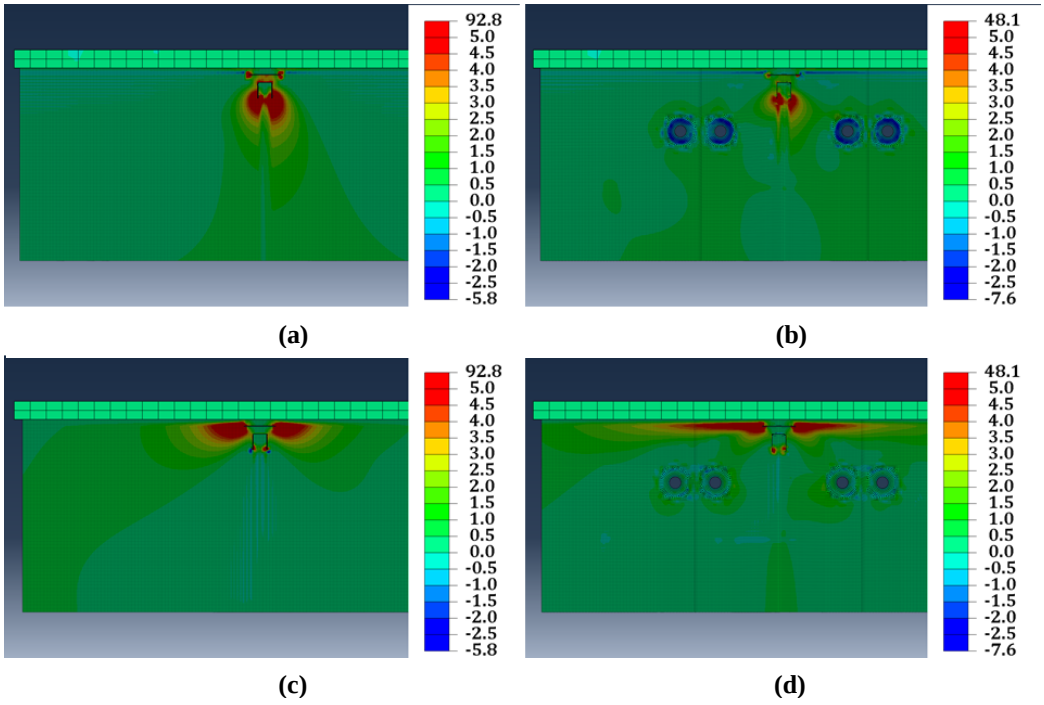

Figure 27: Maximum principal stresses at top web gap for east load truck placement when both the connection plate-to-web and flange-to-web weld cracks are present for (a) stiffener side, before retrofit (b) stiffener side, after retrofit (c) non-stiffener side, before retrofit (d) non-stiffener side, after retrofit. Legend stresses are in ksi.

Figure 28 shows maximum principal stresses from all three truck location loadings, both before and after retrofit application, for the top web gap when only the connection plate-to-web weld crack was present. After application of the retrofit, HSS 1 stress was reduced under the bridge center, west lane, and east lane truck loadings by 63%, 26%, and 50%, respectively. Figure 29 shows maximum principal stresses, both before and after retrofit application, for the top web gap when only the flange-to-web weld crack was present. Application of the retrofit reduced HSS 2 stress demand under the bridge center, west lane, and east lane truck loadings by 23%, 14%, and 2%, respectively.

HSS 1 stresses were reduced only slightly more for the case where both connection plate-to-web weld and flange-to-web weld cracks were present than in the case where only the connection plate-to-web weld crack was present. HSS 2 stresses, however, were reduced significantly less in the case where only the flange-to-web weld crack was present compared to the case where both cracks were present. These results indicate that the flange-to-web weld crack

stresses are affected more by the appearance of connection plate-to-web weld crack, and that the appearance of the flange-to-web weld crack has little effect on the connection plate-to-web weld crack.

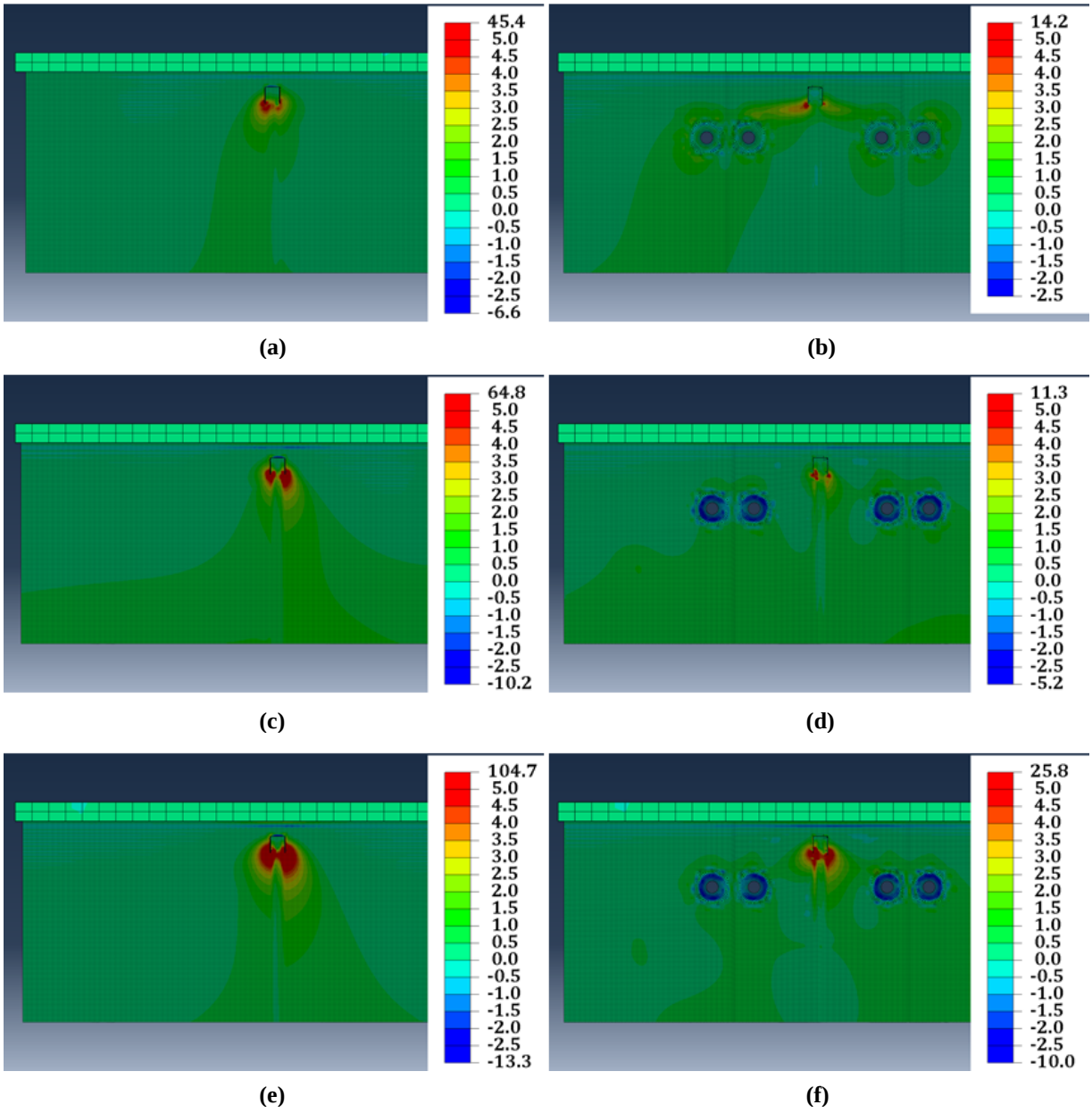

Figure 28: Maximum principal stresses at top web gap when only connection plate-to-web weld crack is present for (a) west load truck placement, before retrofit (b) west load truck placement, after retrofit (c) center load truck placement, before retrofit (d) center load truck placement, after retrofit (e) east load truck placement, before retrofit (f) east load truck placement, after retrofit. Legend stresses are in ksi.

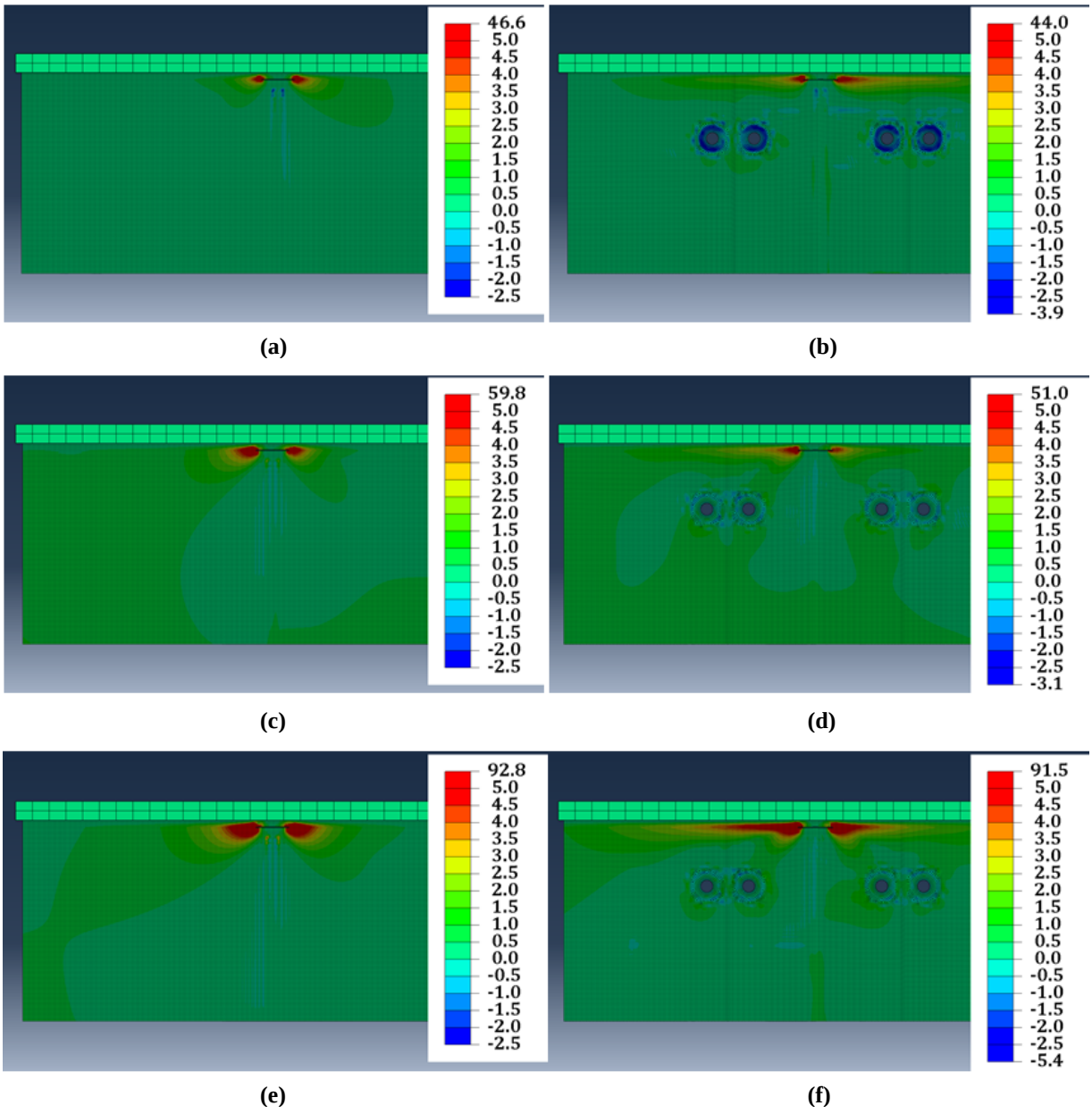

Figure 29: Maximum principal stresses at top web gap when only flange-to-web weld crack is present for (a) west load truck placement, before retrofit (b) west load truck placement, after retrofit (c) center load truck placement, before retrofit (d) center load truck placement, after retrofit (e) east load truck placement, before retrofit (f) east load truck placement, after retrofit. Legend stresses are in ksi.

In all cases, stress demands were reduced in the top web gap region by application of the retrofit. Although stresses were reduced much less when just the flange-to-web weld crack was present, the stress patterns shown in Figure 29 indicate that when the flange-to-web weld crack is present, the stresses in the connection plate-to-web weld crack region are also high and are likely to produce the connection plate-to-web weld crack. The same is true for the case with just the

connection plate-to-web weld crack with respect to the stress patterns in the flange-to-web weld crack region, as shown in Figure 28. These are favorable results in that the appearance of both the connection plate-to-web weld and flange-to-web weld cracks only improves the performance of the angles-with-plate retrofit.

Further investigation of the top web gap region due to concerning results from the field test and corresponding FE analyses led to supportive results for application of the angles-with-plate retrofit. By extending the 19 mm (3/4 in) Type A crack around the connection plate-to-web weld, retrofit performance improved. Since this is the typical propagation for this type of crack, this would be the expected crack pattern if any growth of the Type A crack was to take place in top web gap of Kansas Bridge 135-87(043/044). The results from the additional set of FE analyses shows that performance of the retrofit would only improve if this were to take place, and any further growth of the crack would be unlikely. Even upon addition of a flange-to-web weld crack in the FE models, top web gap stresses were reduced after application of the retrofit. Although stresses in the top web gap region are much smaller in comparison with the bottom web gap region in Kansas Bridge 135-87(043/044), and most fatigue cracking has been reported in the bottom web gap region, these results show that the angles-with-plate retrofit should also be effective in the top web gap region.

8. Conclusions

Kansas Bridge 135-87(043/044) has a history of fatigue cracks, the majority of which are located in the bottom web gap. Field testing was performed on the bridge both before and after the angles-with-plate retrofit was installed at all cross-frame locations. Complementary FE analyses were performed to provide context to the field test results and to obtain an improved overall view of what is occurring in the web gap regions of the bridge and the effect that the angles-with-plate retrofit had on reducing stress demands in those regions. Results for the top web gap region under the east and west lane truck loading scenarios led to the execution of an additional set of FE analyses to develop a better understanding of the top web gap behavior. Based on results from these investigations, it can be concluded that:

1. Readings from the BDI strain transducers and string potentiometer produced the expected global behavior trends of the bridge. Stress and deflection values

corresponded intuitively to the respective east lane, west lane, and bridge center truck loadings and correlated well with FE results.

2. Comparisons between stresses in the top and bottom web gaps for the tests performed before the retrofit was applied showed that stress demands were at least 20% higher in the bottom web gap than in the top web gap. This supports previous research which found that skewed bridges with staggered cross frames are more susceptible to fatigue cracking in the bottom web gap regions than the top. It also explains why more fatigue cracks have been reported in the bottom web gap regions than in the top web gap regions in Kansas Bridge 135-87(043/044).
3. Stress demands decreased after installation of the retrofit in the bottom web gap for each load placement. Since the bottom web gaps are where fatigue cracking has been most critical in Kansas Bridge 135-87(043/044), this indicates that the angles-with-plate retrofit is an effective retrofit for the most problematic areas of the bridge.
4. Stress demands decreased in the top web gap region for the center truck load placement, but increased or stayed nearly the same for the east and west truck load placements for the crack pattern seen in the field tests and FE analyses. Upon further investigation of the top web gap region in an additional suite of FE analyses, retrofit performance was found to improve as the Type A crack was allowed to propagate into its typical horseshoe-shaped pattern around the connection plate-to-web weld. HSS 1 stresses decreased for west and east truck load placements by 26% and 50%, respectively. Upon addition of a separate flange-to-web weld crack, HSS 2 stresses decreased in the top web gap region for west and east truck lane loadings by 14% and 2%, respectively.
5. Analyses of the connection plate-to-web weld crack alone indicated stress patterns that would lead to a flange-to-web weld crack, and vice versa. In FE analyses where both the connection plate-to-web weld and flange-to-web weld cracks were modeled simultaneously, HSS 1 and HSS 2 stresses reduced by 27% and 26%, respectively, for the west truck load placement. For the east truck load placement, HSS 1 and HSS 2 stresses reduced by 53% and 23%, respectively.

Field tests and finite element simulations performed for Kansas Bridge 135-87(043/044) show that the angles-with-plate retrofit is an effective solution for mitigating fatigue cracks in problematic bottom web gap regions of staggered, skewed bridges. In the less demanding top web gap regions of such bridges, the retrofit also shows that it can be used effectively.

The geometry of the cross frame members and their connection directly to the transverse connection plates in Kansas Bridge 135-87(043/044) shows that the angles-with-plate retrofit is a more cost effective and simpler retrofit to install in bridges with similar cross frame construction. Since attachment to the girder flanges is unnecessary, cross frame members do not have to be removed for installation of the angles. The angles can be applied over the cross frame members in both the bottom and top web gap regions. Additionally, if applied in the top web gap region, bridge deck removal is unnecessary, which lowers costs and allows for significantly less traffic interruptions. Thus, in addition to being effective, the angles-with-plate retrofit is a simpler and cost effective technique that can be used to repair distortion-induced fatigue cracking in steel girder bridges.

9. References

Alemdar, F., T. Overman, A. Matamoros, C. Bennett, and S. Rolfe. "Repairing Distortion-Induced Fatigue Cracks in Steel Bridge Girders using Angles-with-Plate Retrofit Technique, Part I: Physical Simulations." *Journal of Structural Engineering* (ASCE), 2013a.

Alemdar, F., T. Overman, A. Matamoros, C. Bennett, and S. Rolfe. "Repairing Distortion-Induced Fatigue Cracks in Steel Bridge Girders using Angles-with-Plate Retrofit Technique, Part II: Computer Simulations." *Journal of Structural Engineering* (ASCE), 2013b.

Connor, R.J. and Fisher, J.W. "Identifying Effective and Ineffective Retrofits for Distortion Induced Fatigue Cracking in Steel Bridges Using Field Instrumentation." *Journal of Bridge Engineering* 11, no. 6 (2006): 745-752.

Fisher, J.W. and Mertz, D.R. "Fatigue and Fracture in Steel Bridges." *The Conference on Bridges*, 1984: 10-21.

Grondin, G.Y., R. Fraser, and M. D'Andrea. "Testing and Evaluation of Fatigue Damaged Girders." *4th Structural Specialty Conference of the Canadian Society for Civil Engineering*, 2002.

Hartman, A. "Analytical and Experimental Investigation for Distortion-Induced Fatigue in Steel Bridges." PhD Thesis, University of Kansas, 2013.

Hartman, A., H. Hassel, C. Adams, C. Bennett, A. Matamoros, and S. and Rolfe. "Effects of Cross-Frame Placement and Skew on Distortion-Induced Fatigue in Steel Bridges." *TRB: Journal of Transporation Research Board* 2200, no. 1 (2010): 62-68.

Hassel, H., C. Bennett, A. Matamoros, and S. and Rolfe. "Parametric Analysis of Cross-Frame Layout on Distortion-Induced fatigue in Skewed Steel Bridges." *Journal of Bridge Engineering* (ASCE) 18, no. 7 (2013): 601-611.

Jones, J., C. Bennett, A. Matamoros, S. Rolfe, and K. and Roddis. "Fighting Fatigue in Steel Bridges." *TR News, Transportation Research Board (TRB)*, no. 259 (Nov/Dec 2008).

Liu, H. "A Finite-Element-Based Approach to Modeling Cracking & Repairs for Disotortion-Induced Fatigue in Steel Bridges." PhD Thesis, University of Kansas, 2015.

Richardson, T. "Analytical Investigation of Repair Methods for Fatigue Cracks in Steel Bridges." MS Thesis, University of Kansas, 2012.

Roddis, W.M.K, and Y. Zhao. "Out-of-Plane Fatigue Cracking in Welded Steel Bridges." *Welding Innovation* 27, no. 2 (2001): 2-7.

Zhao, Y., and W.M.K. Roddis. "Fatigue Behavior and Retrofit Investigation of Distortion-Induced Web Gap Cracking." *Journal of Bridge Engineering* 12, no. 6 (2007): 737-745.

Appendix A: Calibration Constants

Strain Transducers from Bridge Diagnostics Inc. (BDI)

Calibrations are provided by Bridge Diagnostics Inc. but must be modified based on supplied voltage. A supply voltage of 5 V was applied to each strain transducer.

$$\text{Calibration Constant} = \frac{\text{General Factor } \mu\varepsilon/mV/\text{V} \cdot 1000\ mV/V}{\text{Input Voltage } V}$$

These modified constants for the strain transducers can be found in Table A. 1.

Table A. 1: Calibration Constants for Strain Transducers

Strain Transducer Label	General Factor	Calibration Constant (5V)
BDI 1269	503.9 με/mV/V	100,780 με/V
BDI 1270	497.0 με/mV/V	99,400 με/V
BDI 1271	503.5 με/mV/V	100,700 με/V
BDI 1272	496.7 με/mV/V	99,340 με/V
BDI 1273	493.6 με/mV/V	98,720 με/V
BDI 1274	502.4 με/mV/V	100,480 με/V

Appendix B: Kansas Bridge 135-087 (043/044) Plans

Original Plans

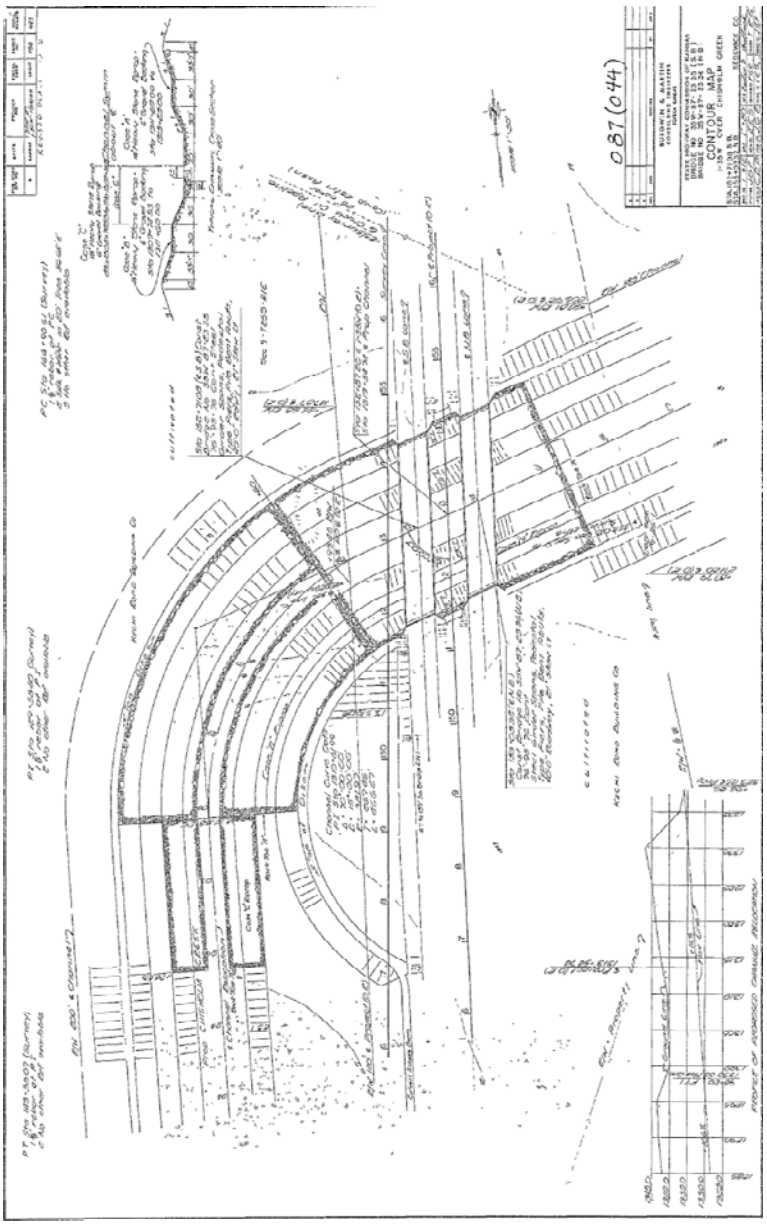

Figure B. 1: Contour map.

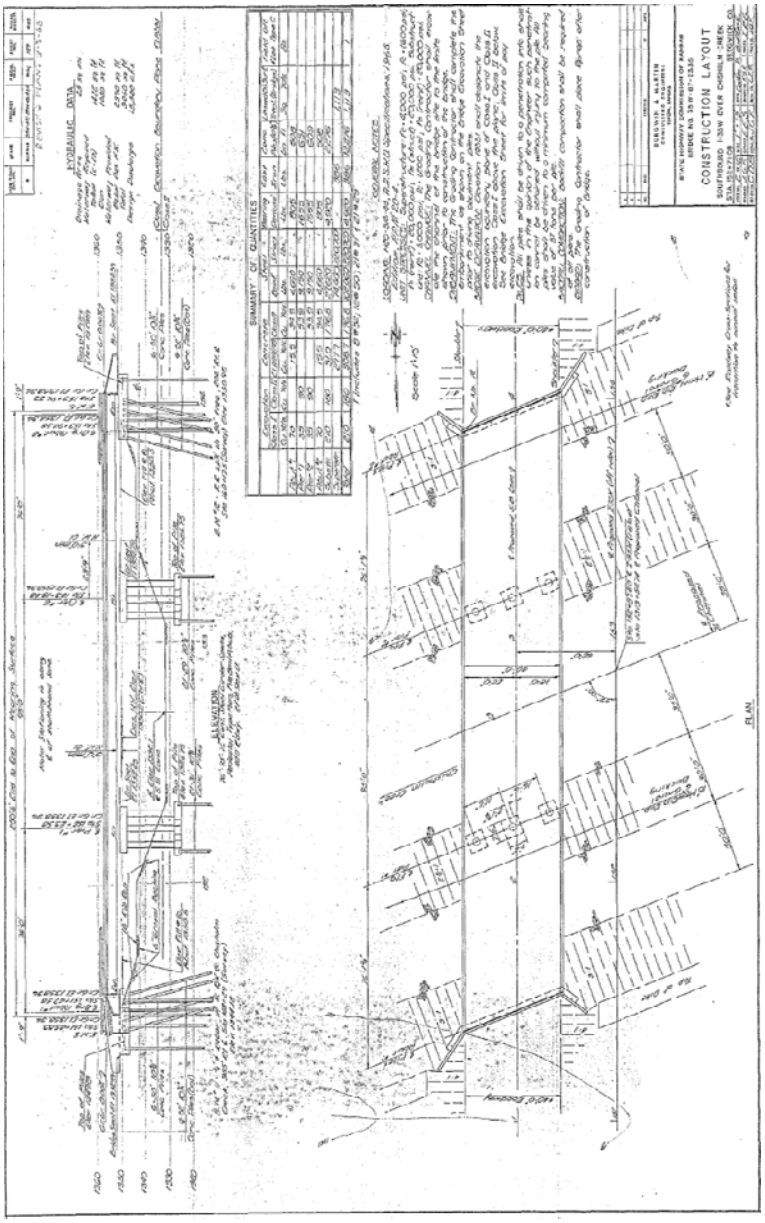

Figure B. 2: Construction layout of southbound bridge.

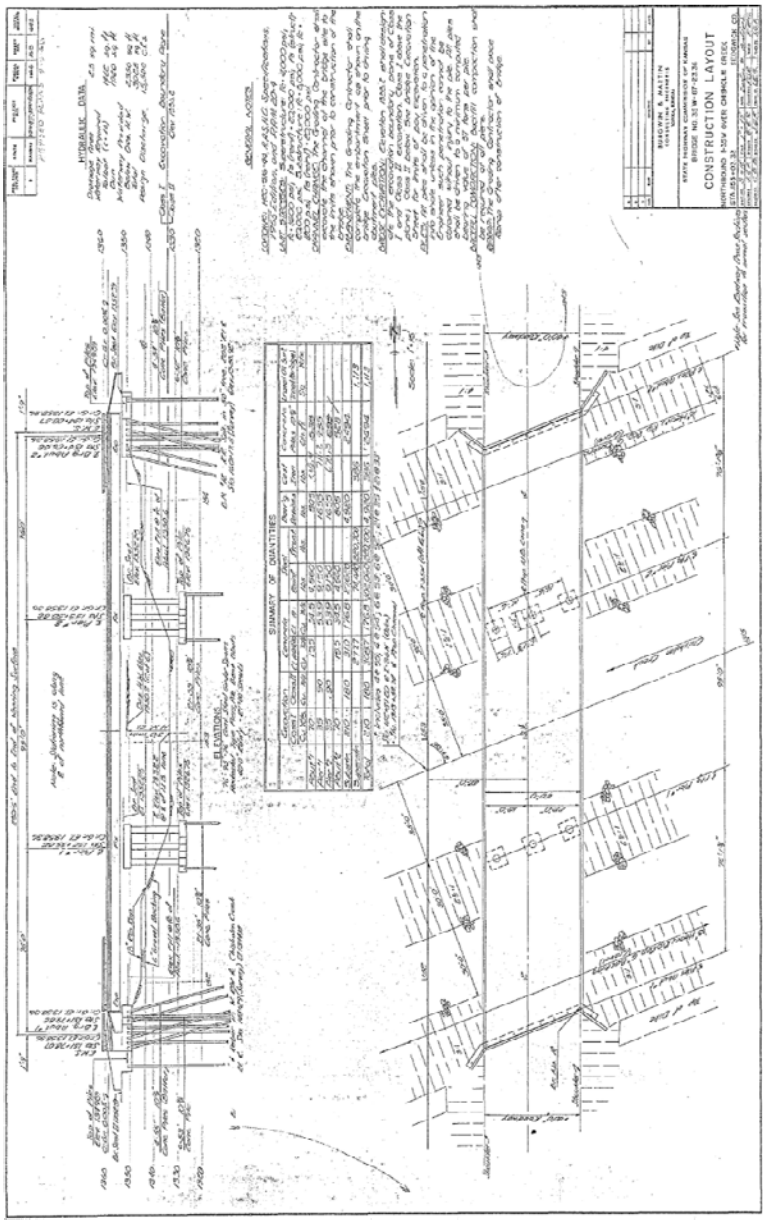

Figure B. 3: Construction layout of northbound bridge.

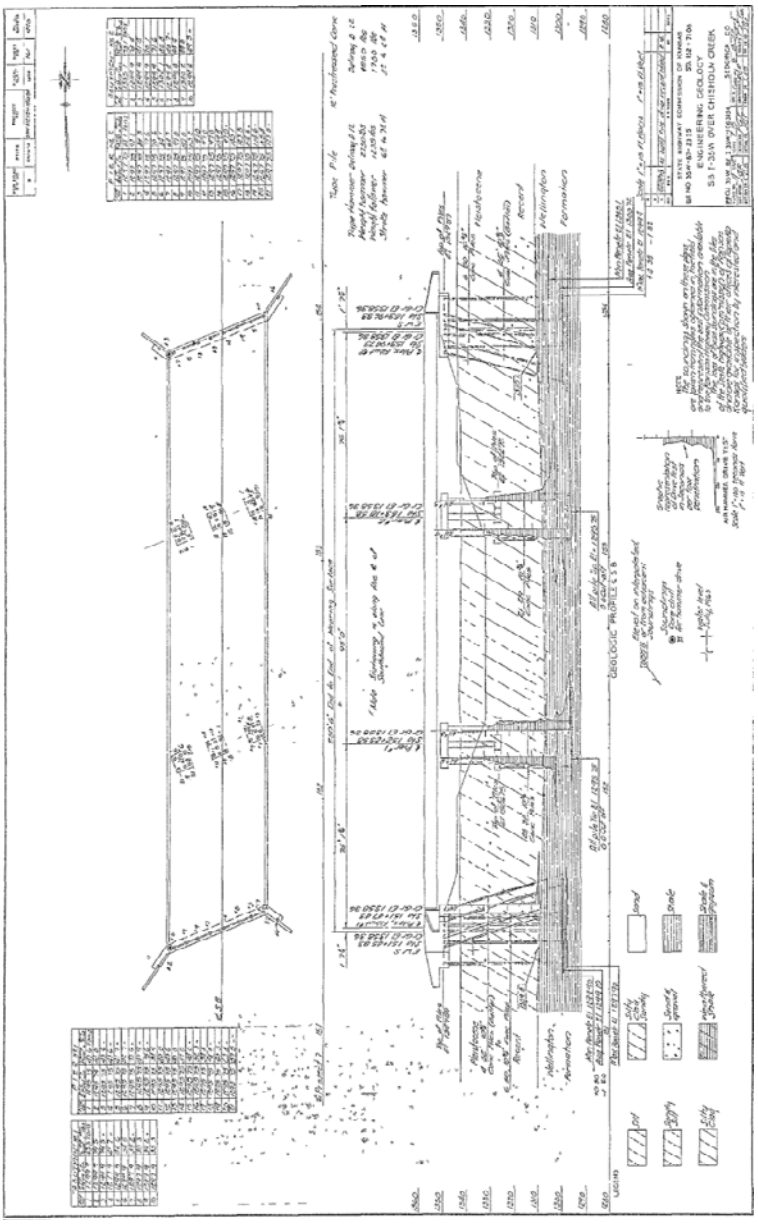

Figure B. 4: Engineering geology.

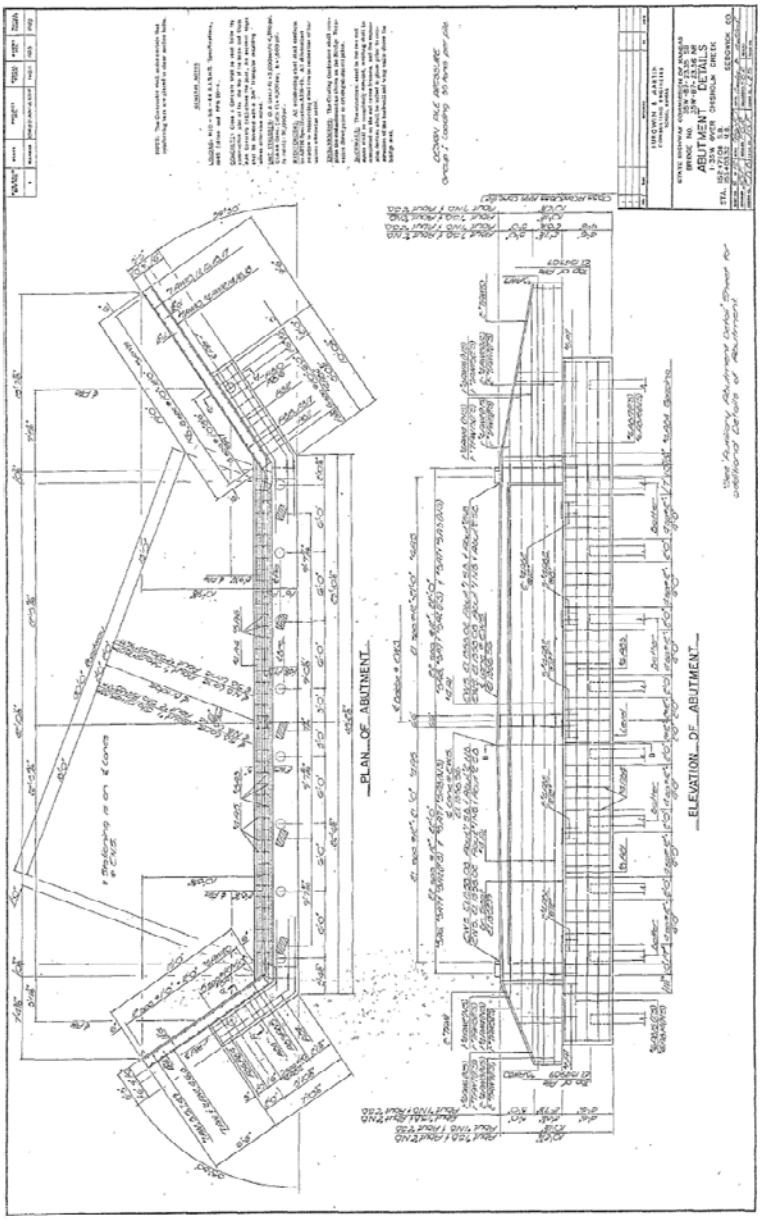

Figure B. 5: Abutment details.

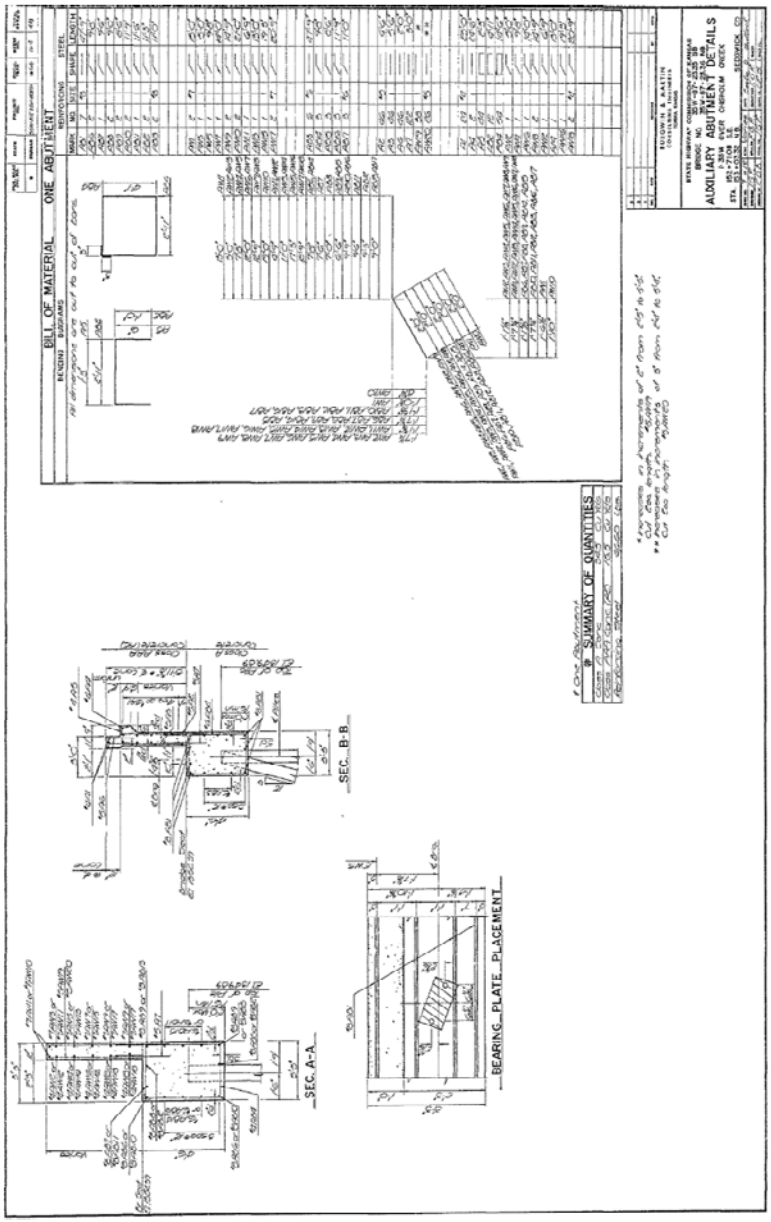

Figure B. 6: Auxiliary abutment details.

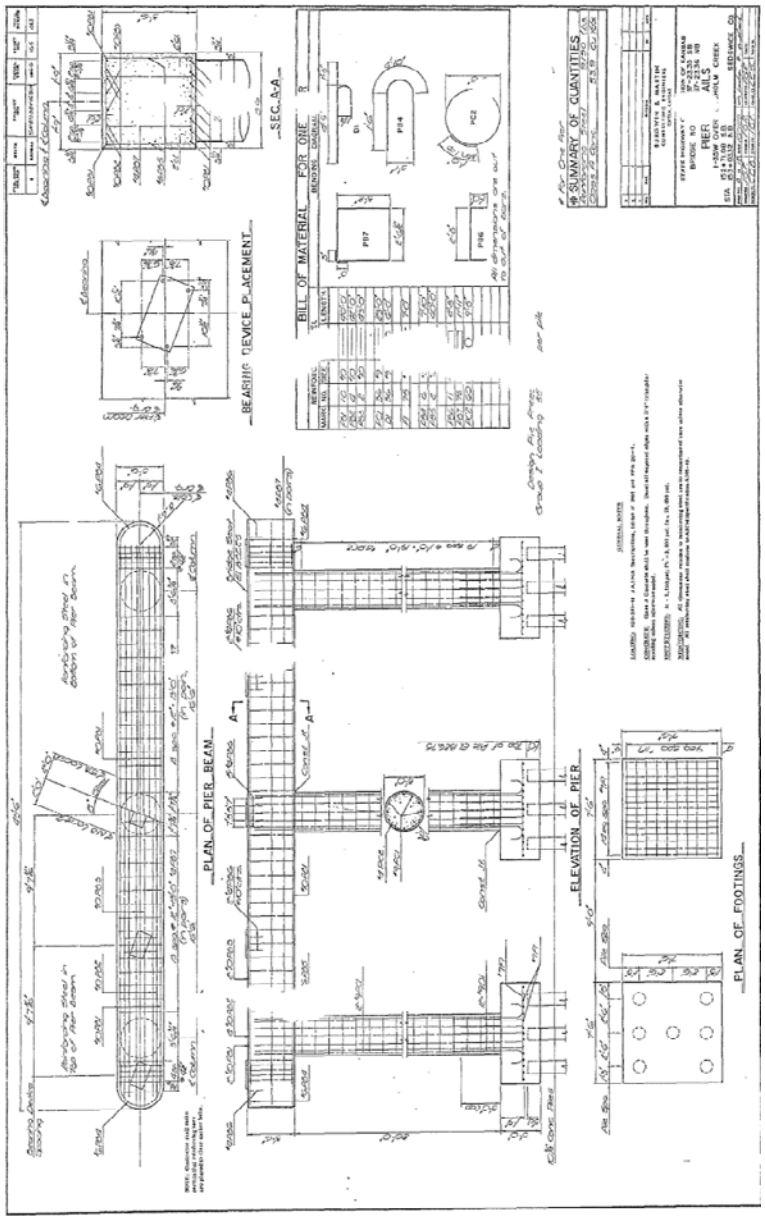

Figure B. 7: Pier details.

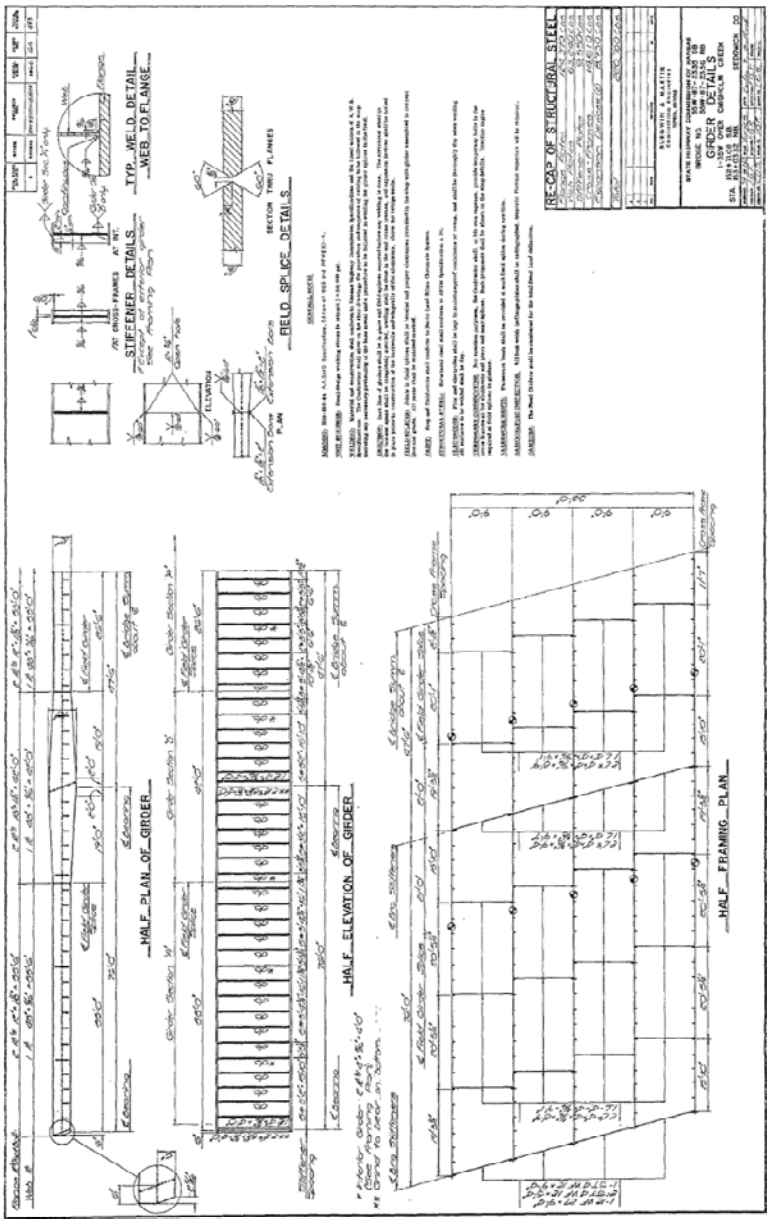

Figure B. 8: Girder details.

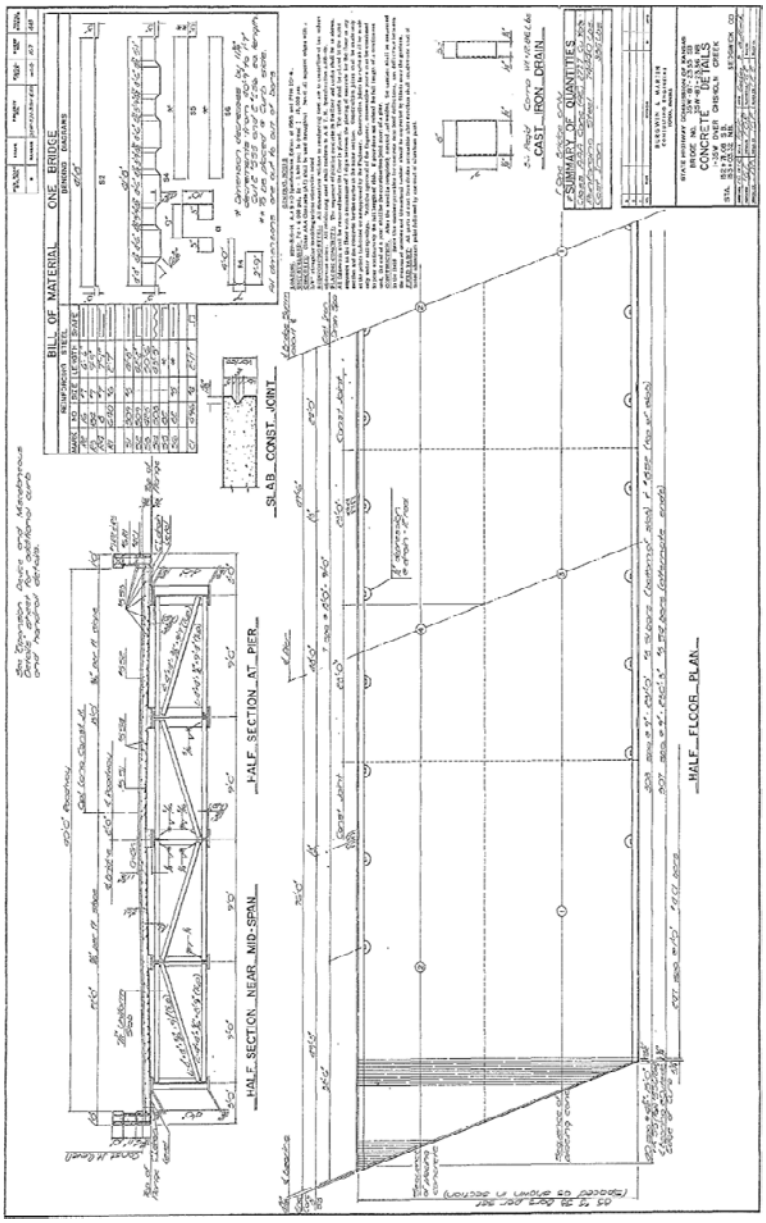

Figure B. 9: Concrete details.

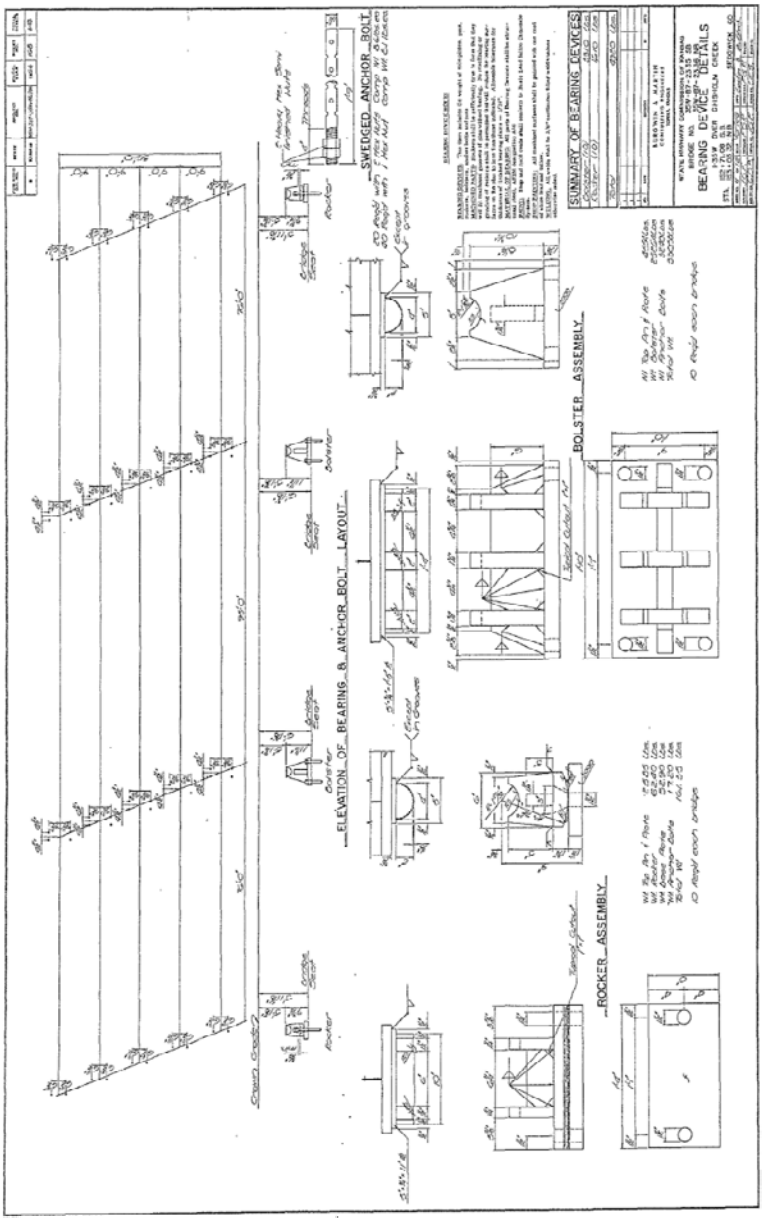

Figure B. 10: Bearing device details.

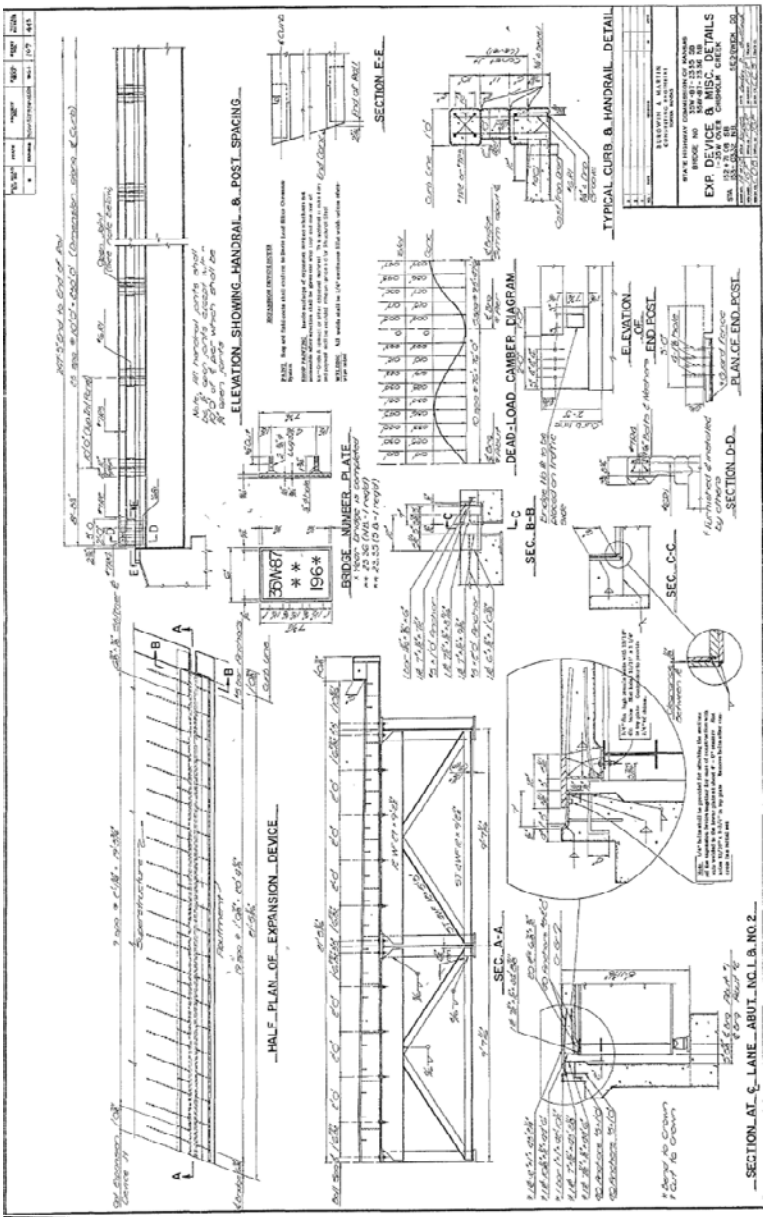

Figure B. 11: Expansion device and miscellaneous details.

Repair Plans

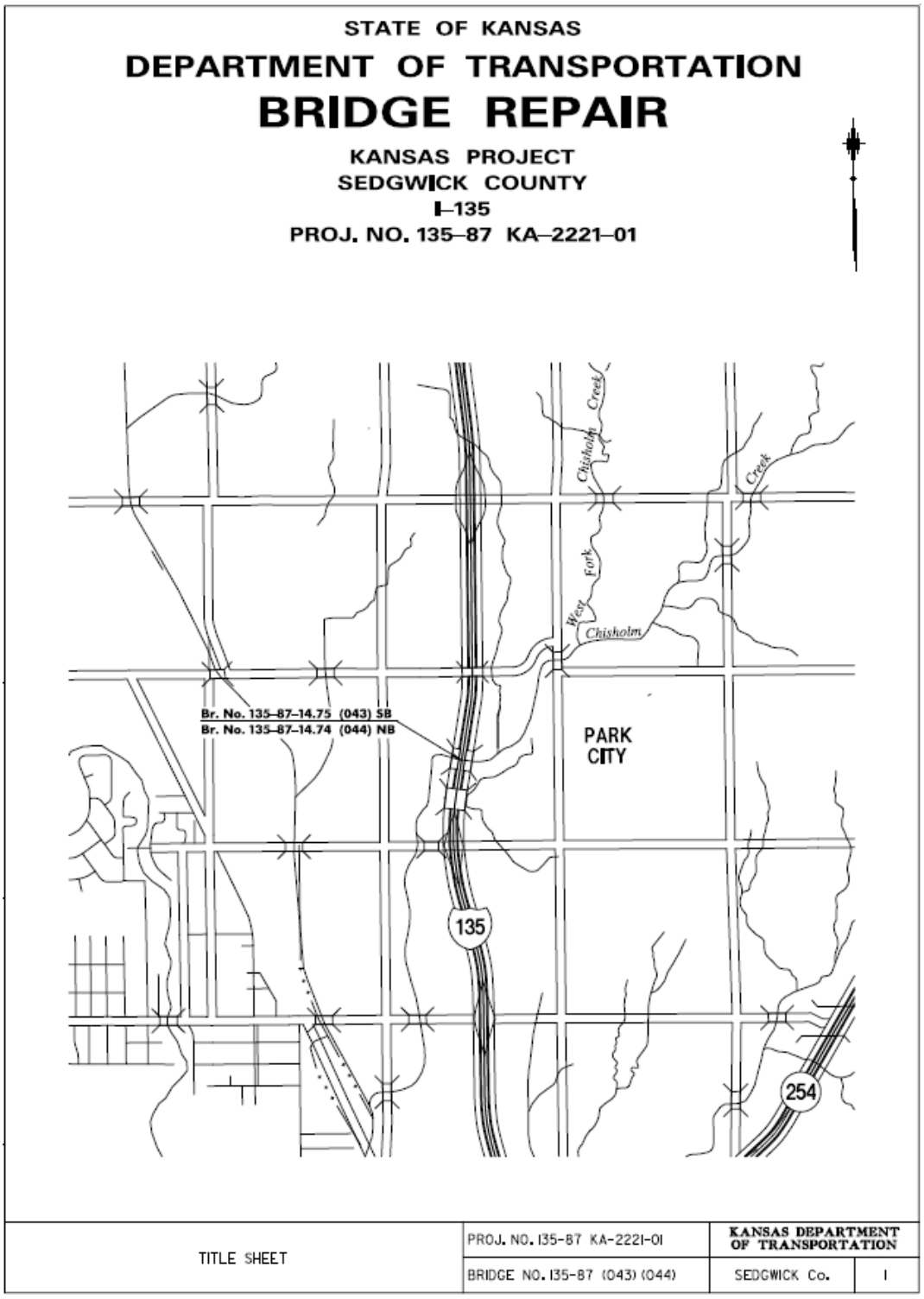

Figure B. 12: Title sheet.

SUMMARY OF STRUCTURAL STEEL QUANTITIES (For Information only)						
Bridge Number	Connection Angle 8" x 6" x 3/4" x 3 1/2" (Each)	* Plate 1" x 7 1/4" x 10 1/2" (Each)	* Plate 3/4" x 3 1/4" x 7 1/4" (Each)	Backing Plate 1" x 7 1/4" x 1'-10" (Each)	Fill Plate 5/16" x 3 1/2" x 7 1/4" (Each)	Fill Plate 5/16" x 3 1/2" x 3 1/2" (Each)
(043)	160	60	60	50	60	80
(044)	320	120	120	100	120	160
Total	480	180	180	150	180	240

* To be used in "Fabricated Backing Plate Angle".

POUNDS OF STRUCTURAL STEEL:
Single Web Stiffener Locations
Br. No. (043)....3,300 lbs.
Br. No. (044)....6,600 lbs.
Double Web Stiffener Locations
Br. No. (043)....2,354 lbs.
Br. No. (044)....4,708 lbs.
TOTAL:
Br. No. (043)....5,654 lbs
Br. No. (044)...11,308 lbs.
TOTAL.....16,962 lbs.

3/4"ø A325 Bolts:
3 1/2" - 960 Total
3 3/4" - 330 Total

INDEX TO DRAWINGS	
Sheet No.	Drawing
1	Title Sheet
2-3	General Notes and Quantities
4	Construction Layout
5	Framing Plan
6	Existing Girder Details at Cross Frames
7-8	Proposed Girder Web Repair Details at Cross Frames (Single Web Stiffener Locations)
9-10	Proposed Girder Web Repair Details at Cross Frames (Double Web Stiffener Locations)
11	Structural Steel Details

SUMMARY OF QUANTITIES		
ITEM	UNITS	QUANTITY
Bridge Repair	Lump Sum	Lump Sum
Flagger (Set)	Hour	1
Mobilization	Lump Sum	Lump Sum

ID #1: 150 Single Web Stiffener Locations
ID #2: 90 Double Web Stiffener Locations

Note: On Bridge (043), repair connections at the bottom flanges only.
On Bridge (044), repair connections at both the bottom and top flanges.

GENERAL NOTES AND QUANTITIES	PROJ. NO. 135-87 KA-2221-01	KANSAS DEPARTMENT OF TRANSPORTATION	
	BRIDGE NO. 135-87 (043) (044)	SEDGWICK Co.	2

Figure B. 13: General notes and quantities.

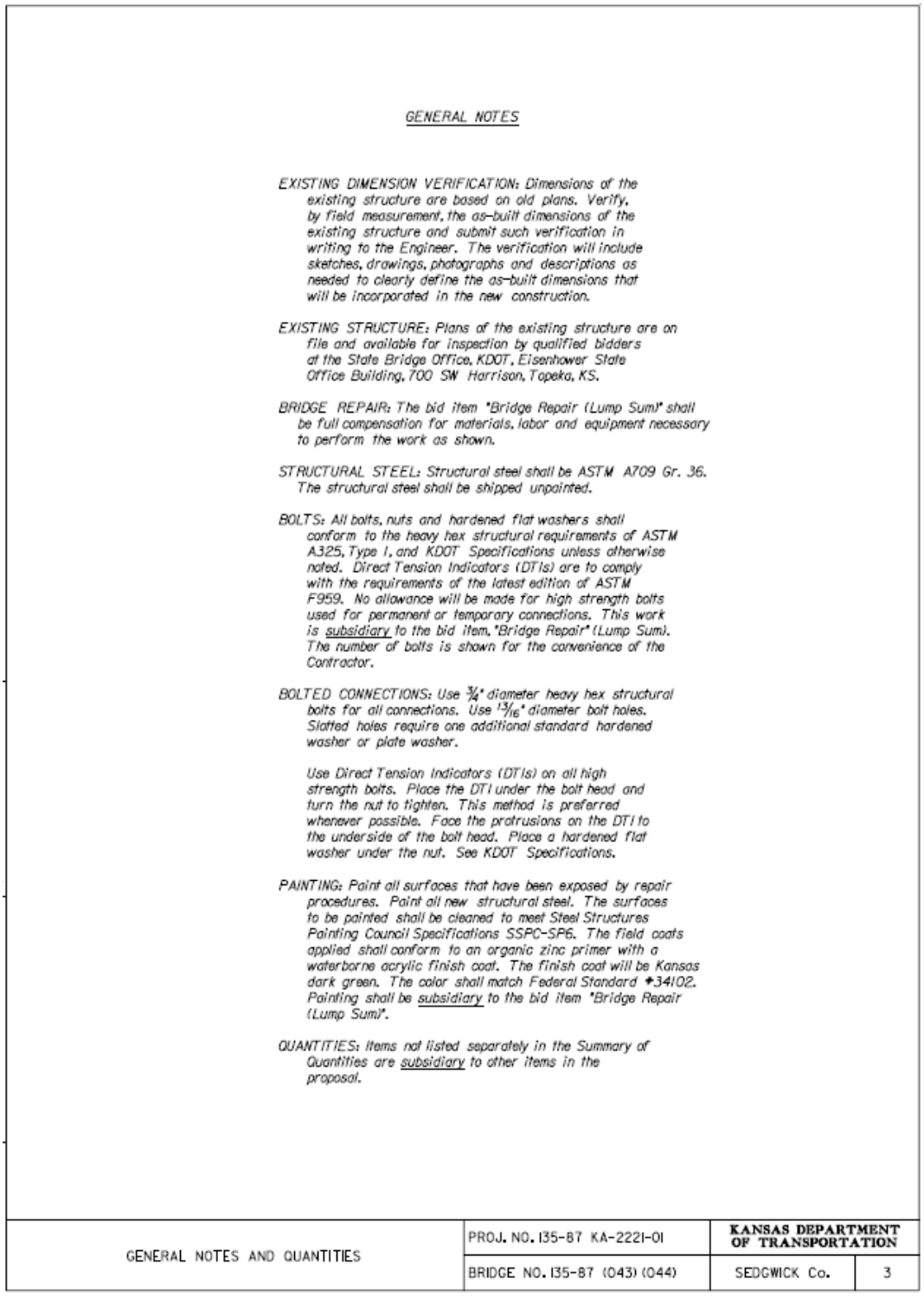

GENERAL NOTES

EXISTING DIMENSION VERIFICATION: Dimensions of the existing structure are based on old plans. Verify, by field measurement, the as-built dimensions of the existing structure and submit such verification in writing to the Engineer. The verification will include sketches, drawings, photographs and descriptions as needed to clearly define the as-built dimensions that will be incorporated in the new construction.

EXISTING STRUCTURE: Plans of the existing structure are on file and available for inspection by qualified bidders at the State Bridge Office, KDOT, Eisenhower State Office Building, 700 SW Harrison, Topeka, KS.

BRIDGE REPAIR: The bid item "Bridge Repair (Lump Sum)" shall be full compensation for materials, labor and equipment necessary to perform the work as shown.

STRUCTURAL STEEL: Structural steel shall be ASTM A709 Gr. 36. The structural steel shall be shipped unpainted.

BOLTS: All bolts, nuts and hardened flat washers shall conform to the heavy hex structural requirements of ASTM A325, Type 1, and KDOT Specifications unless otherwise noted. Direct Tension Indicators (DTIs) are to comply with the requirements of the latest edition of ASTM F959. No allowance will be made for high strength bolts used for permanent or temporary connections. This work is subsidiary to the bid item, "Bridge Repair" (Lump Sum). The number of bolts is shown for the convenience of the Contractor.

BOLTED CONNECTIONS: Use ¾" diameter heavy hex structural bolts for all connections. Use 13/16" diameter bolt holes. Slotted holes require one additional standard hardened washer or plate washer.

Use Direct Tension Indicators (DTIs) on all high strength bolts. Place the DTI under the bolt head and turn the nut to tighten. This method is preferred whenever possible. Face the protrusions on the DTI to the underside of the bolt head. Place a hardened flat washer under the nut. See KDOT Specifications.

PAINTING: Paint all surfaces that have been exposed by repair procedures. Paint all new structural steel. The surfaces to be painted shall be cleaned to meet Steel Structures Painting Council Specifications SSPC-SP6. The field coats applied shall conform to an organic zinc primer with a waterborne acrylic finish coat. The finish coat will be Kansas dark green. The color shall match Federal Standard #34102. Painting shall be subsidiary to the bid item "Bridge Repair (Lump Sum)".

QUANTITIES: Items not listed separately in the Summary of Quantities are subsidiary to other items in the proposal.

GENERAL NOTES AND QUANTITIES	PROJ. NO. 135-87 KA-2221-01	KANSAS DEPARTMENT OF TRANSPORTATION	
	BRIDGE NO. 135-87 (043) (044)	SEDGWICK Co.	3

Figure B. 14: General notes and quantities.

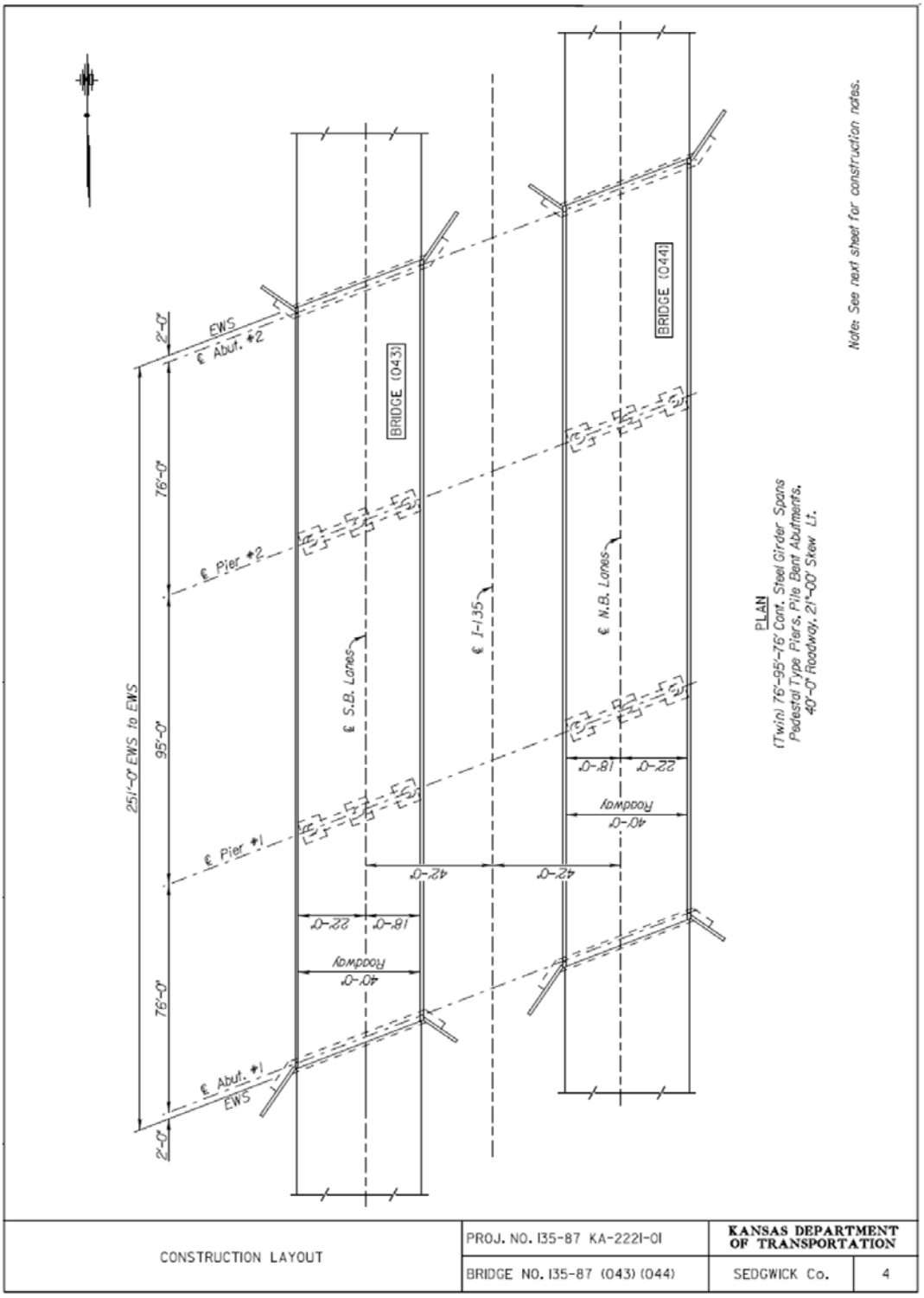

Figure B. 15: Construction layout.

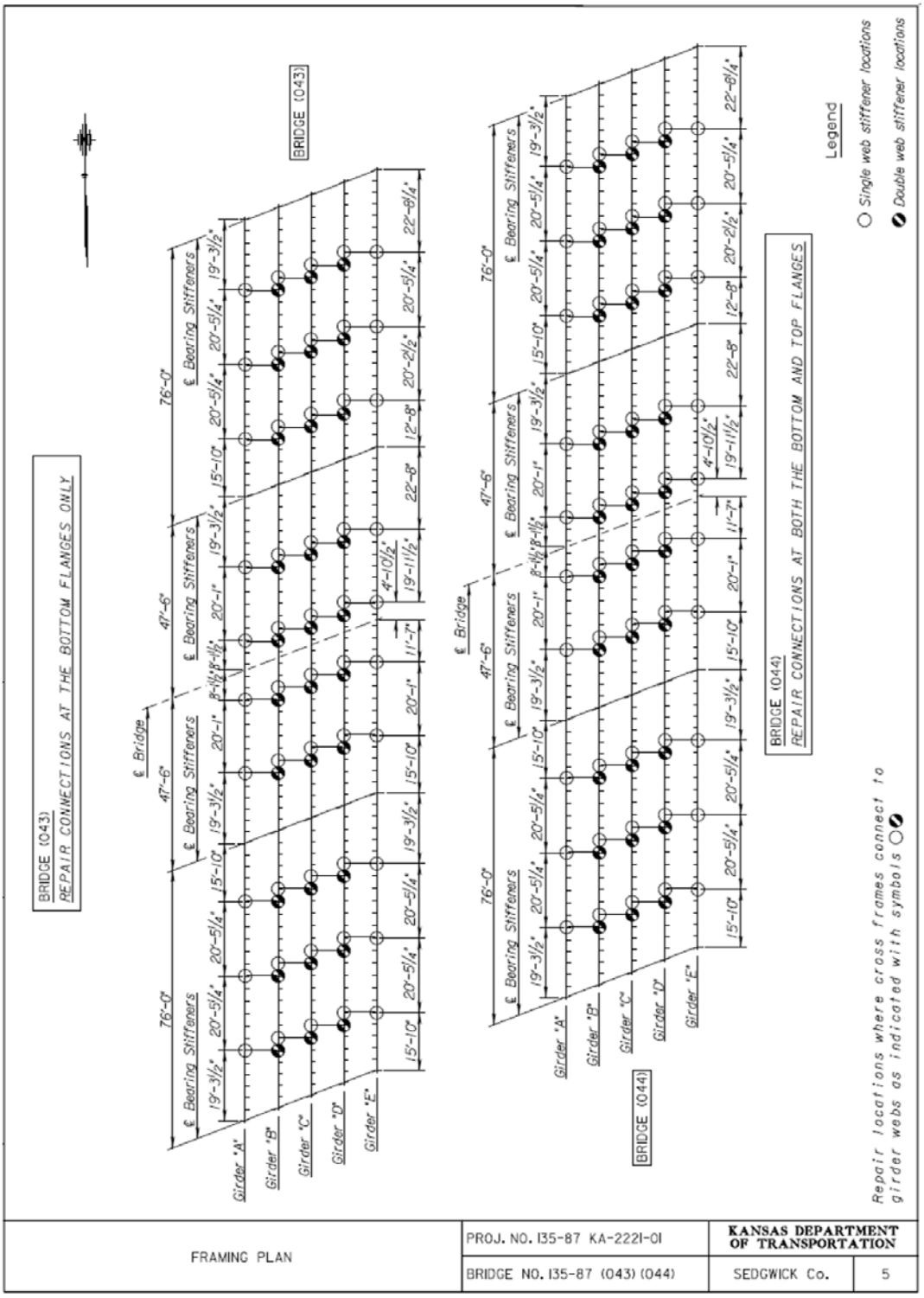

Figure B. 16: Framing plan.

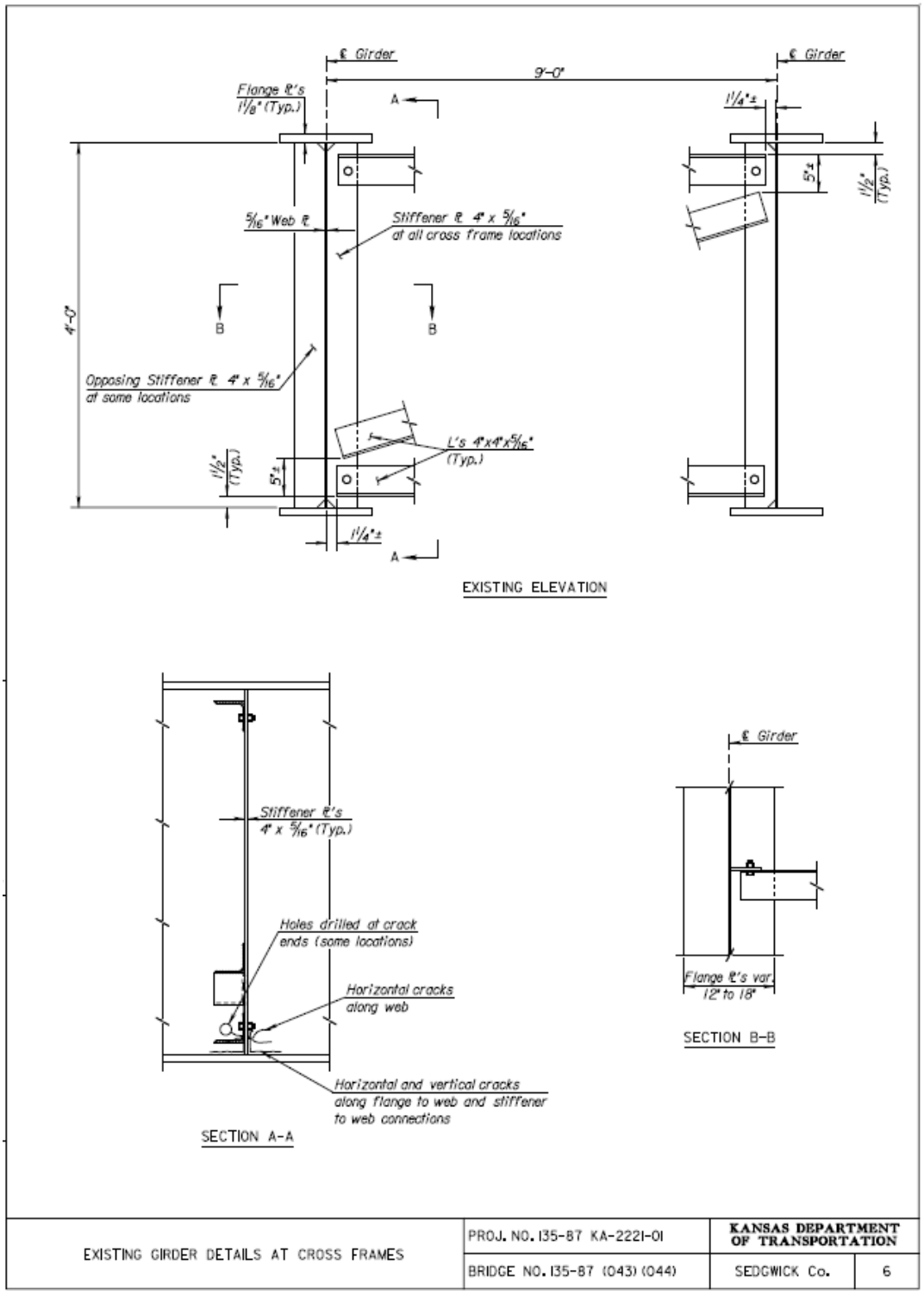

Figure B. 17: Existing girder details at cross frames.

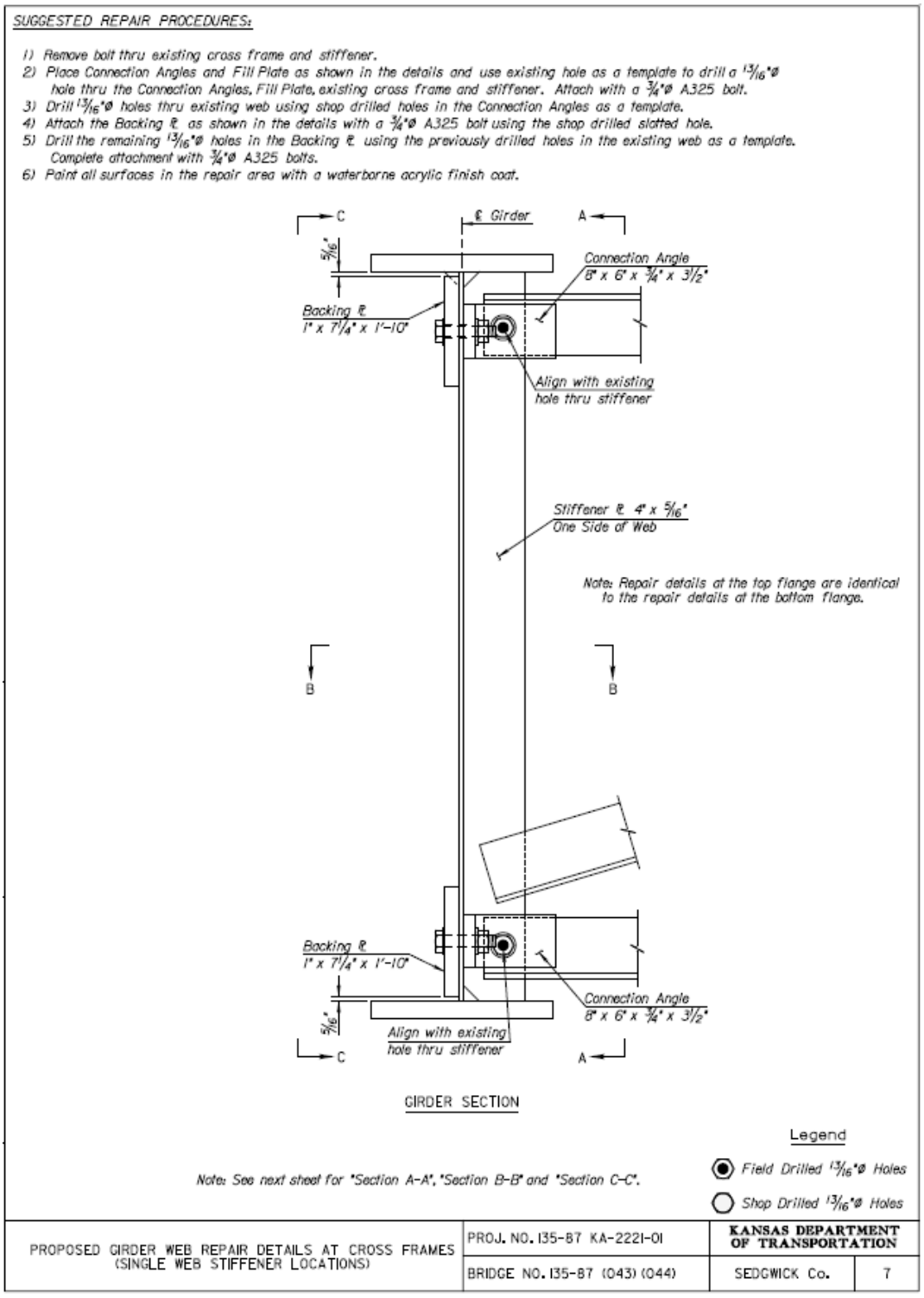

Figure B. 18: Proposed girder web repair details at cross frames (single web stiffener locations).

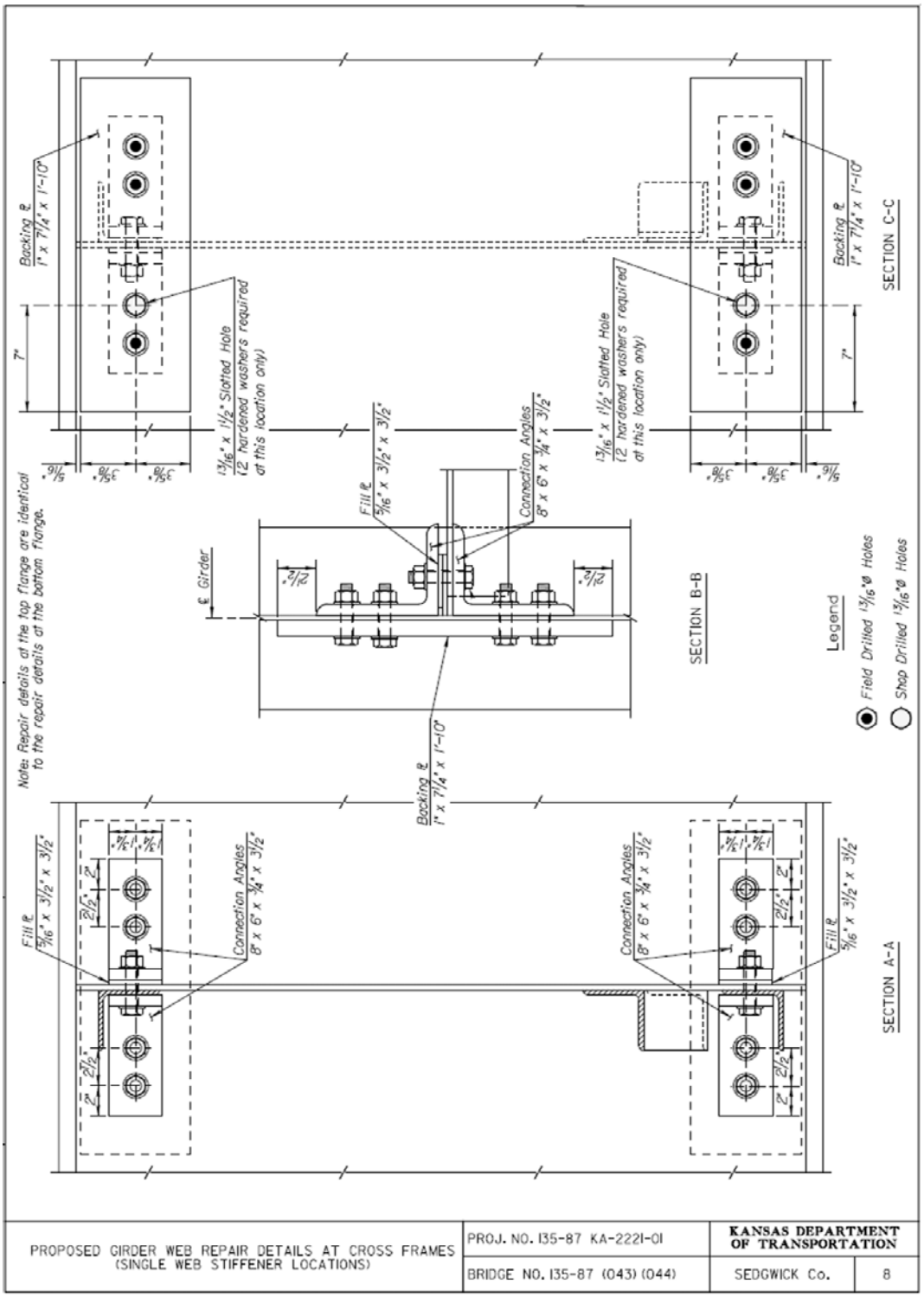

Figure B. 19: Proposed girder web repair details at cross frames (single web stiffener locations).

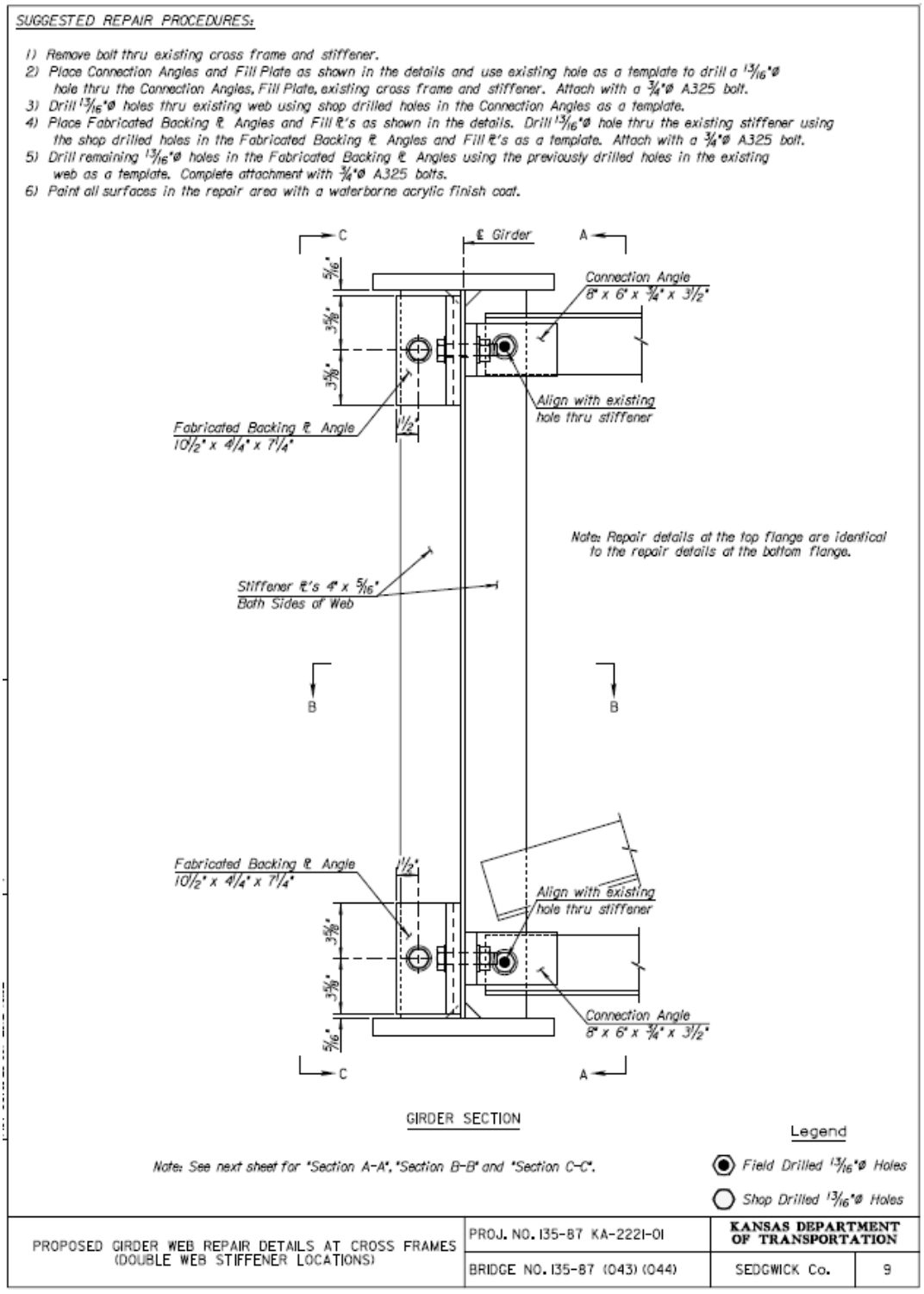

Figure B. 20: Proposed girder web repair details at cross frames (double web stiffener locations).

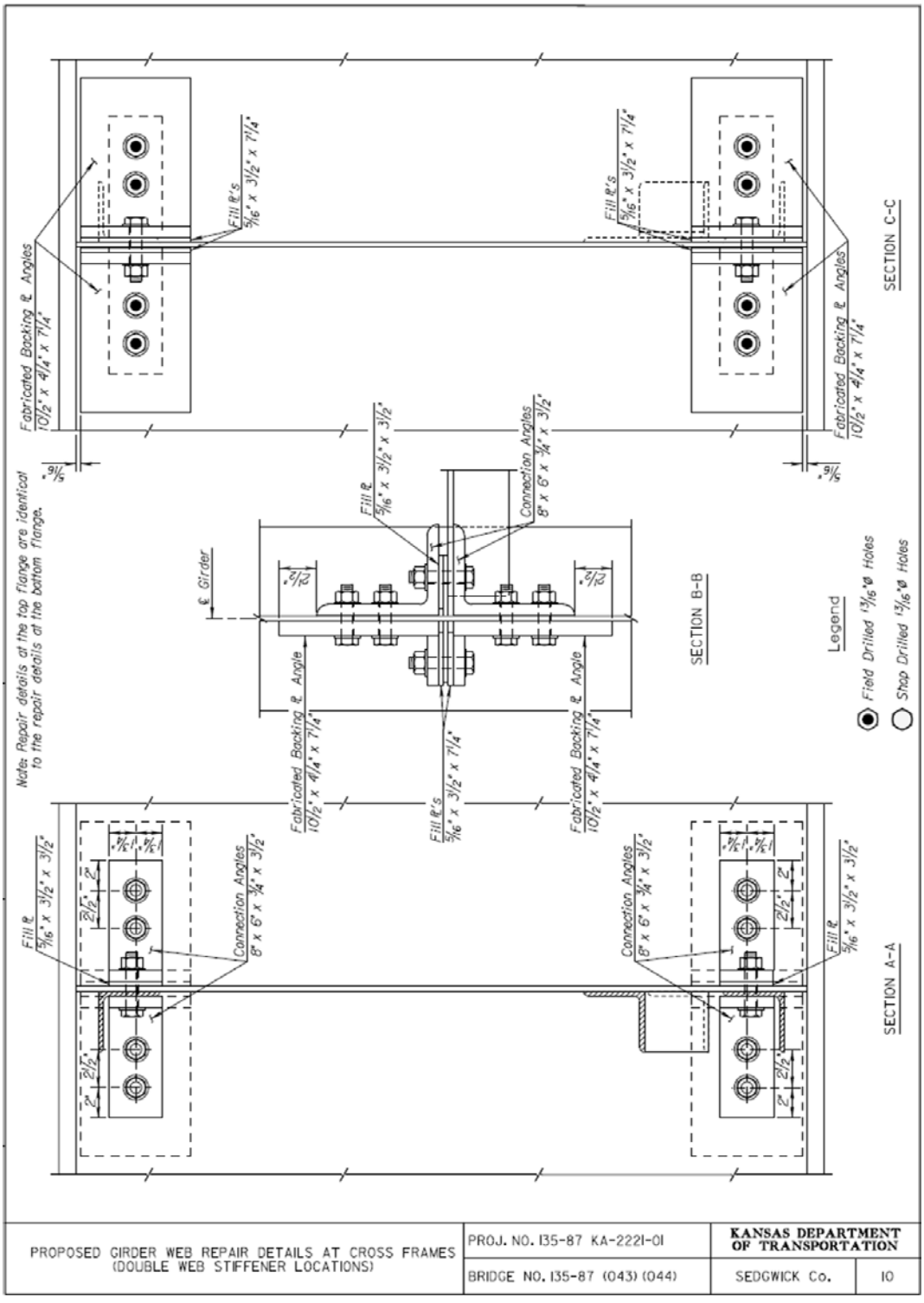

Figure B. 21: Proposed girder web repair details at cross frames (double web stiffener locations).

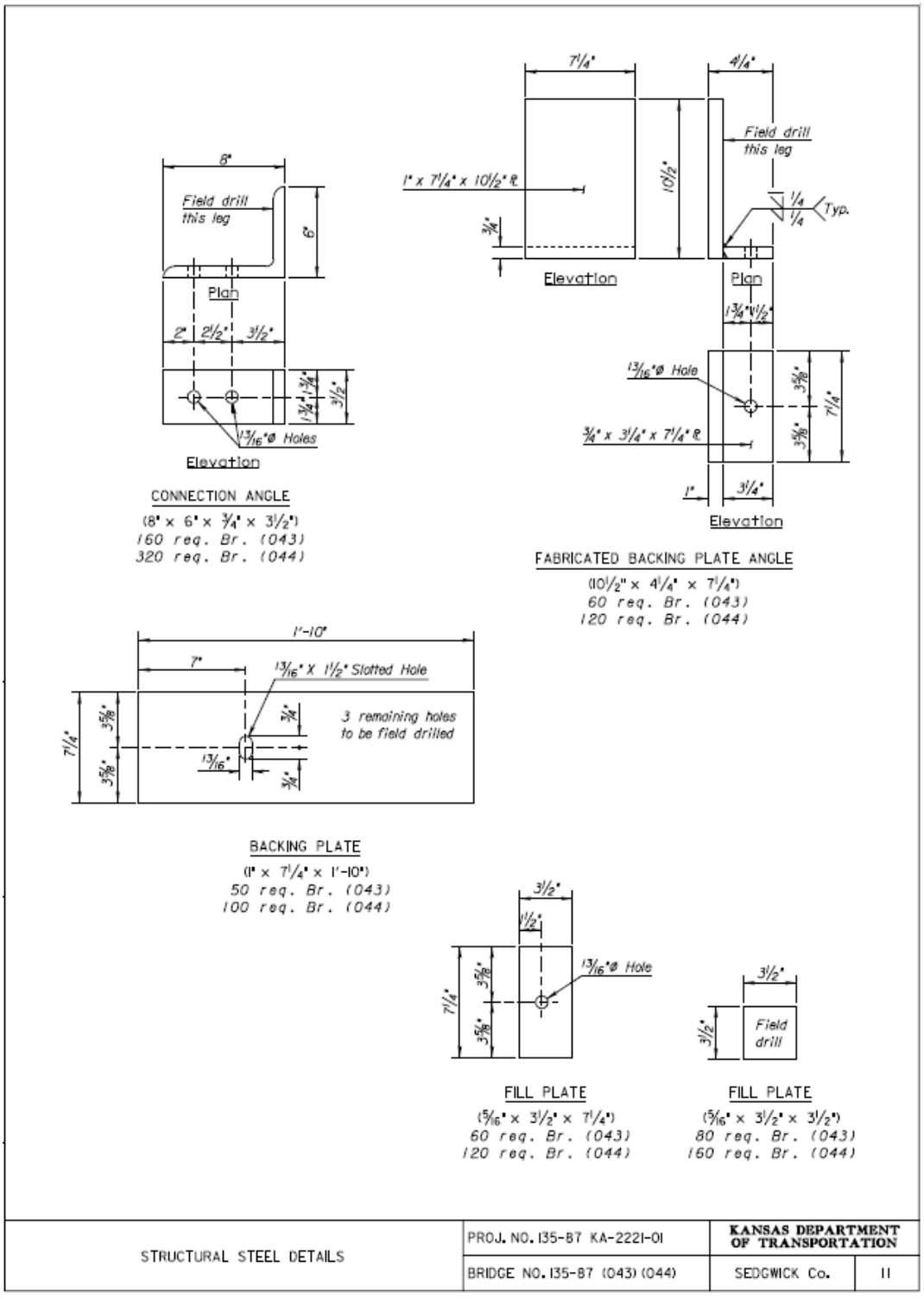

Figure B. 22: Structural steel details.

Appendix C: Filtered Field Test Data

Before Retrofit

Figure C. 1: West Truck Load Placement 8-16 kph (5-10 mph).

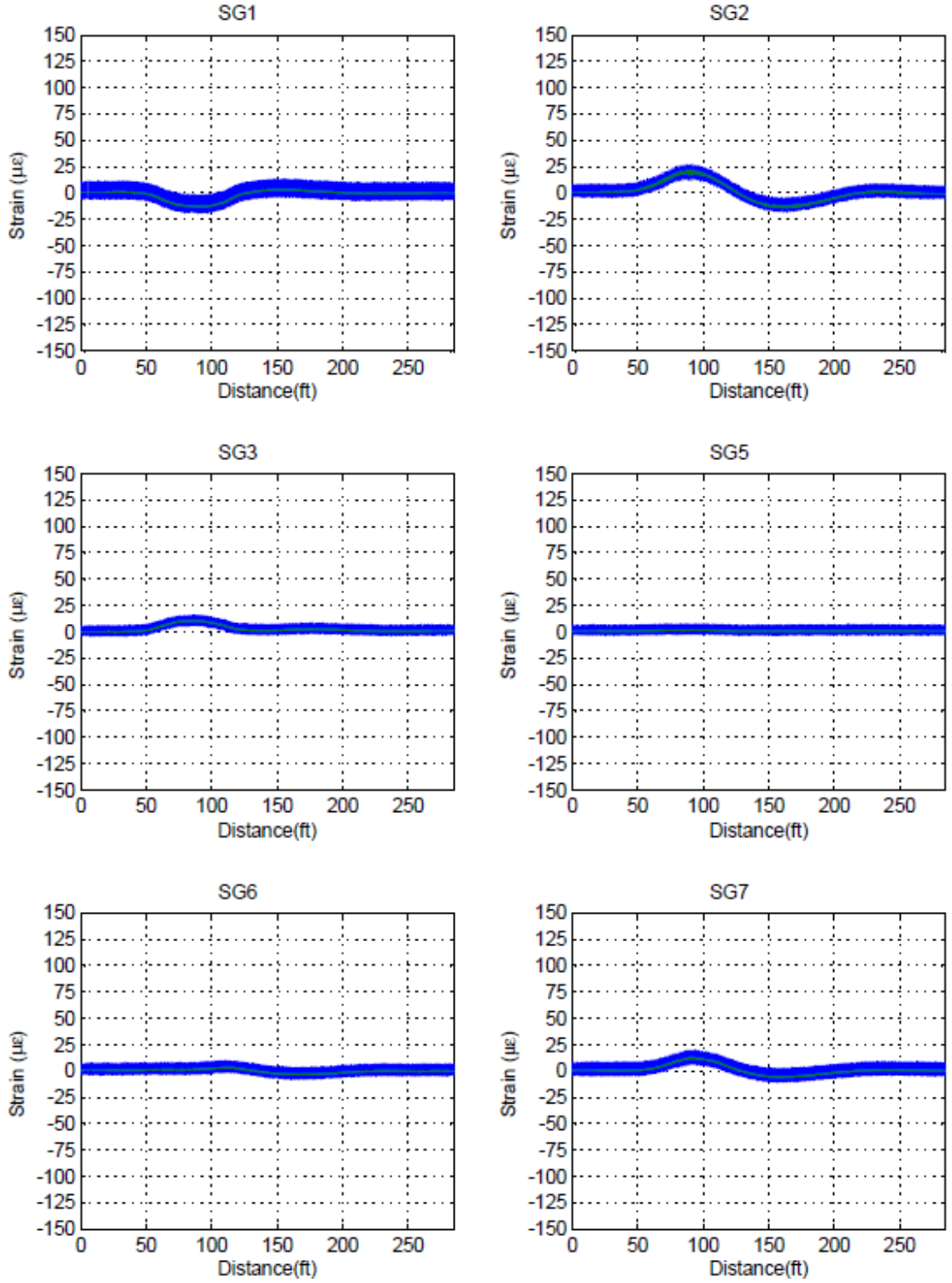

Figure C. 2: West Truck Load Placement 8-16 kph (5-10 mph).

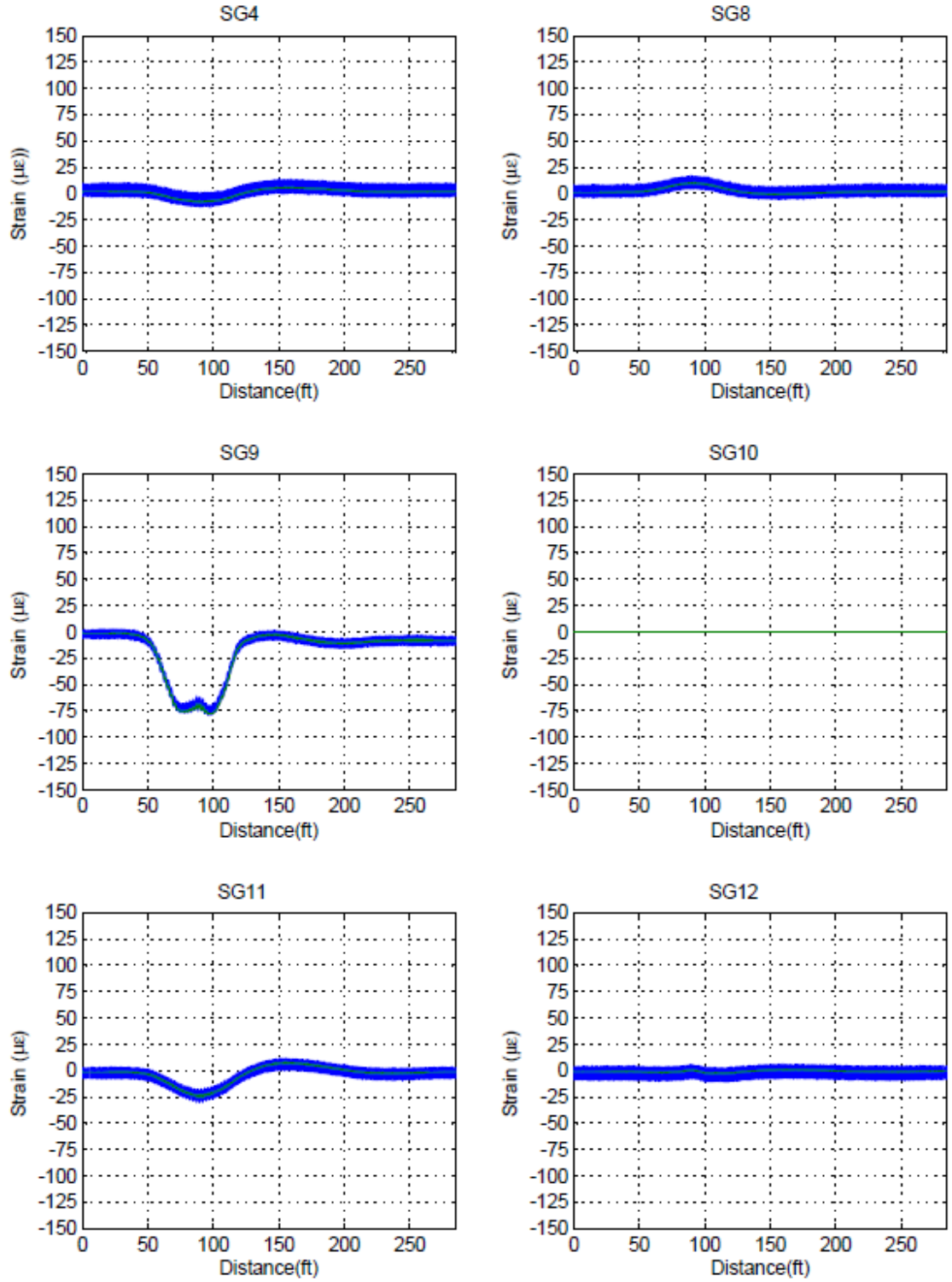

Figure C. 3: West Truck Load Placement 8-16 kph (5-10 mph).

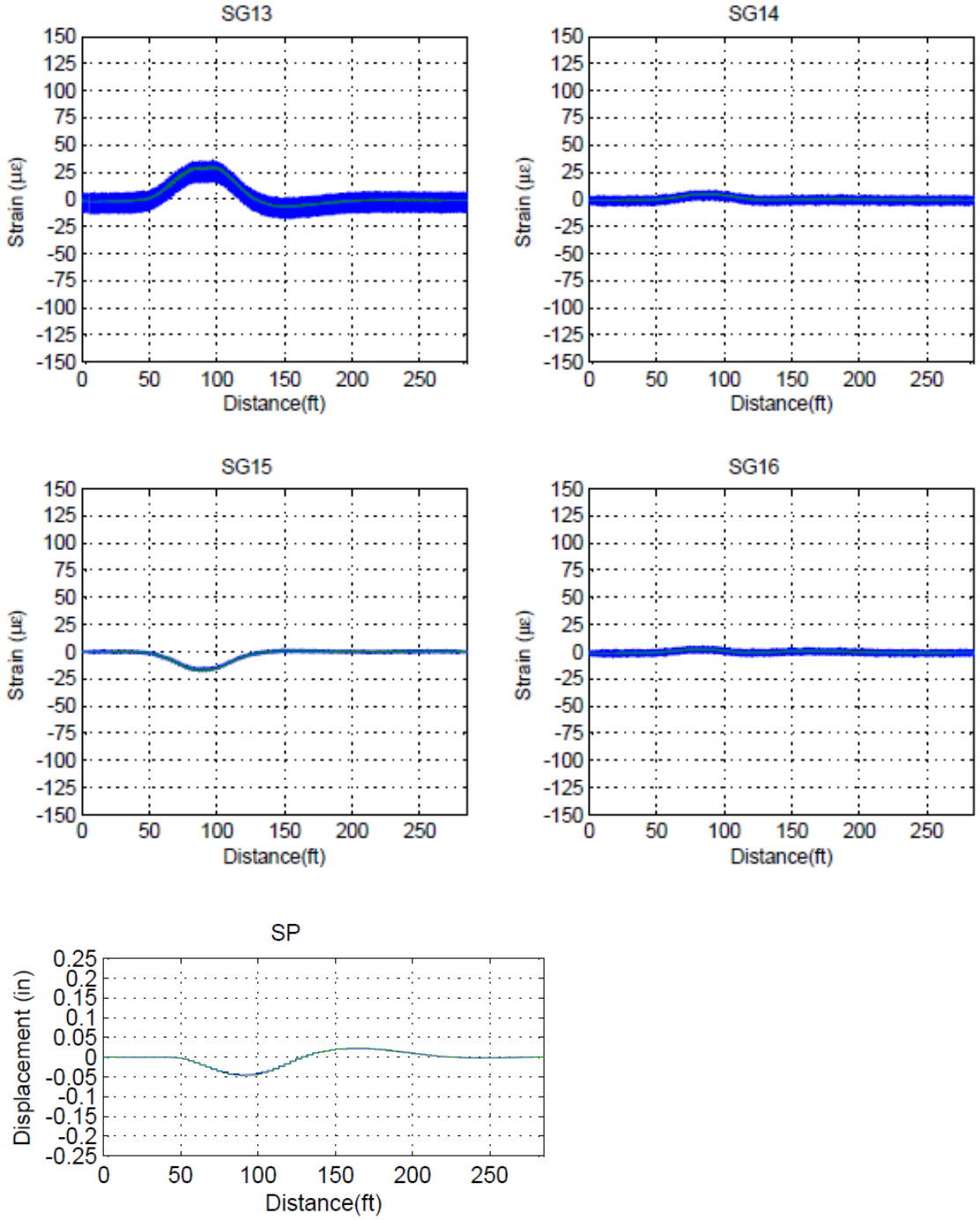

Figure C. 4: West Truck Load Placement 105-121 kph (65-75 mph).

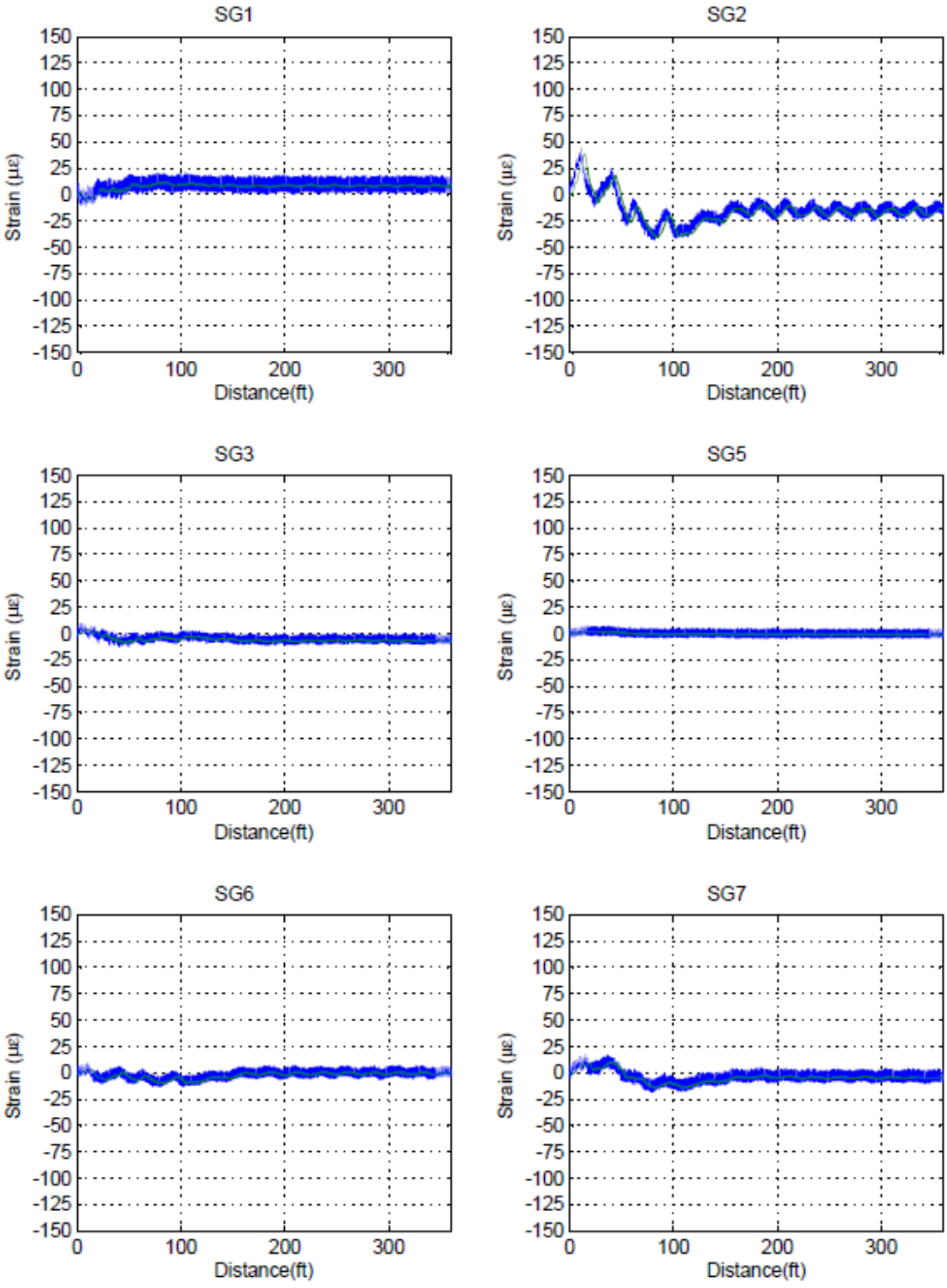

Figure C. 5: West Truck Load Placement 105-121 kph (65-75 mph).

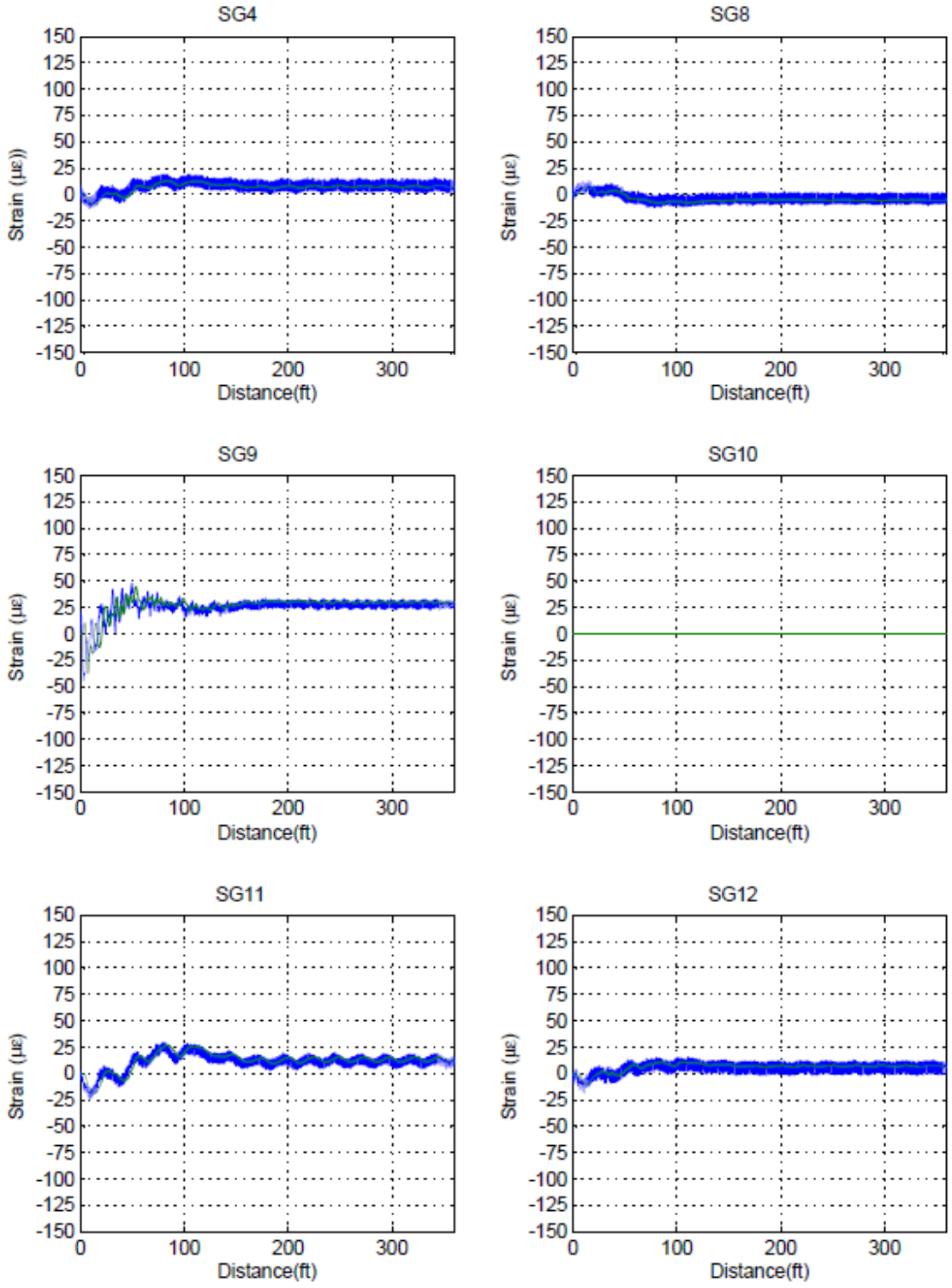

Figure C. 6: West Truck Load Placement 105-121 kph (65-75 mph).

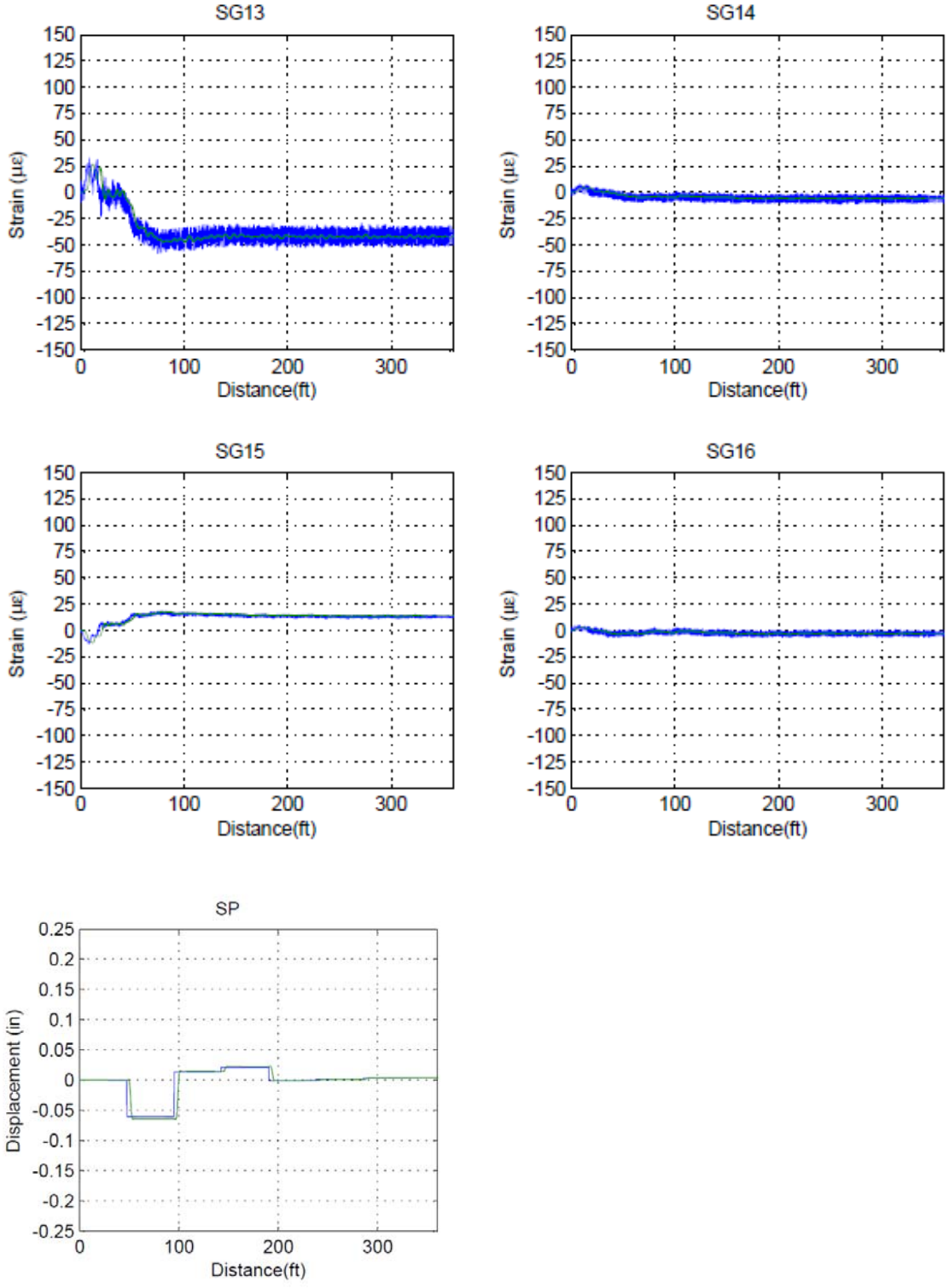

Figure C. 7: Center Truck Load Placement 8-16 kph (5-10 mph).

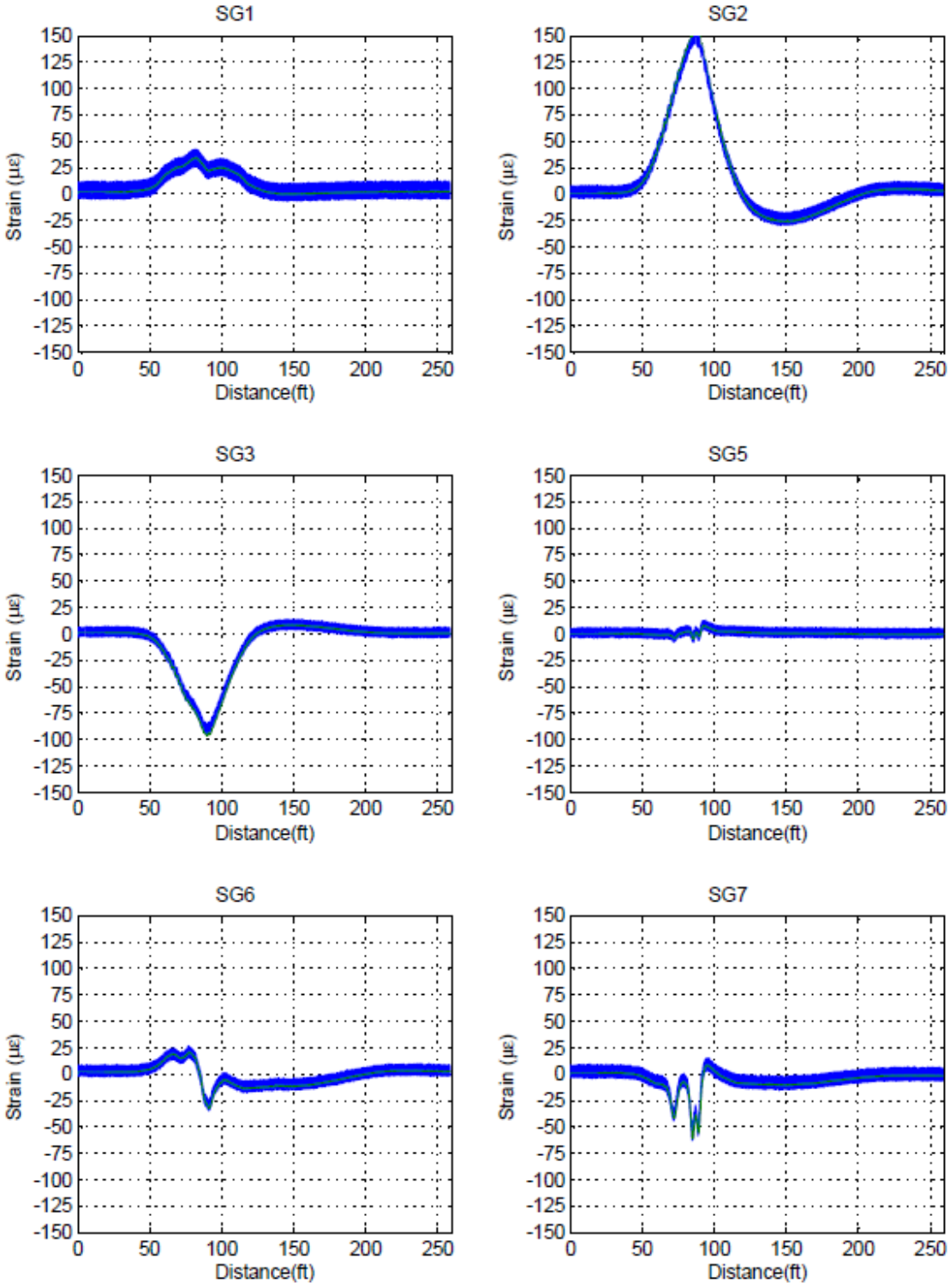

Figure C. 8: Center Truck Load Placement 8-16 kph (5-10 mph).

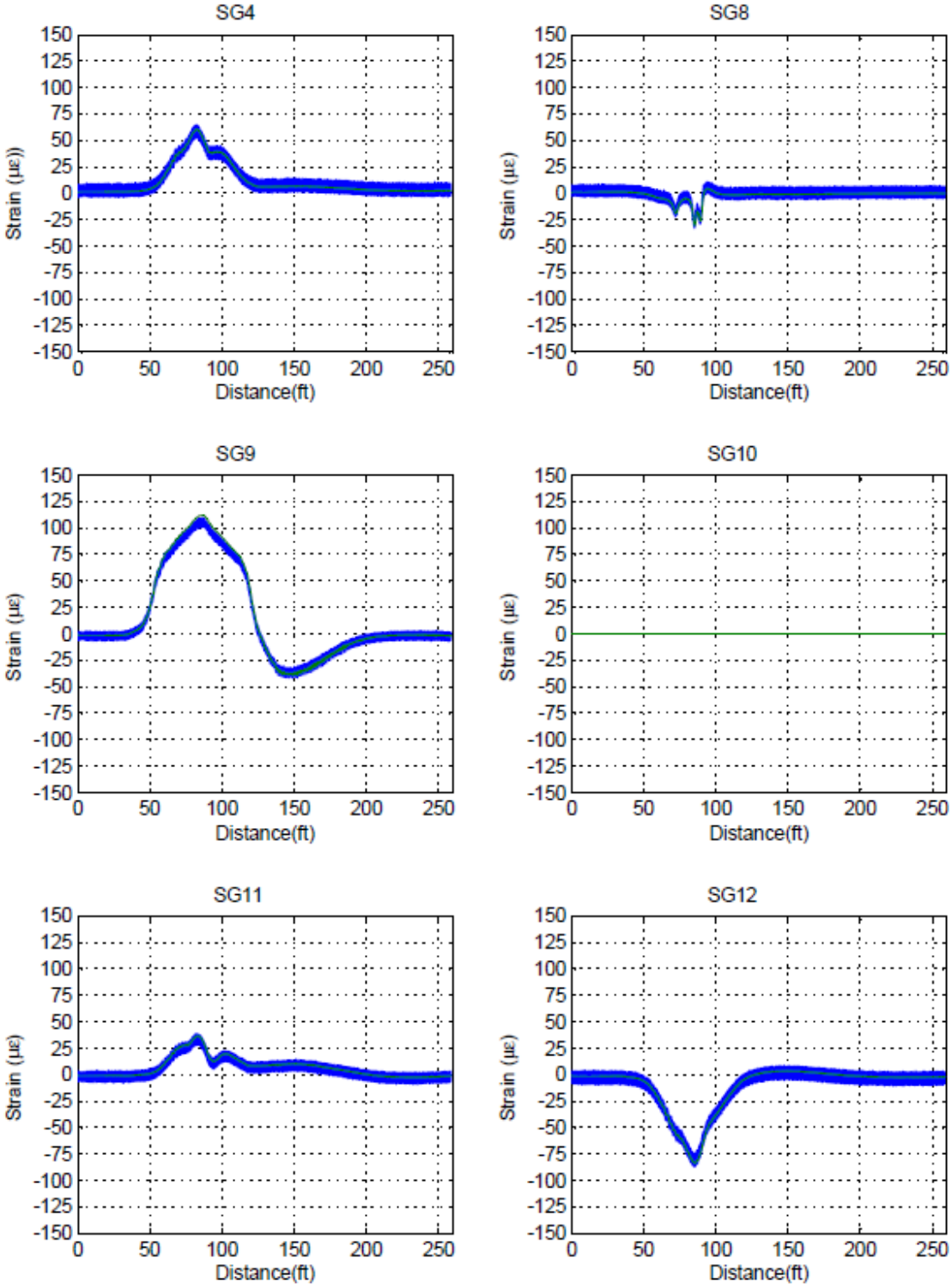

Figure C. 9: Center Truck Load Placement 8-16 kph (5-10 mph).

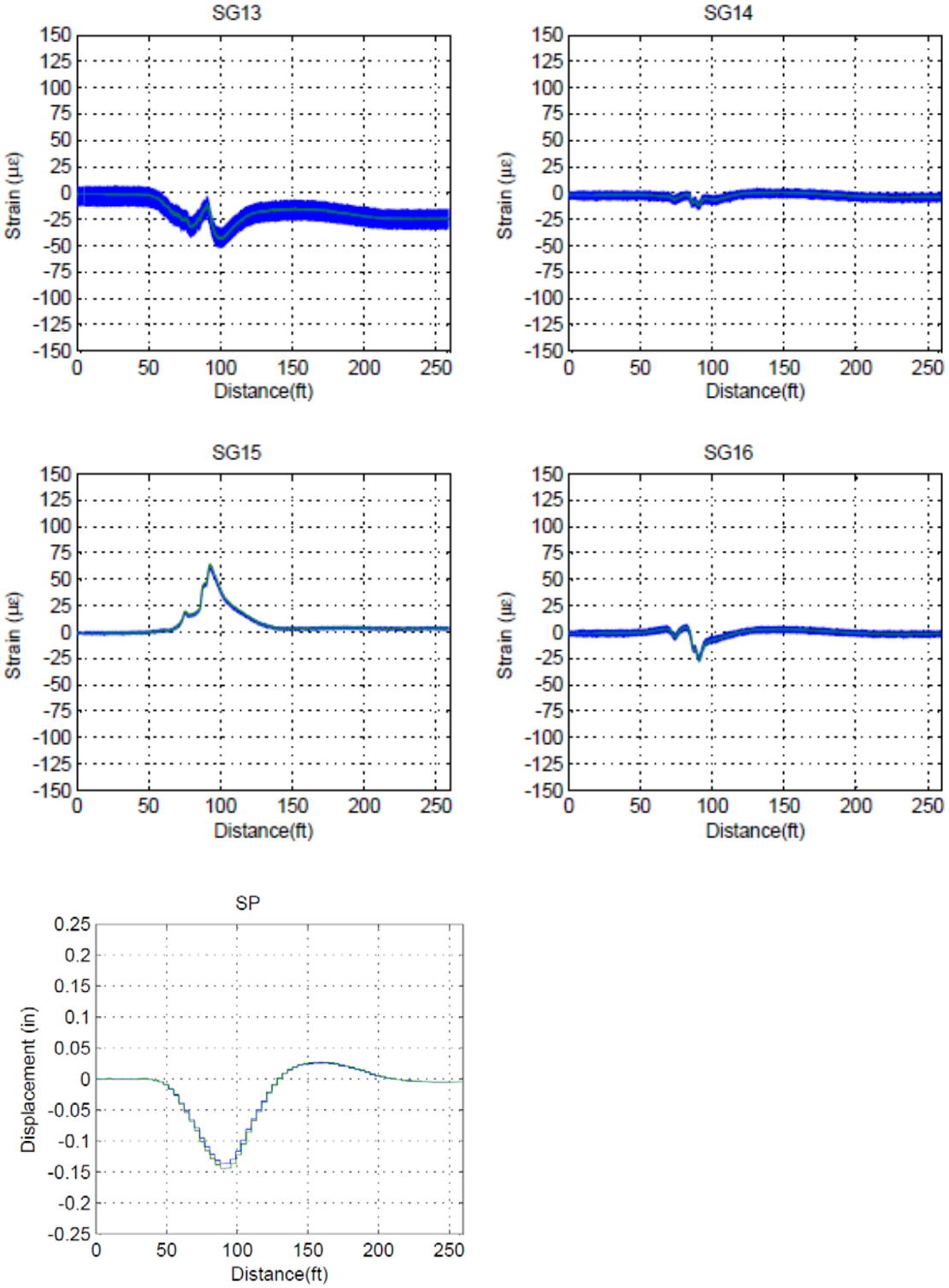

Figure C. 10: Center Truck Load Placement 105-121 kph (65-75 mph).

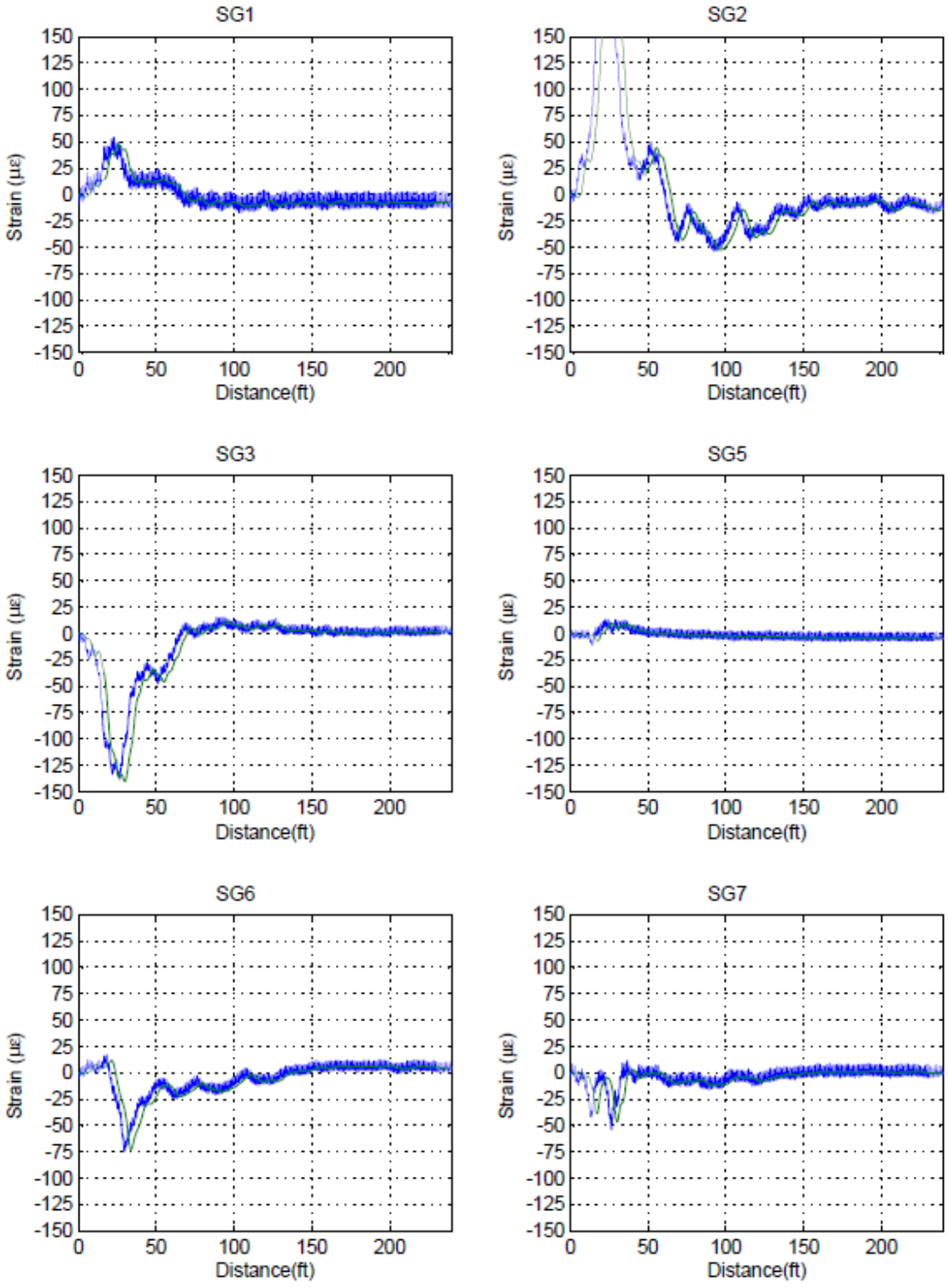

Figure C. 11: Center Truck Load Placement 105-121 kph (65-75 mph).

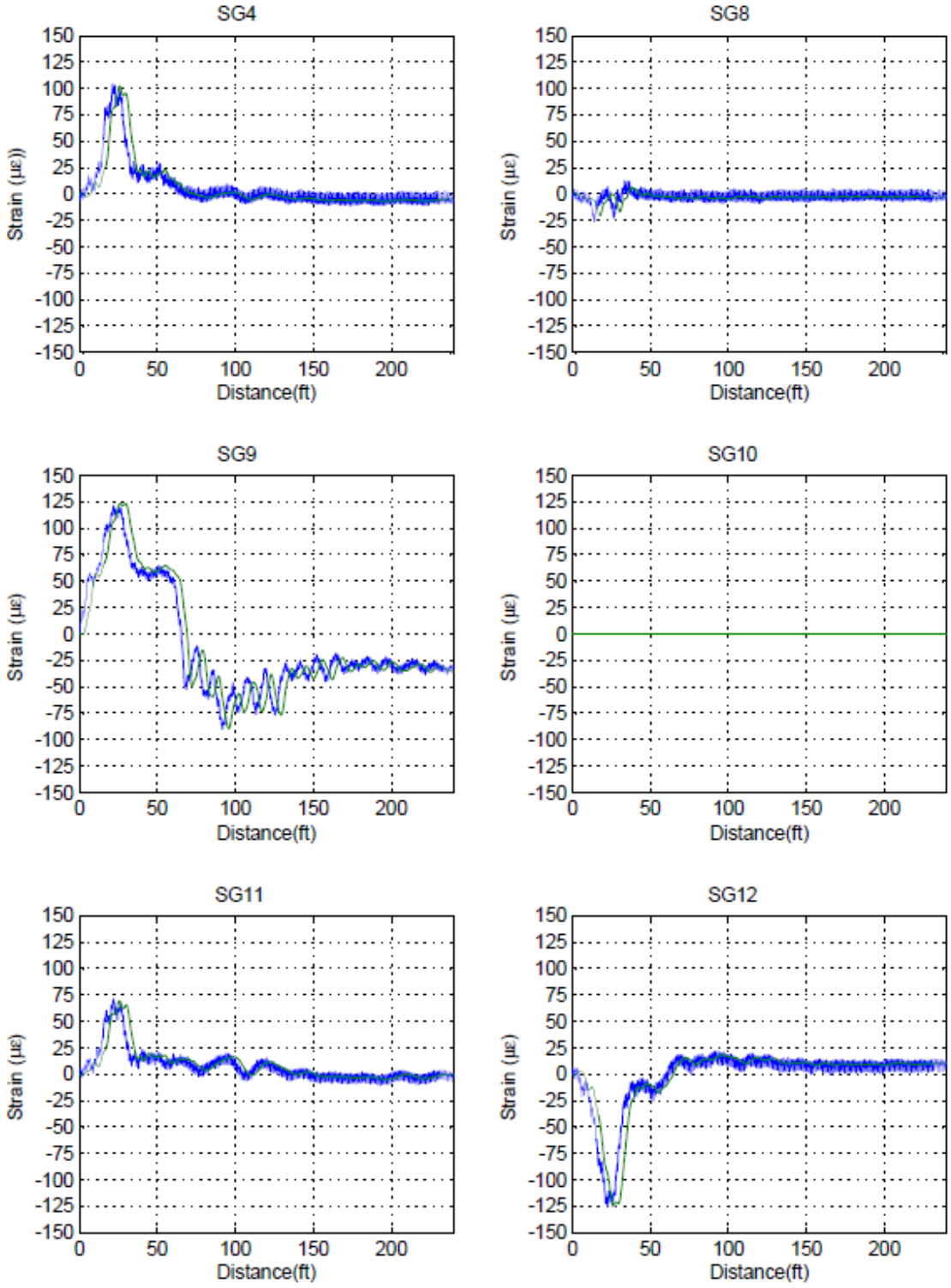

Figure C. 12: Center Truck Load Placement 105-121 kph (65-75 mph).

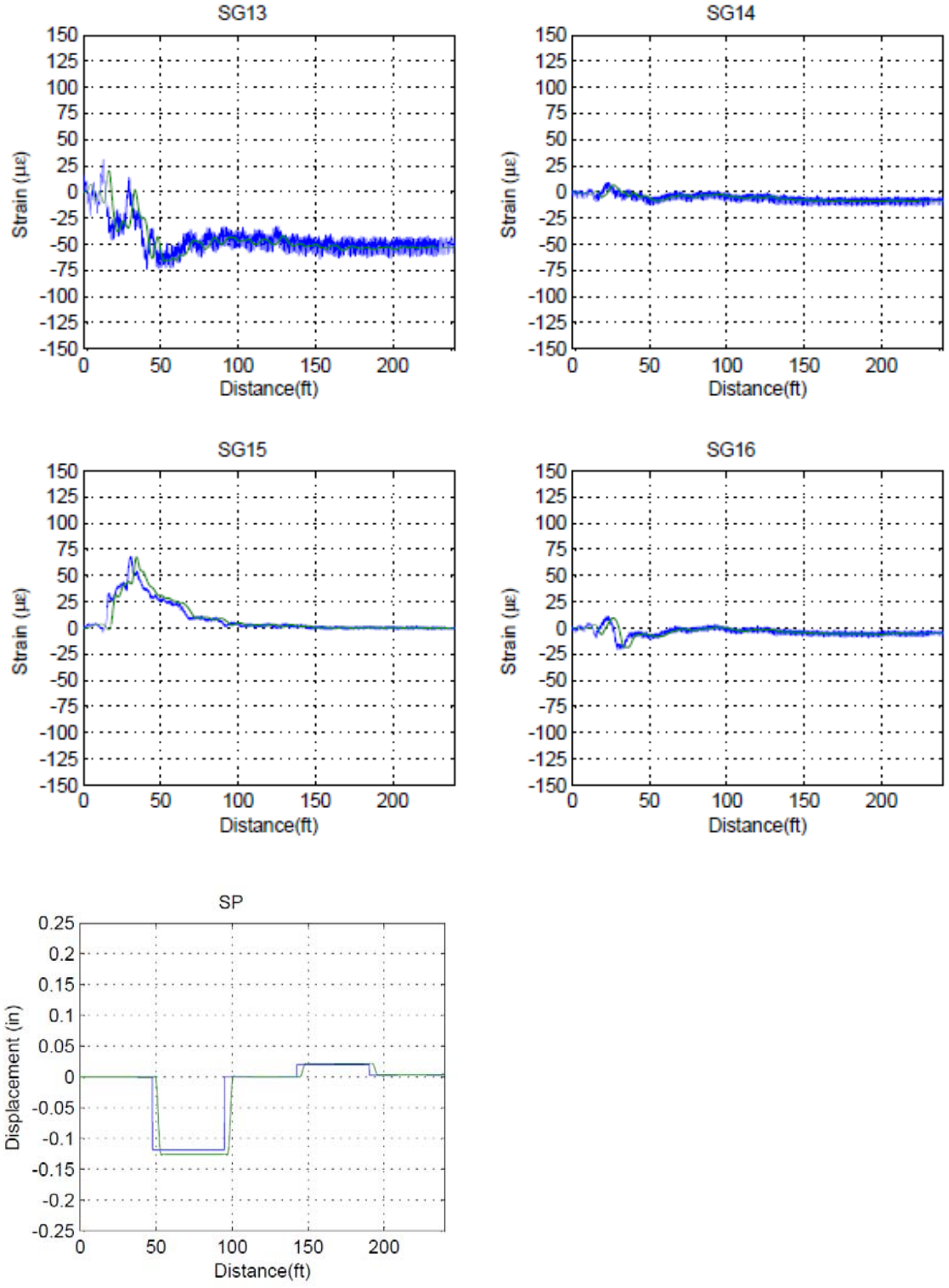

Figure C. 13: East Truck Load Placement 8-16 kph (5-10 mph).

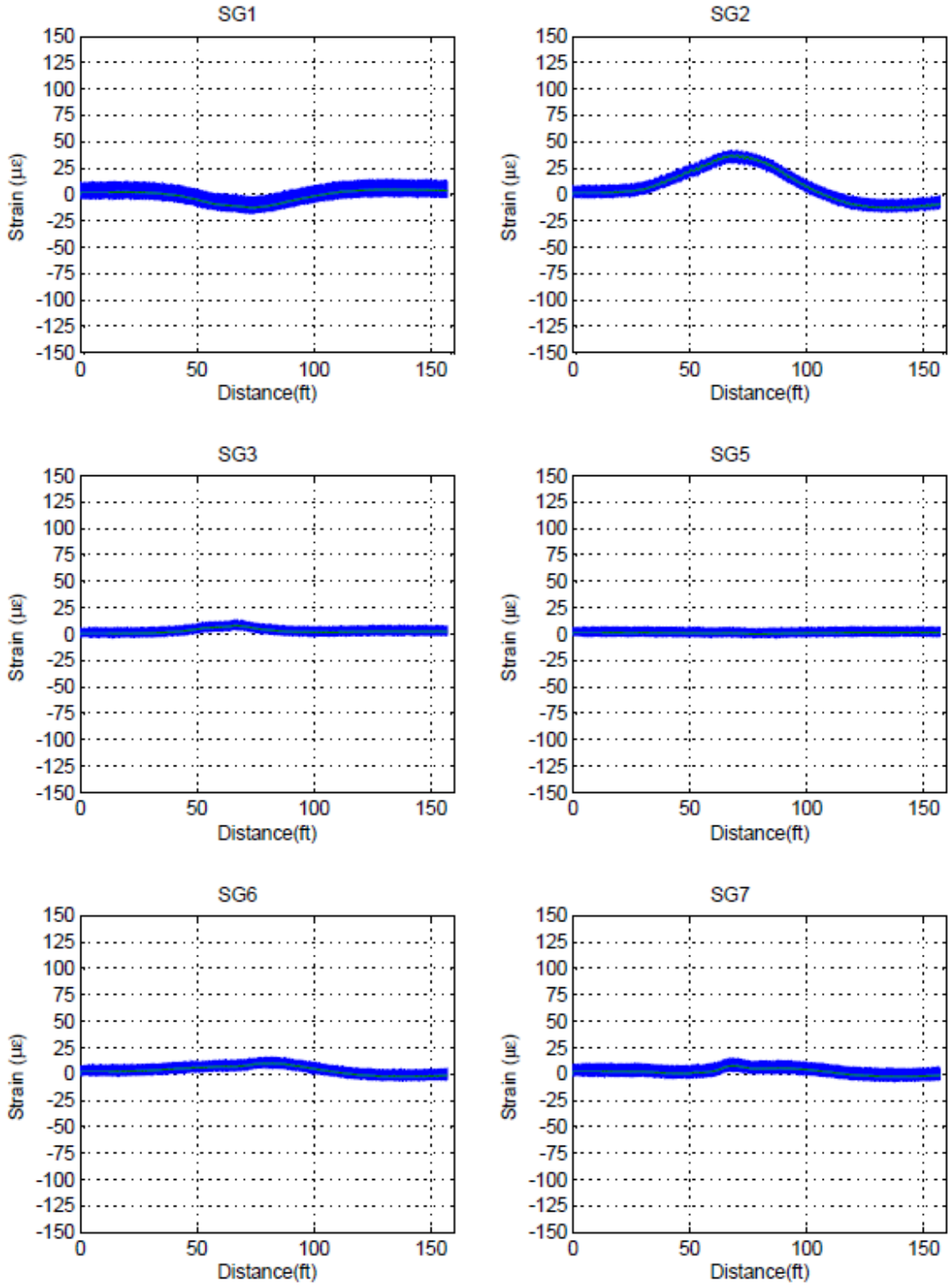

Figure C. 14: East Truck Load Placement 8-16 kph (5-10 mph).

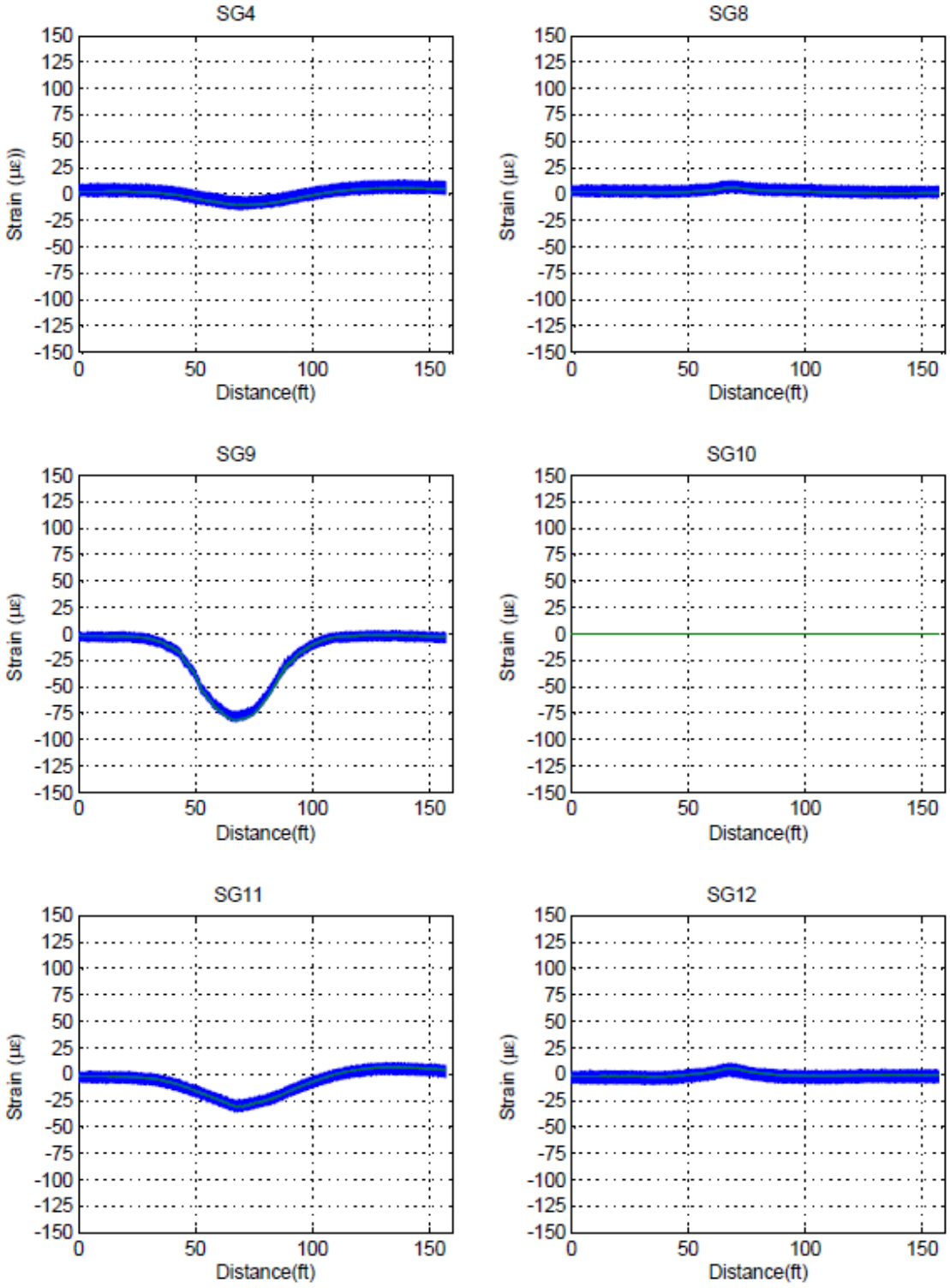

Figure C. 15: East Truck Load Placement 8-16 kph (5-10 mph).

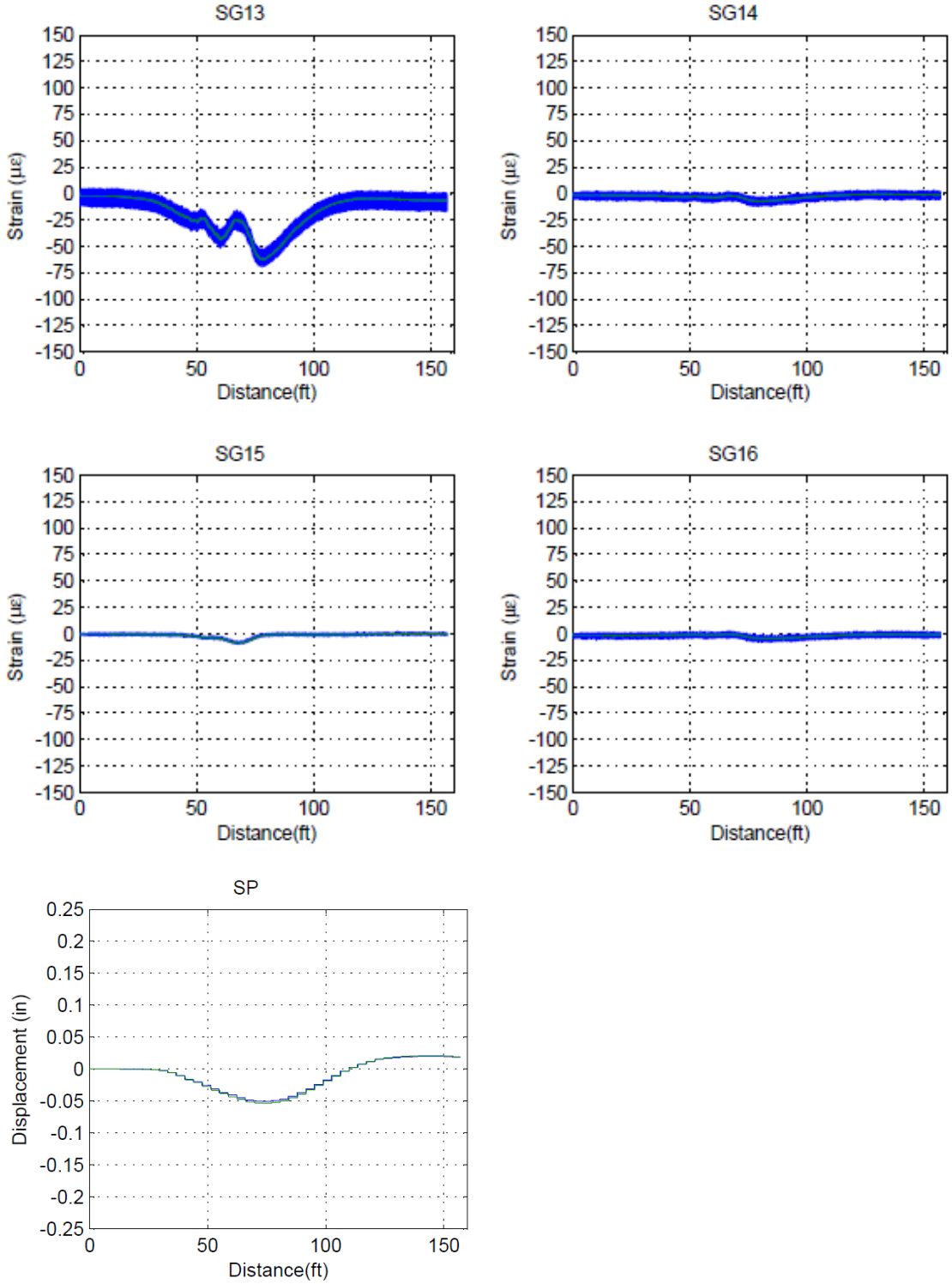

Figure C. 16: East Truck Load Placement 105-121 kph (65-75 mph).

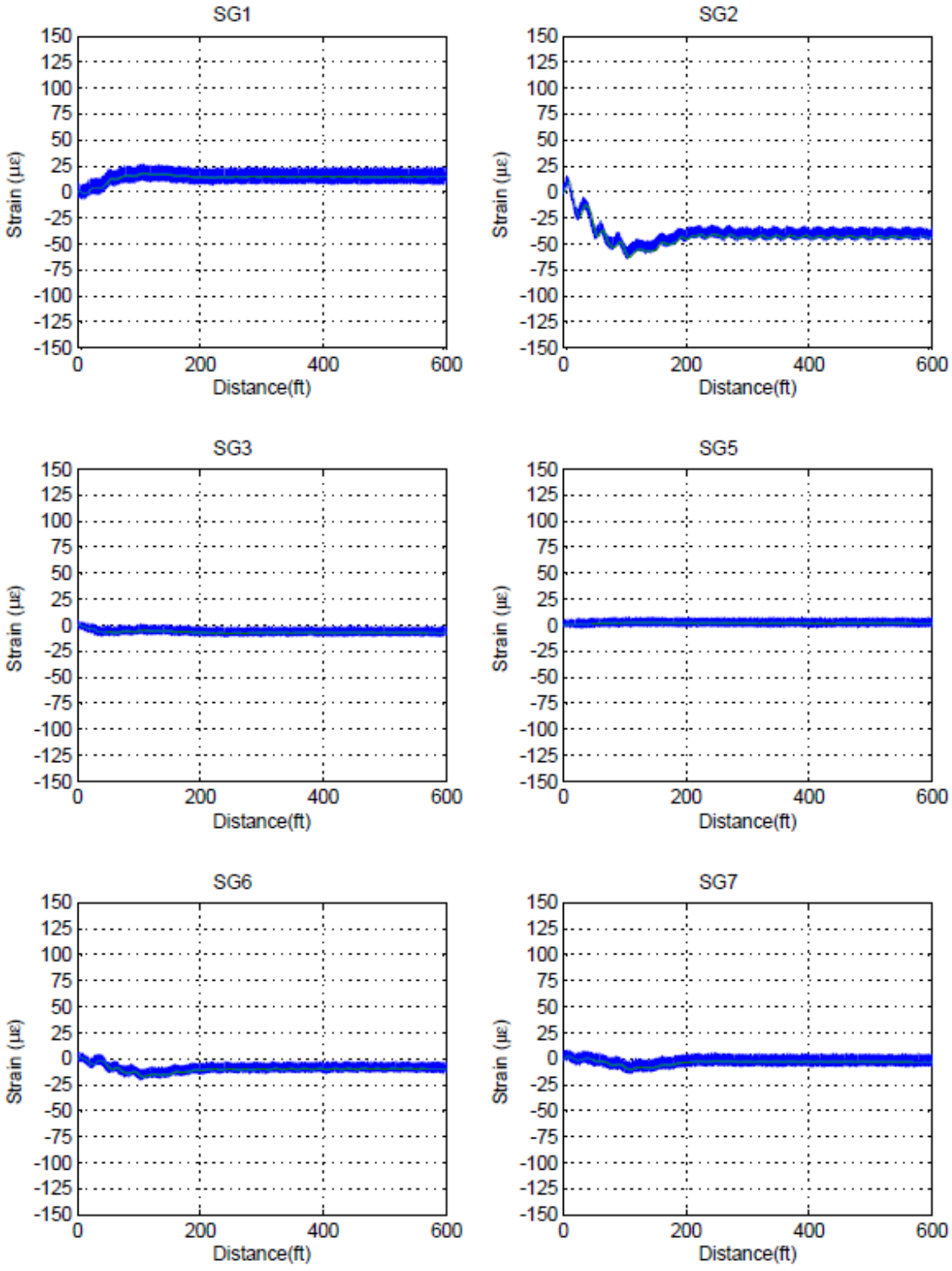

Figure C. 17: East Truck Load Placement 105-121 kph (65-75 mph).

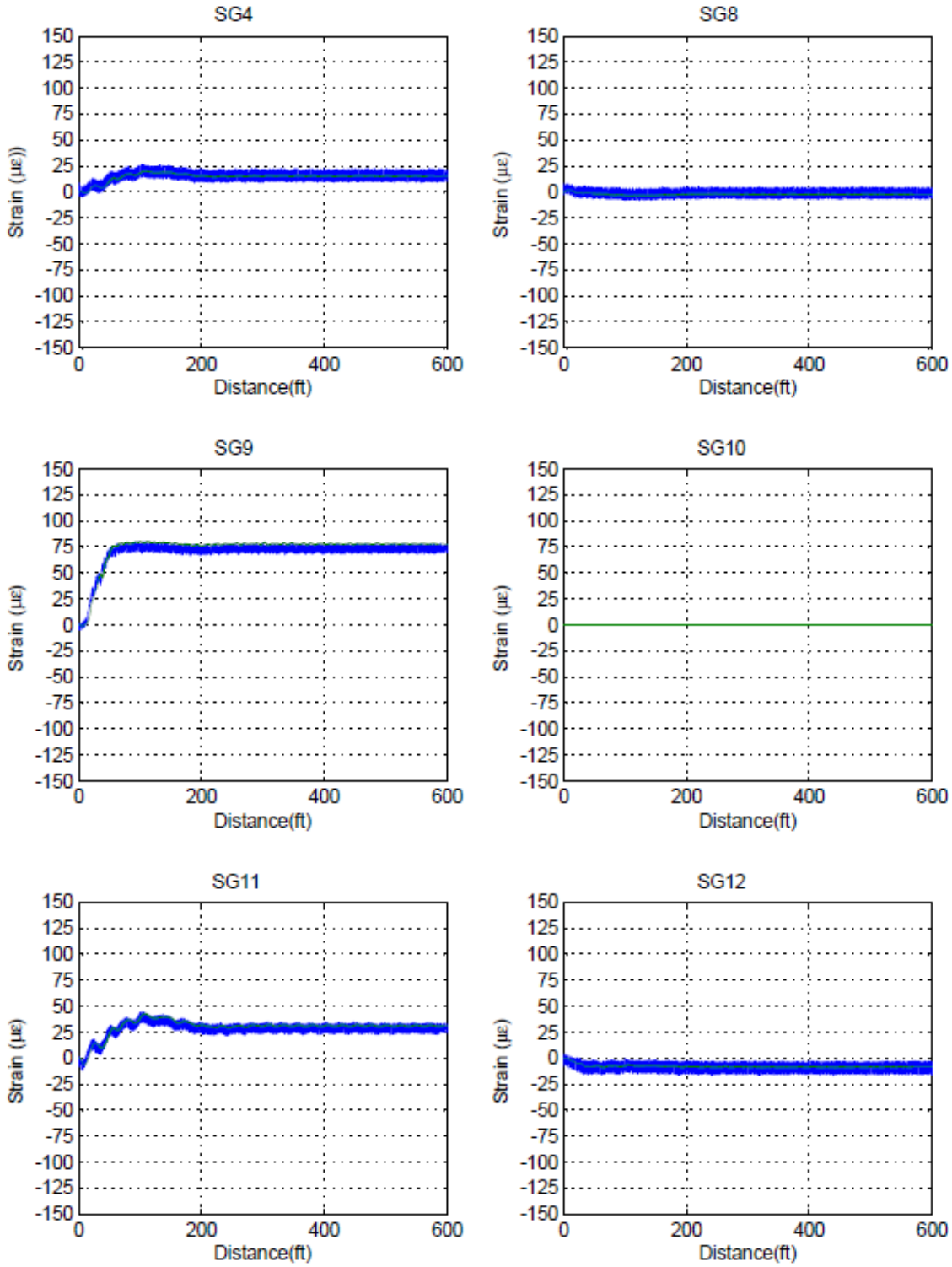

Figure C. 18: East Truck Load Placement 105-121 kph (65-75 mph).

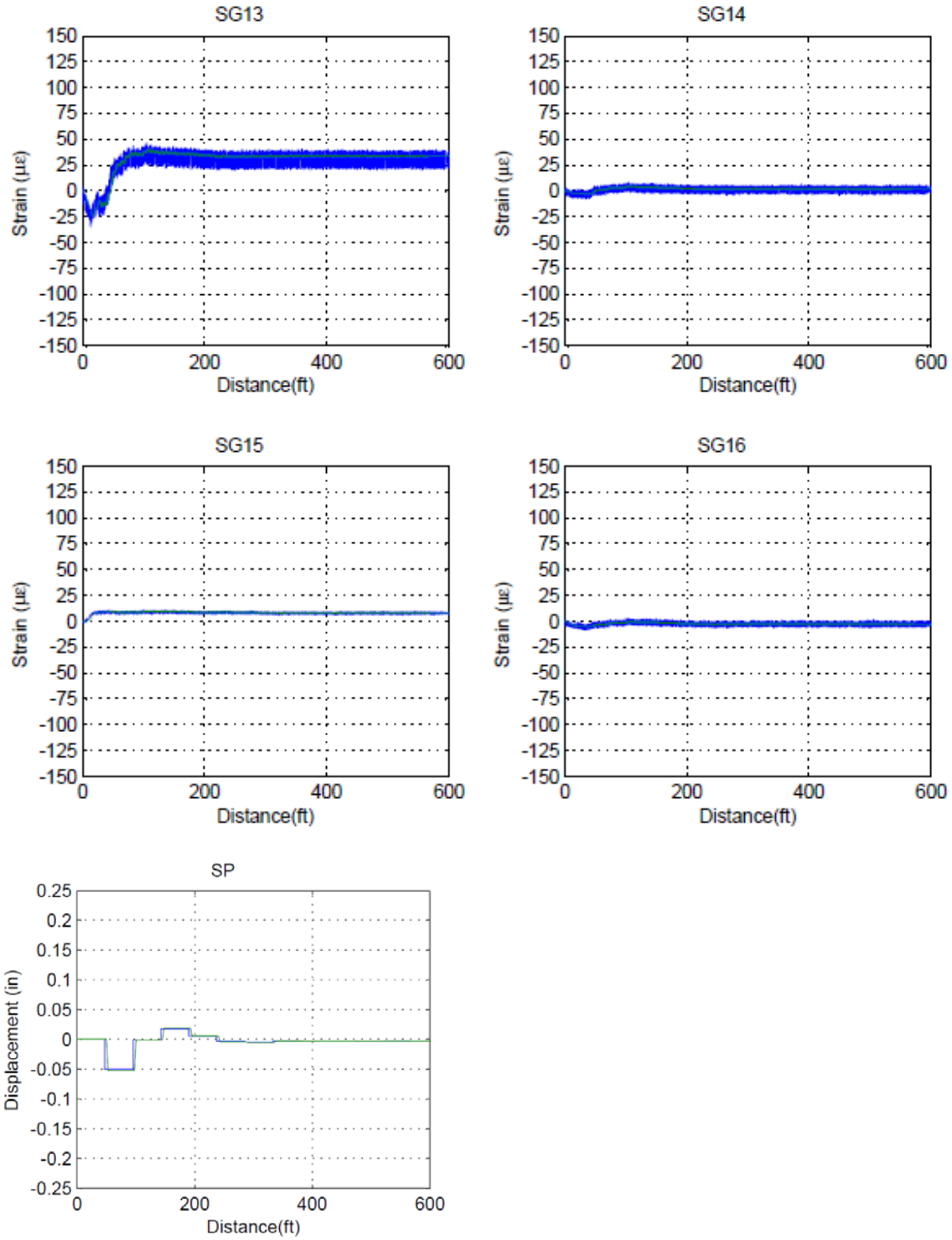

After Retrofit

Figure C. 19: West Truck Load Placement 8-16 kph (5-10 mph).

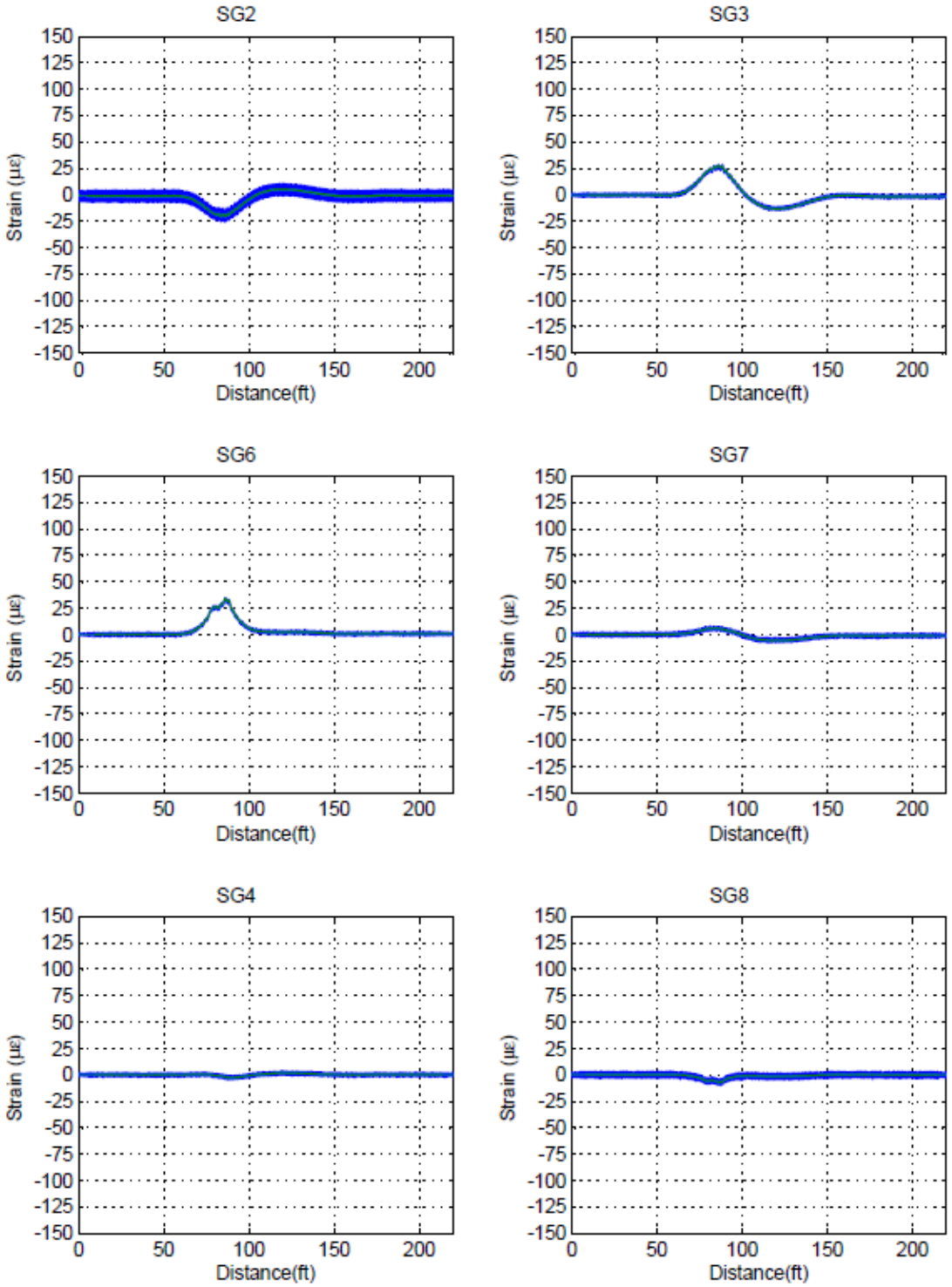

Figure C. 20: West Truck Load Placement 8-16 kph (5-10 mph).

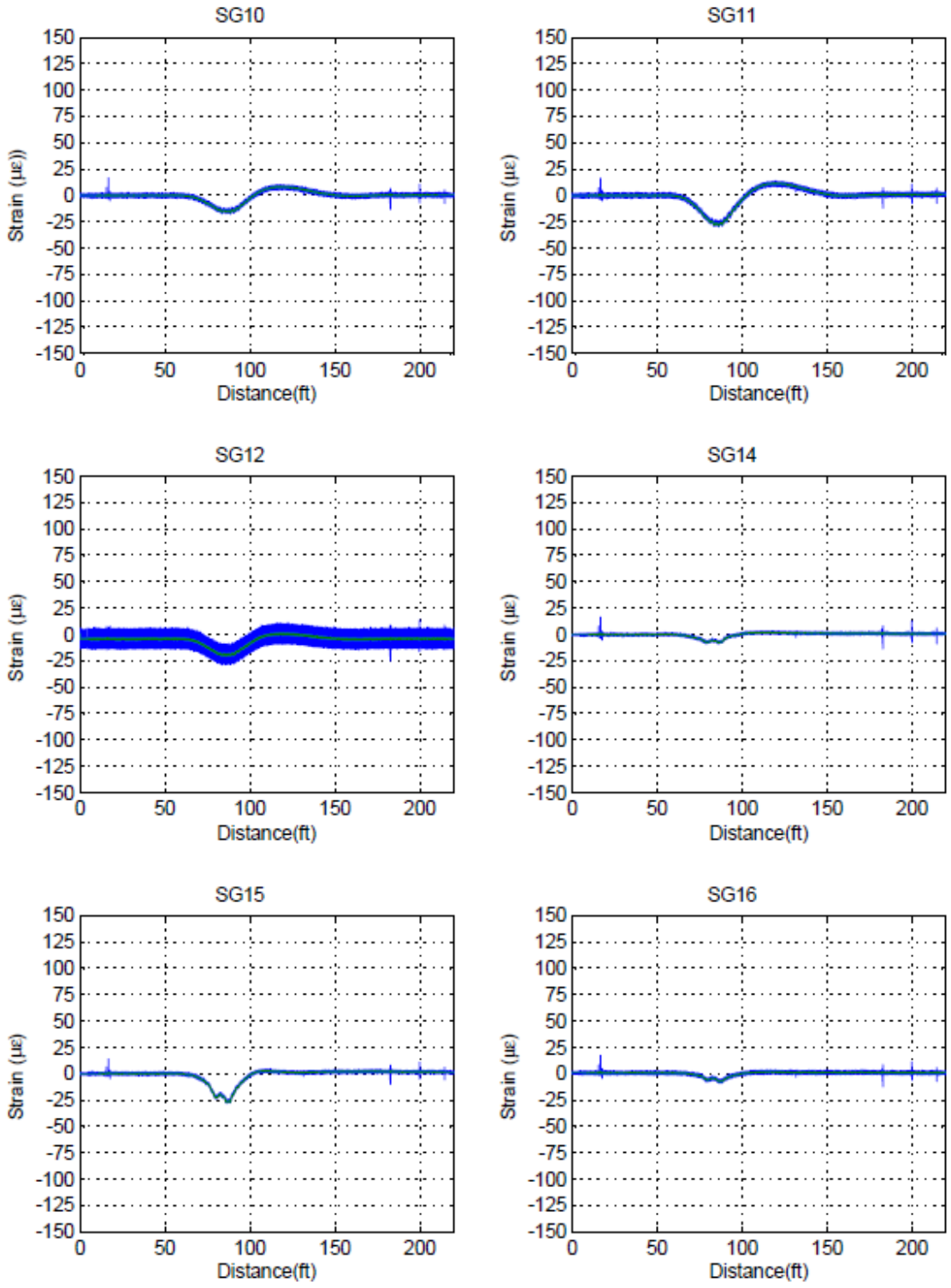

Figure C. 21: West Truck Load Placement 8-16 kph (5-10 mph).

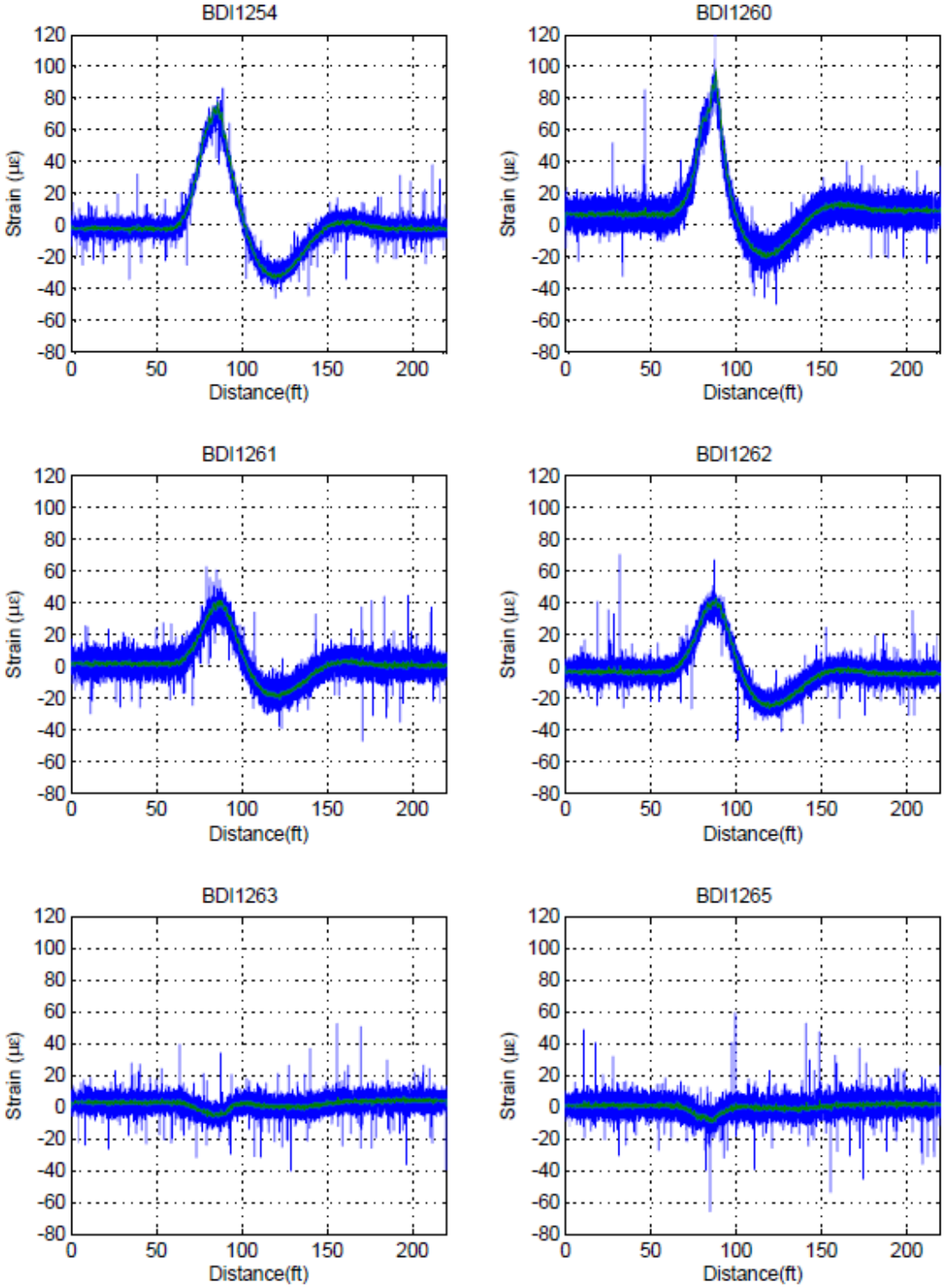

Figure C. 22: West Truck Load Placement 8-16 kph (5-10 mph).

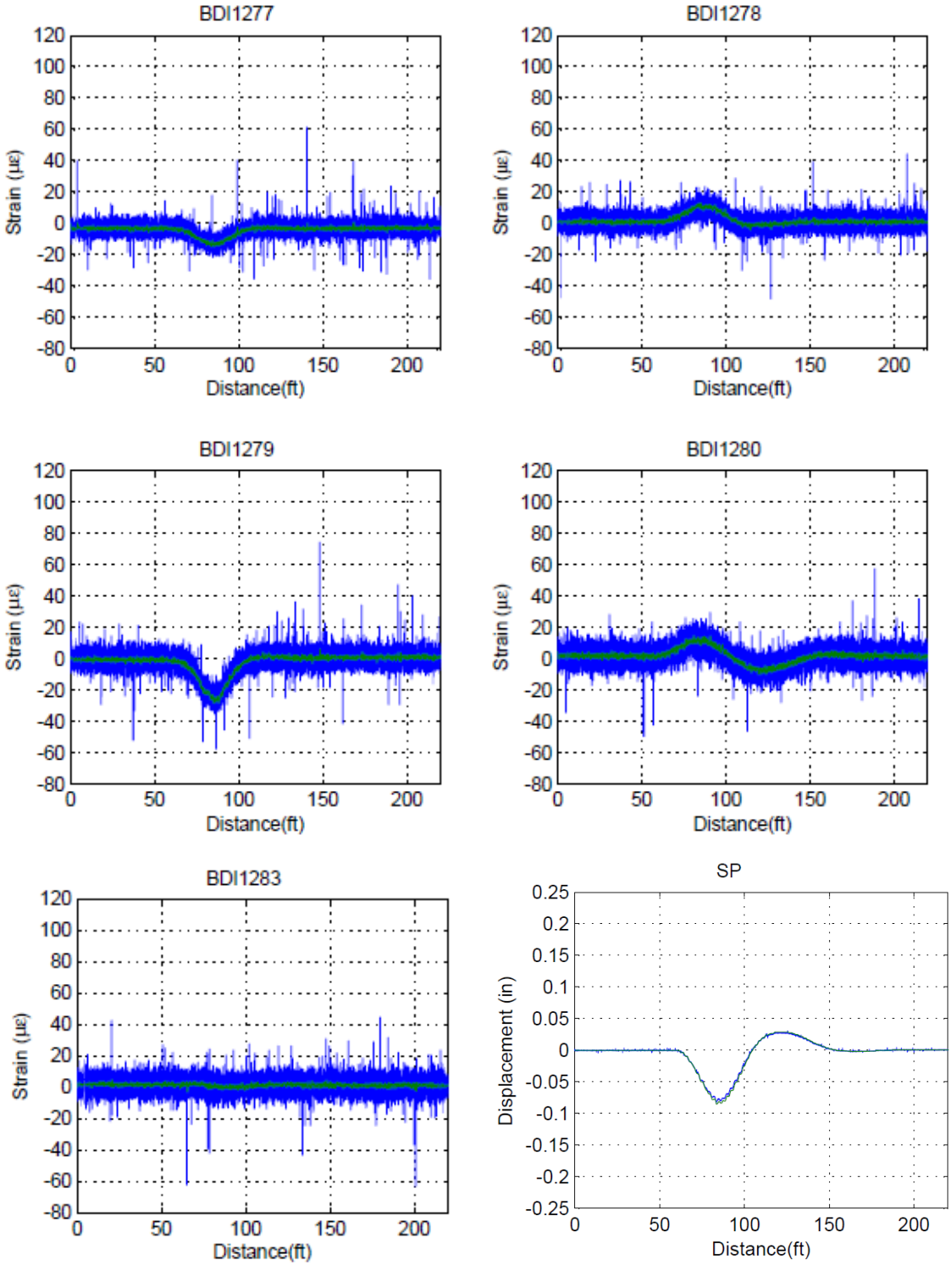

Figure C. 23: West Truck Load Placement 105-121 kph (65-75 mph).

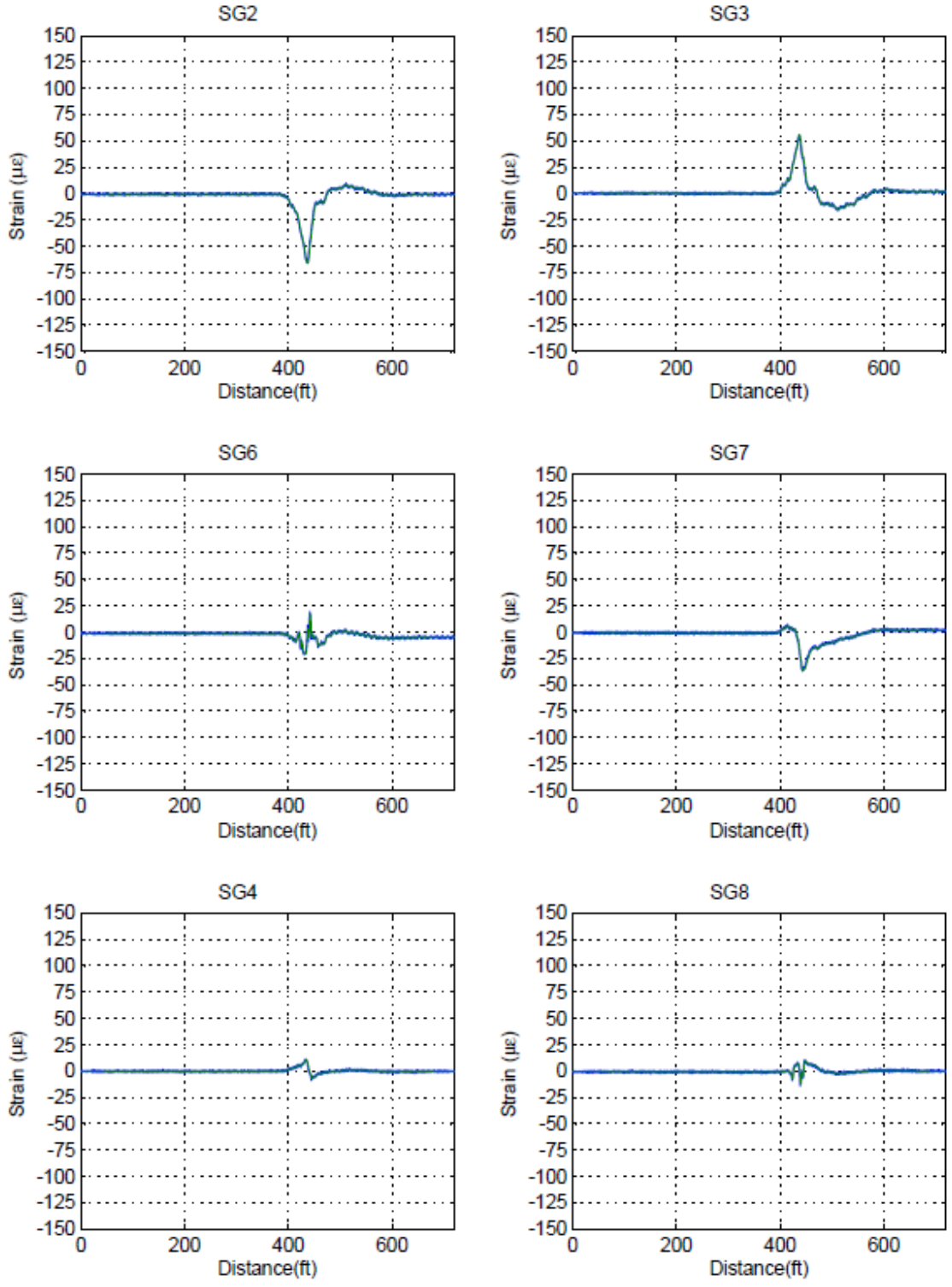

Figure C. 24: West Truck Load Placement 105-121 kph (65-75 mph).

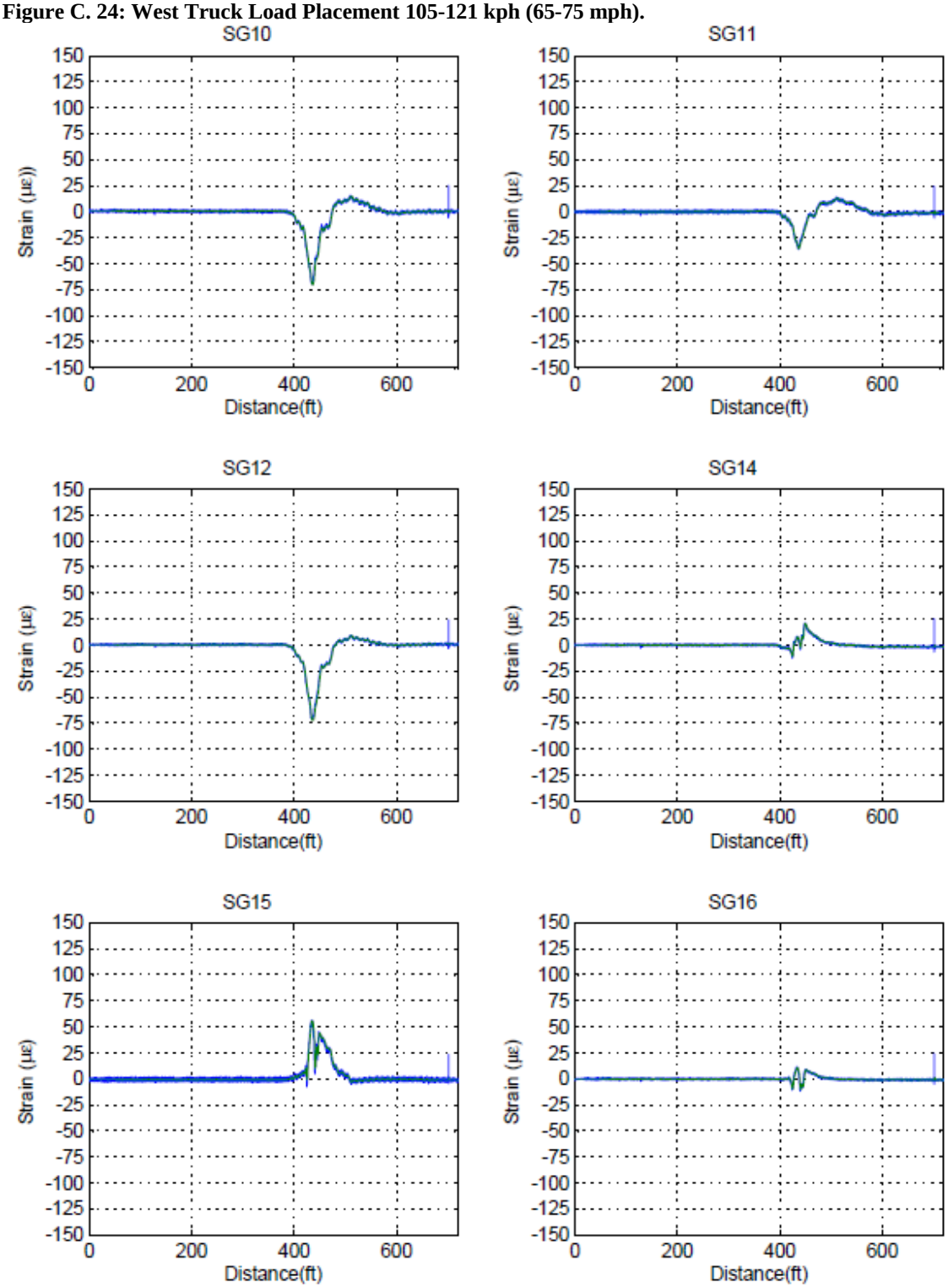

Figure C. 25: West Truck Load Placement 105-121 kph (65-75 mph).

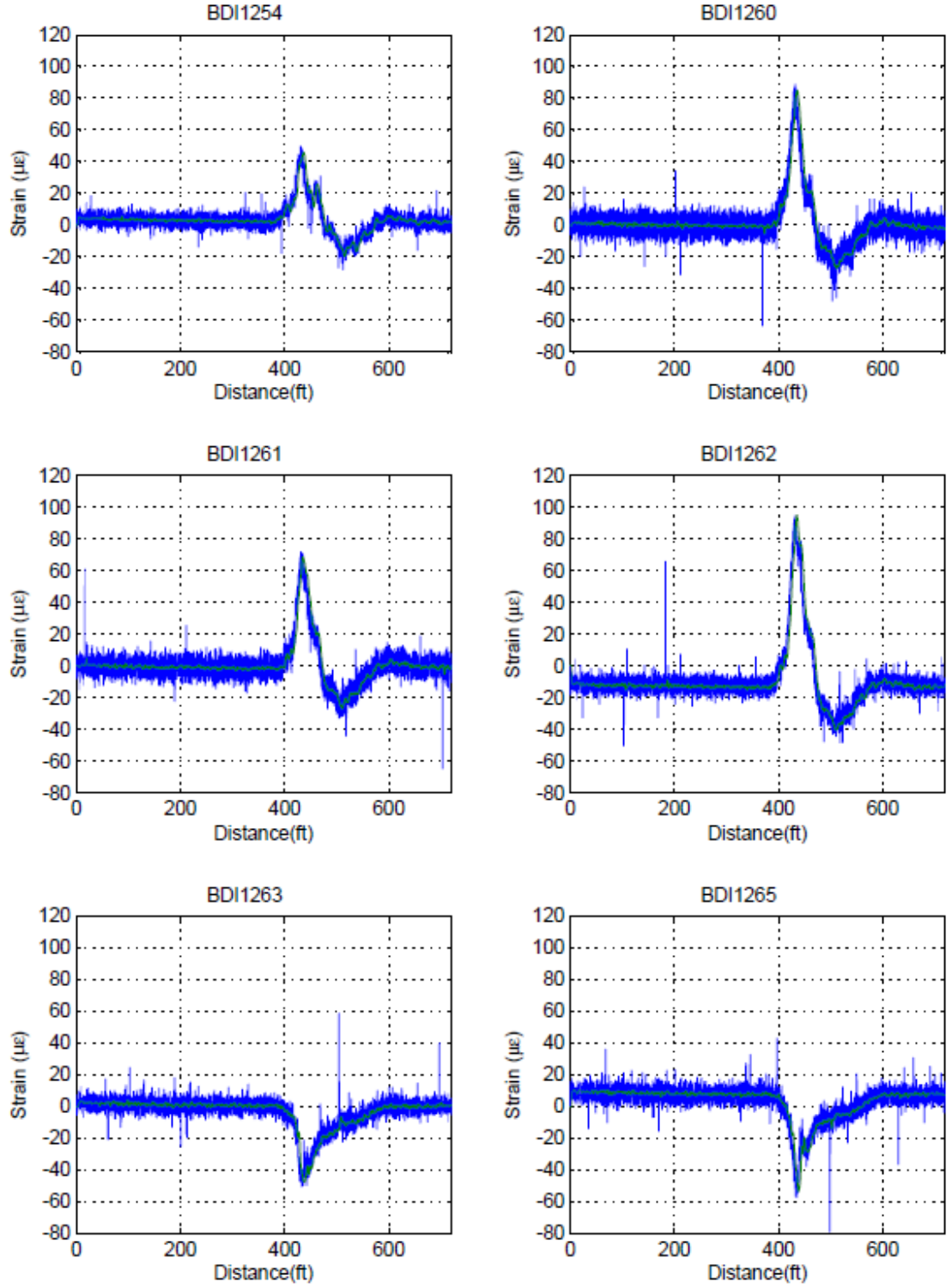

Figure C. 26: West Truck Load Placement 105-121 kph (65-75 mph).

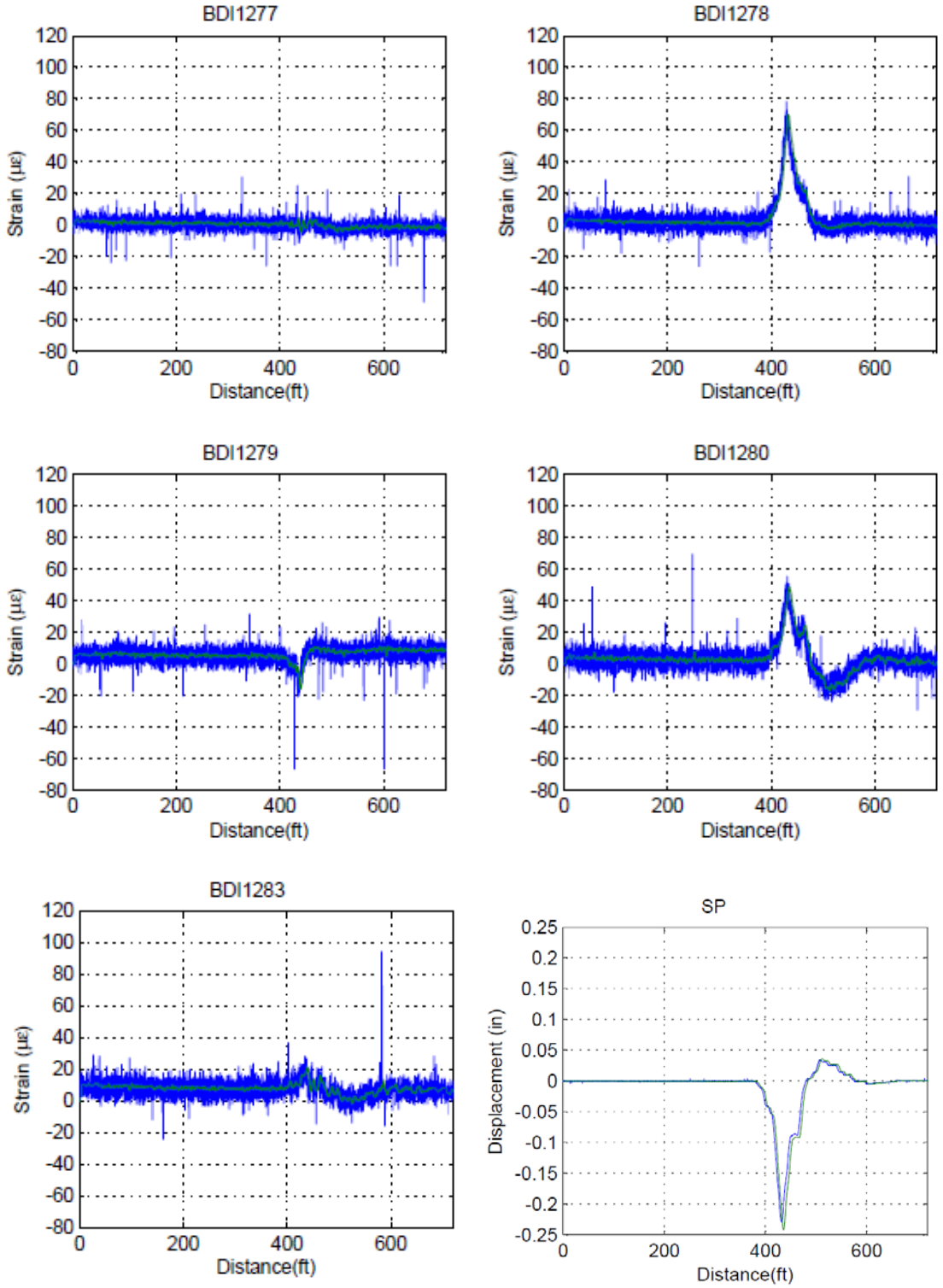

Figure C. 27: Center Truck Load Placement 8-16 kph (5-10 mph).

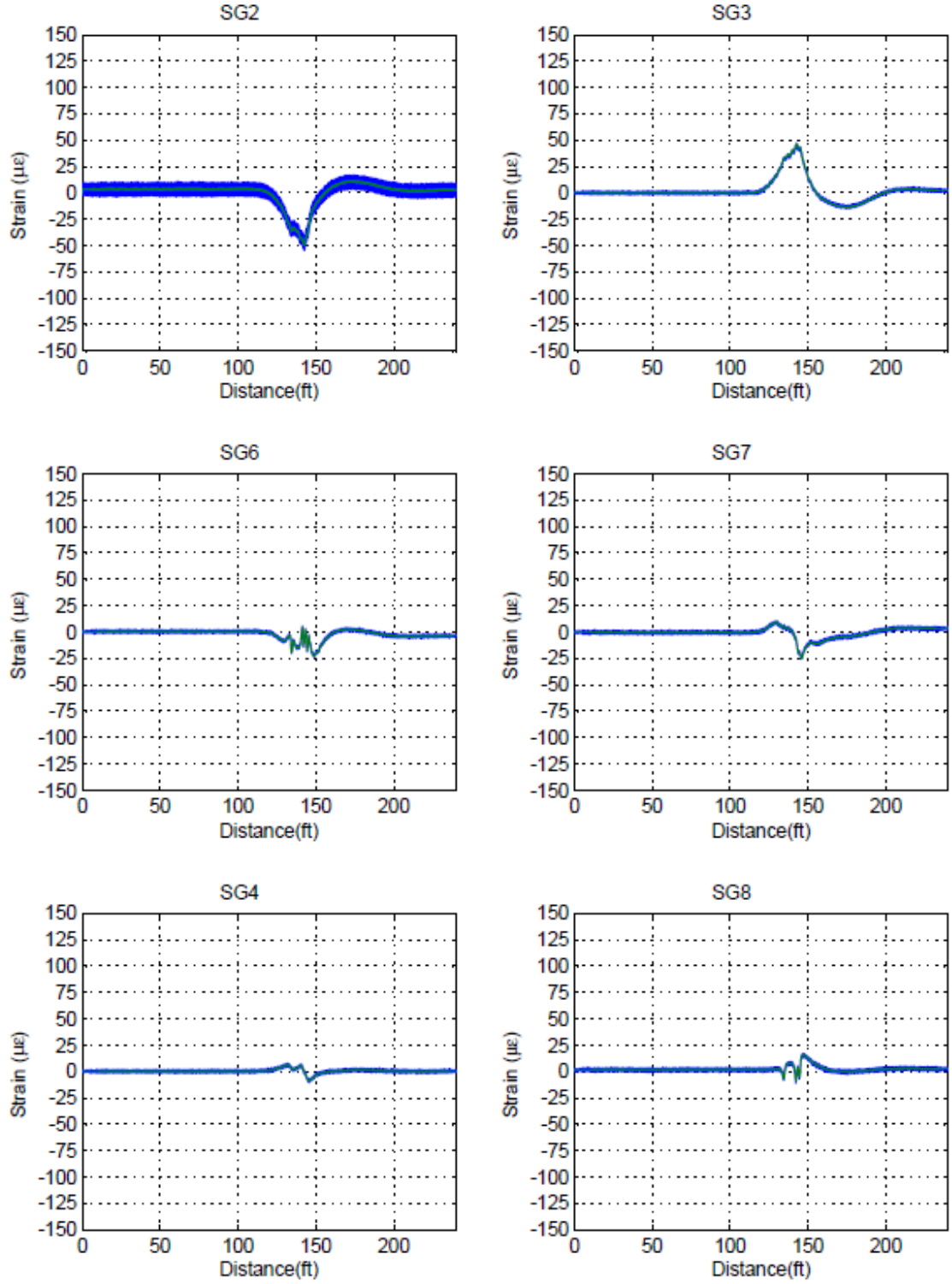

Figure C. 28: Center Truck Load Placement 8-16 kph (5-10 mph).

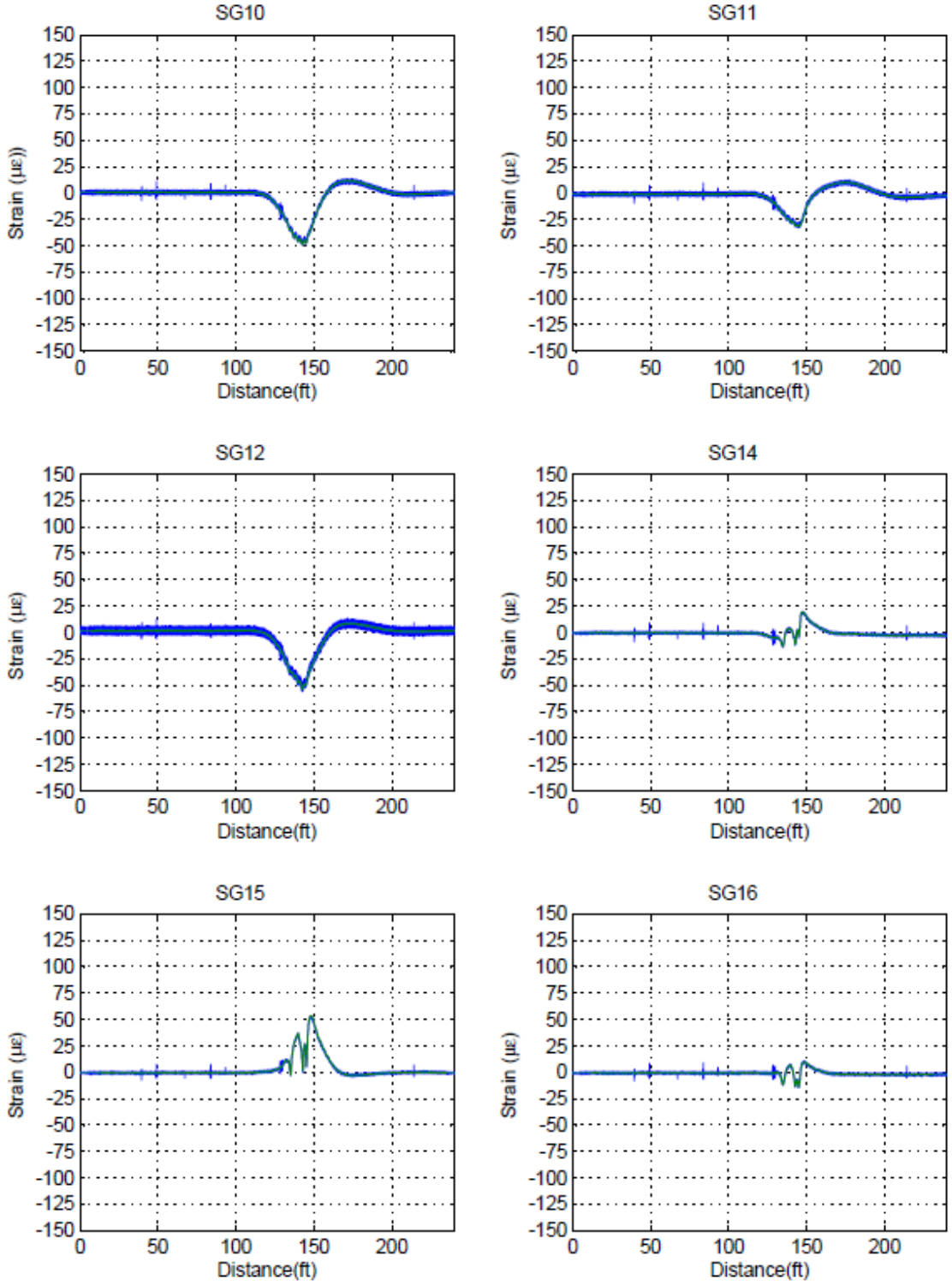

Figure C. 29: Center Truck Load Placement 8-16 kph (5-10 mph).

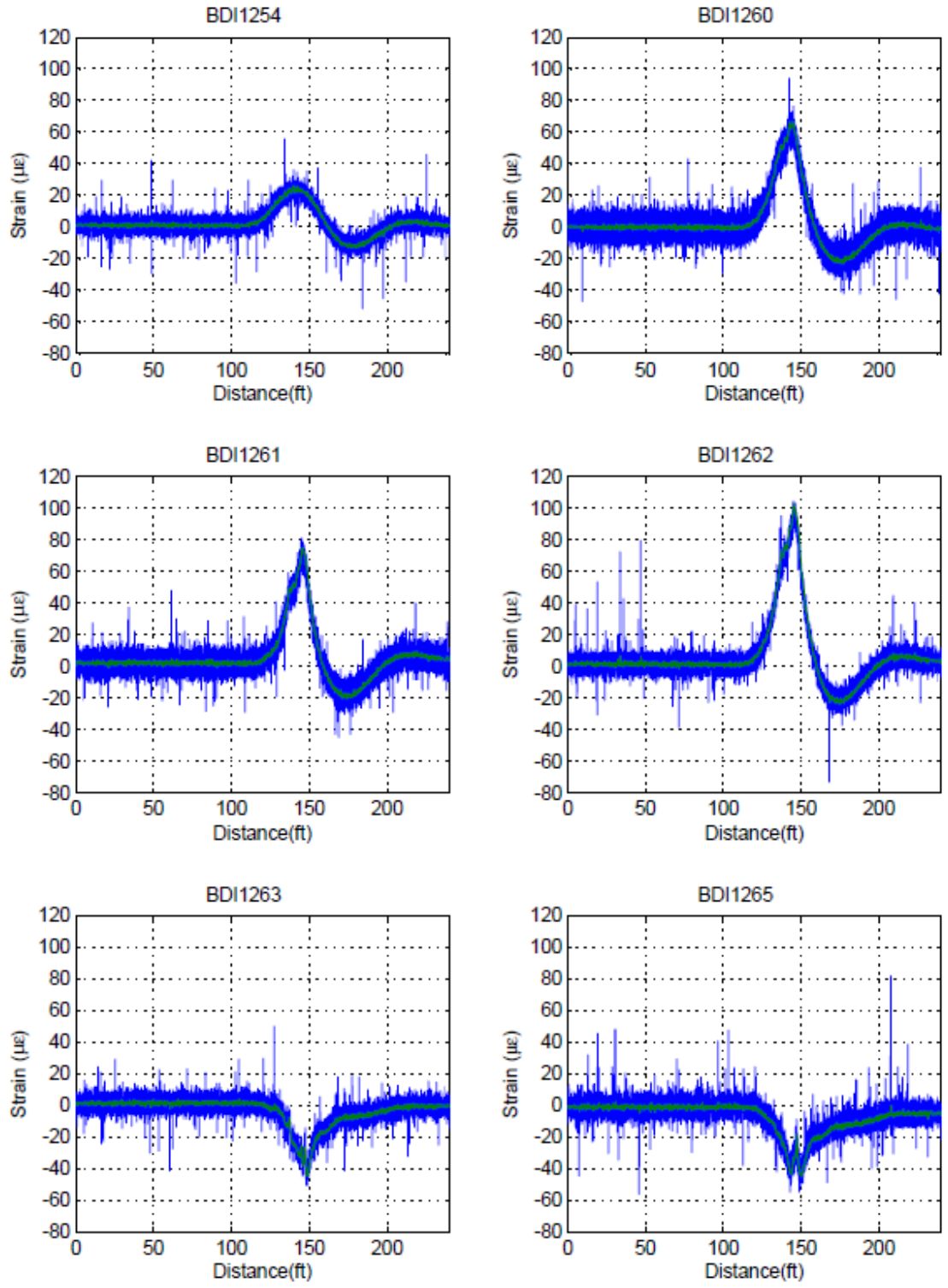

Figure C. 30: Center Truck Load Placement 8-16 kph (5-10 mph).

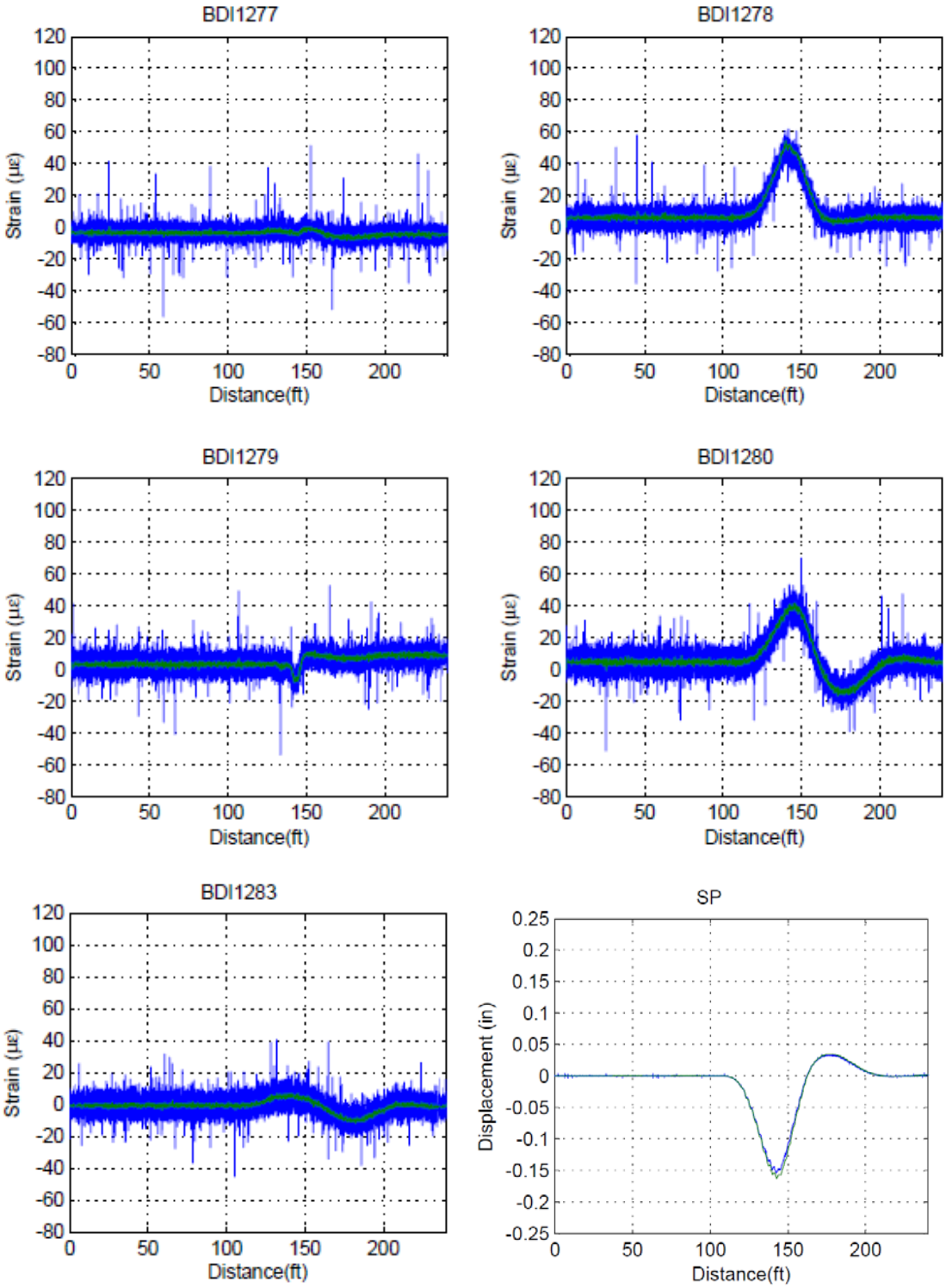

Figure C. 31: Center Truck Load Placement 105-121 kph (65-75 mph).

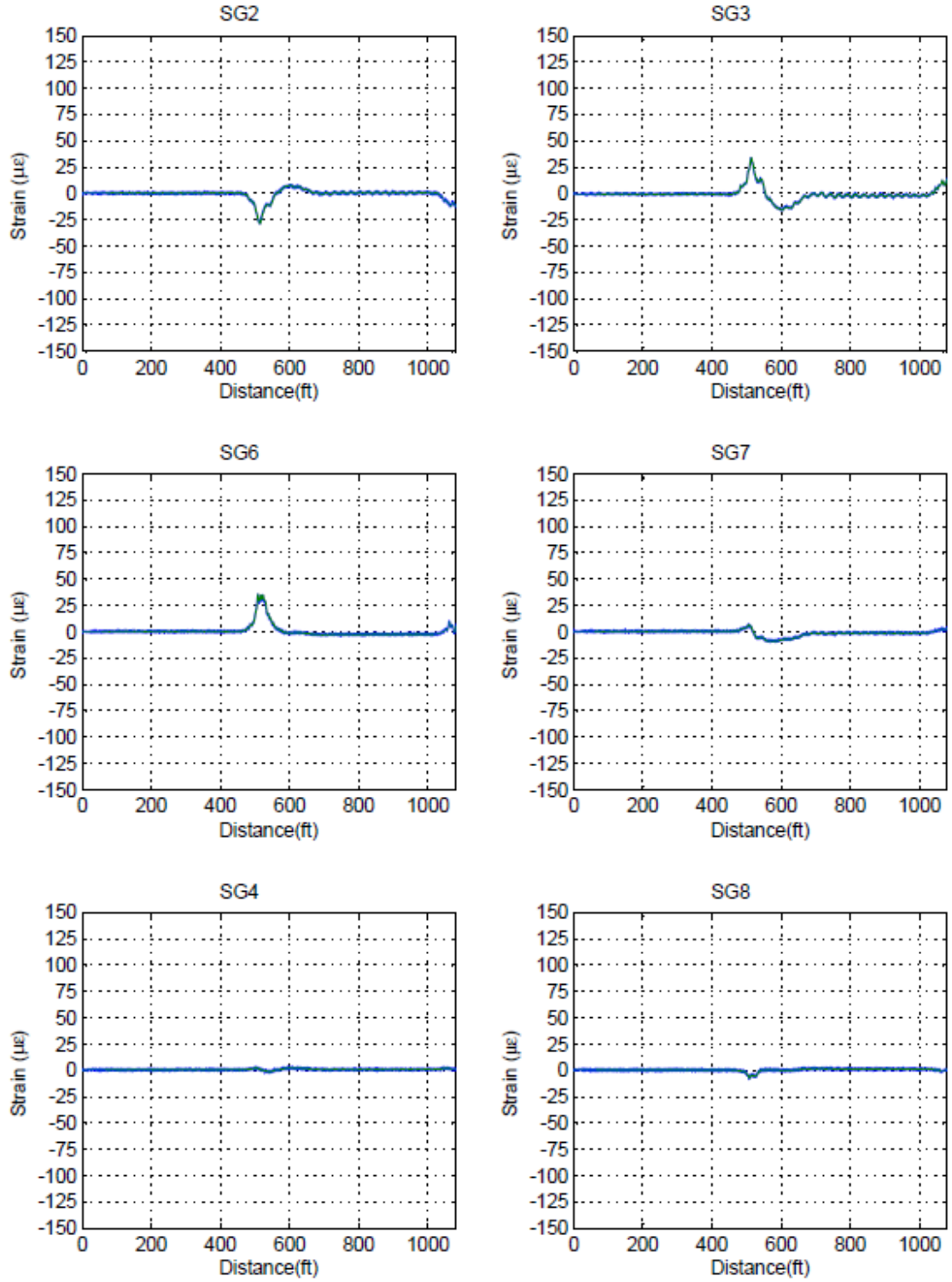

Figure C. 32: Center Truck Load Placement 105-121 kph (65-75 mph).

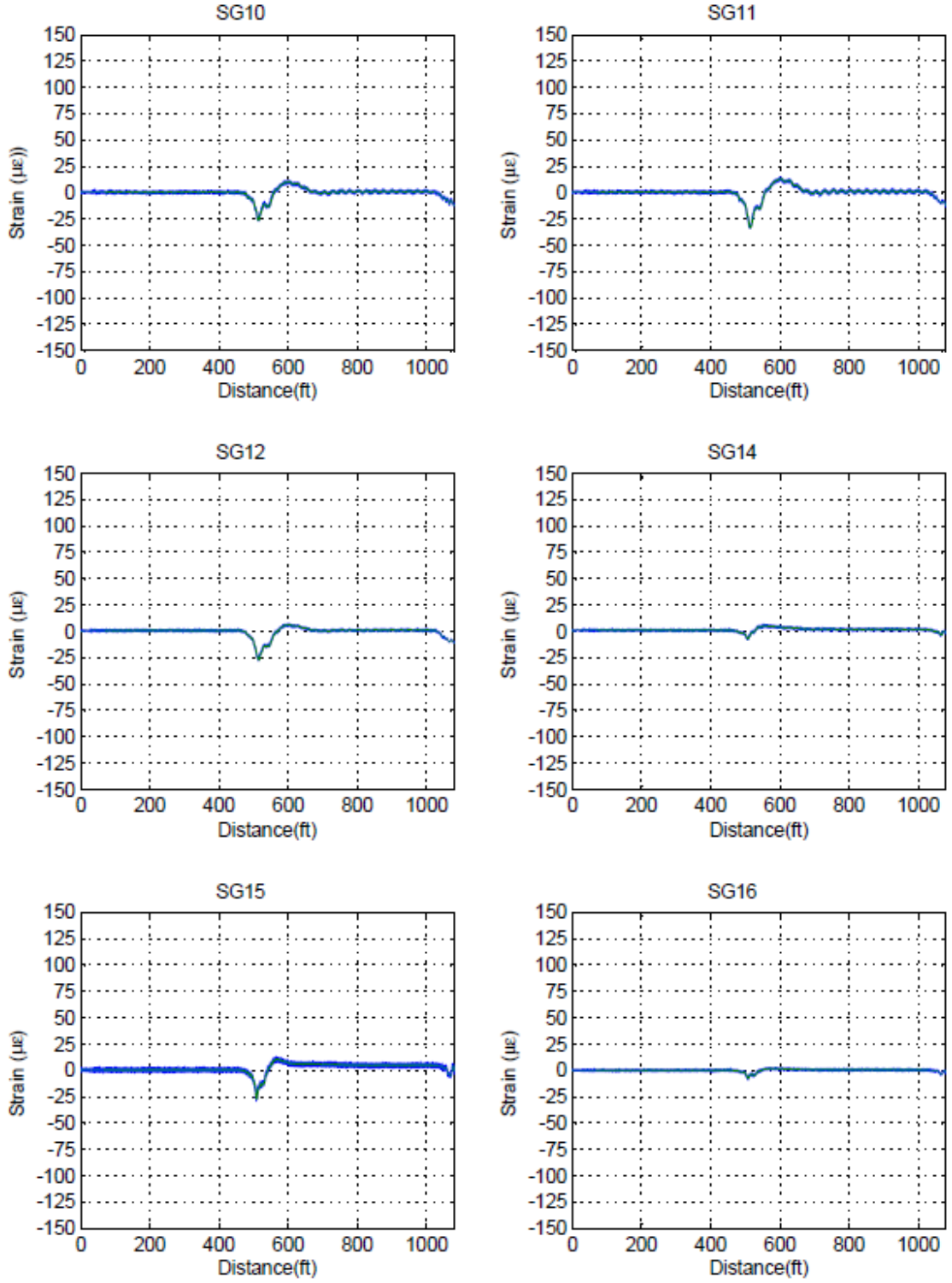

Figure C. 33: Center Truck Load Placement 105-121 kph (65-75 mph).

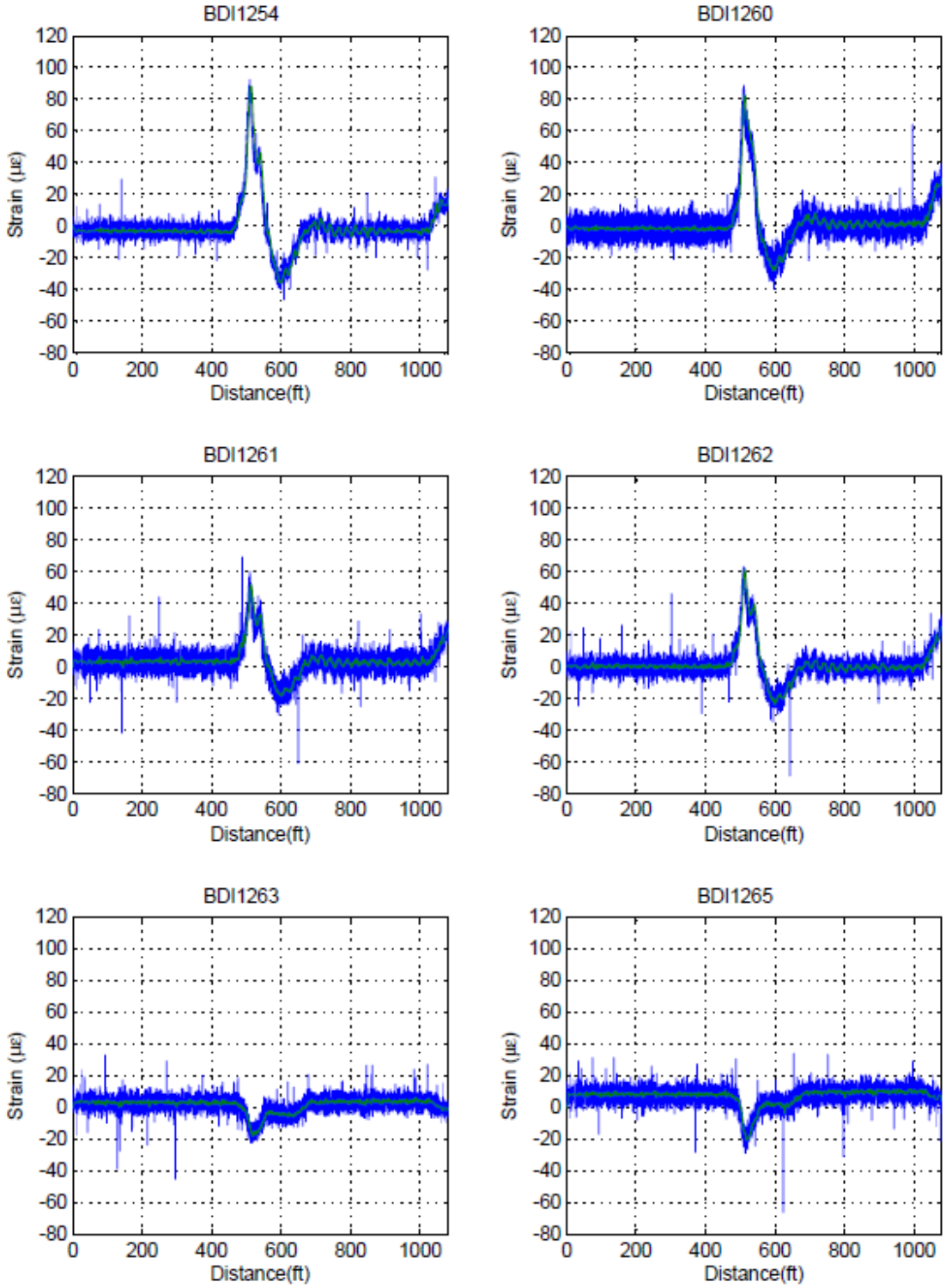

Figure C. 34: Center Truck Load Placement 105-121 kph (65-75 mph).

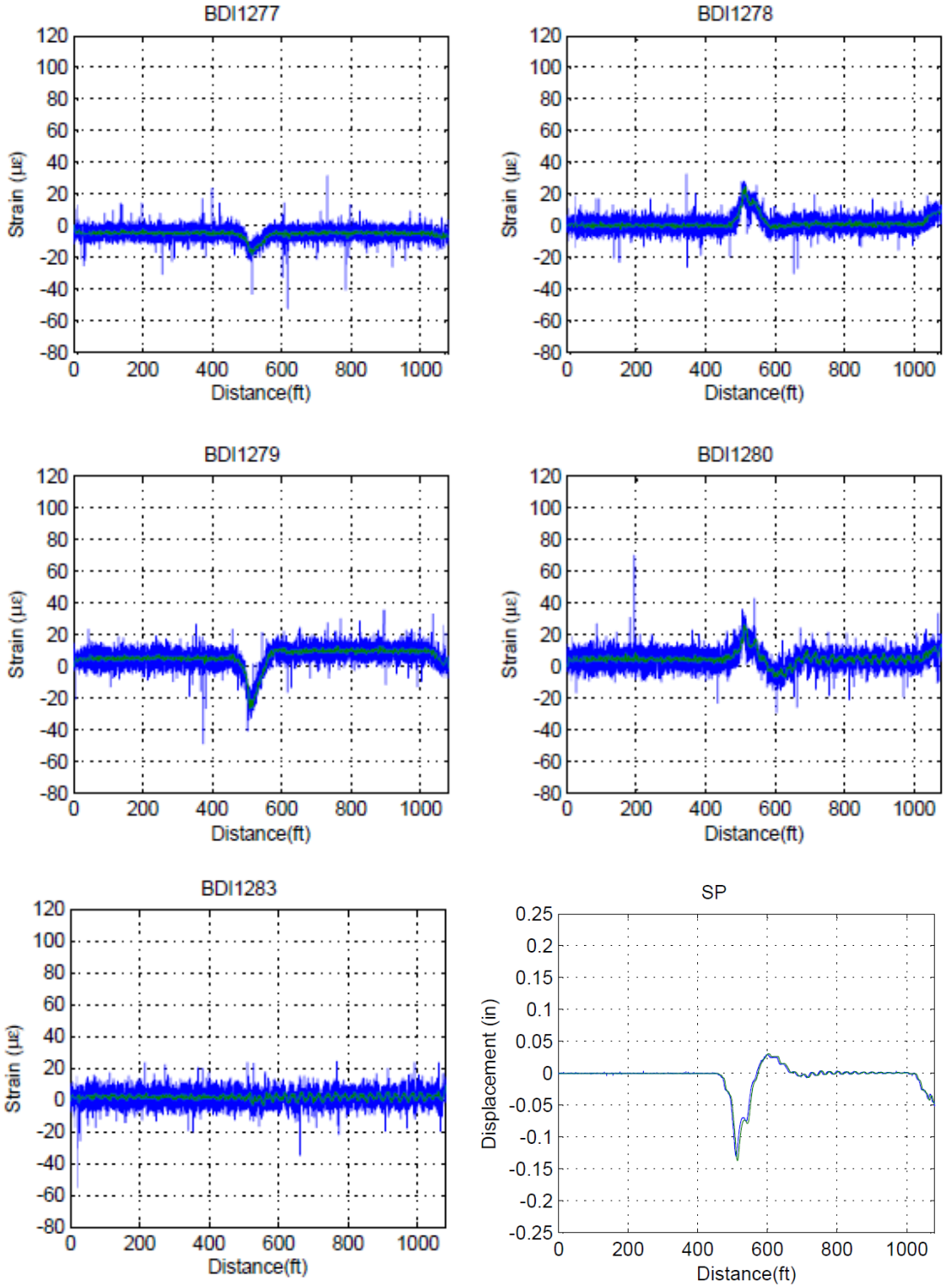

Figure C. 35: East Truck Load Placement 8-16 kph (5-10 mph).

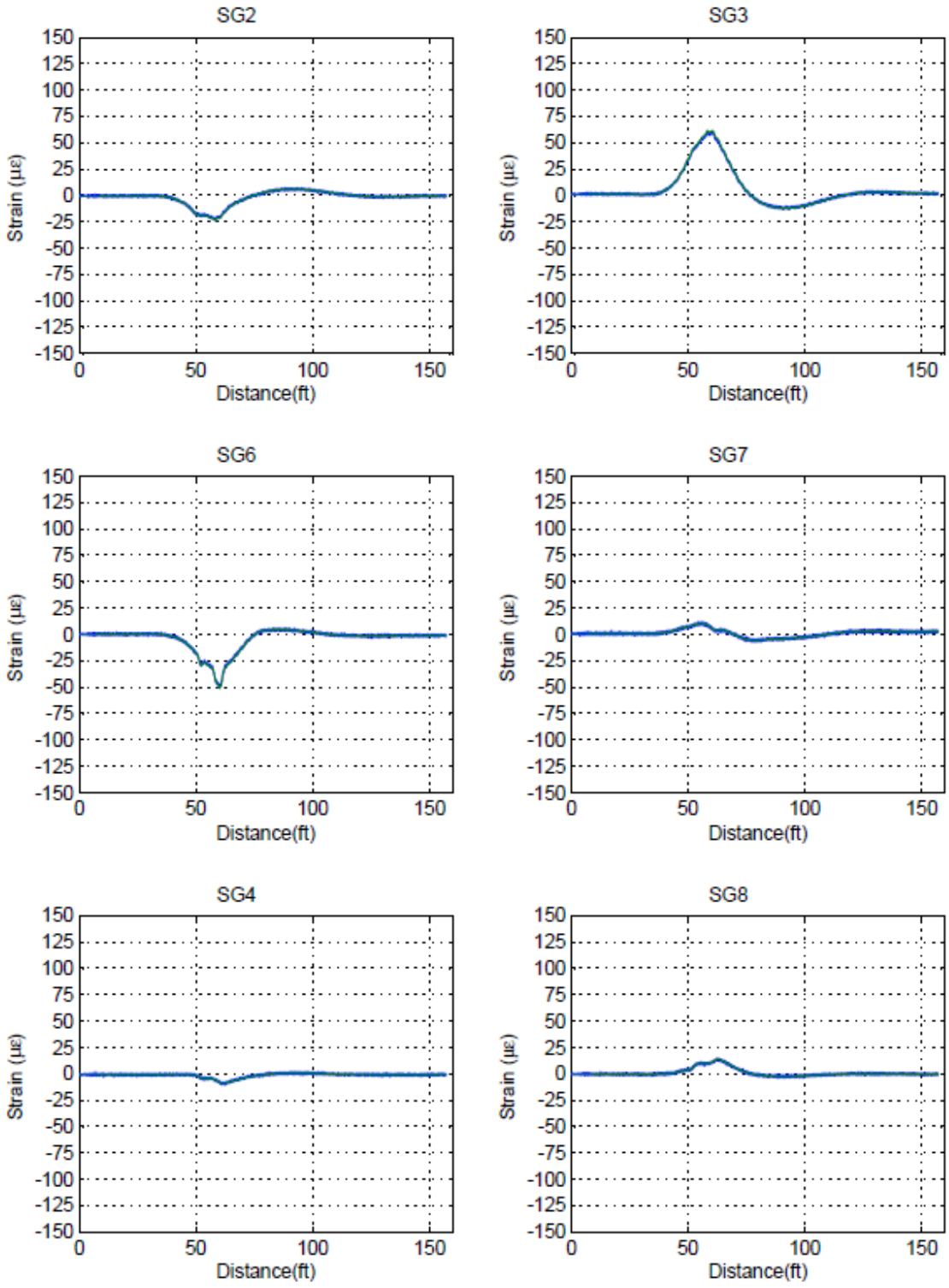

Figure C. 36: East Truck Load Placement 8-16 kph (5-10 mph).

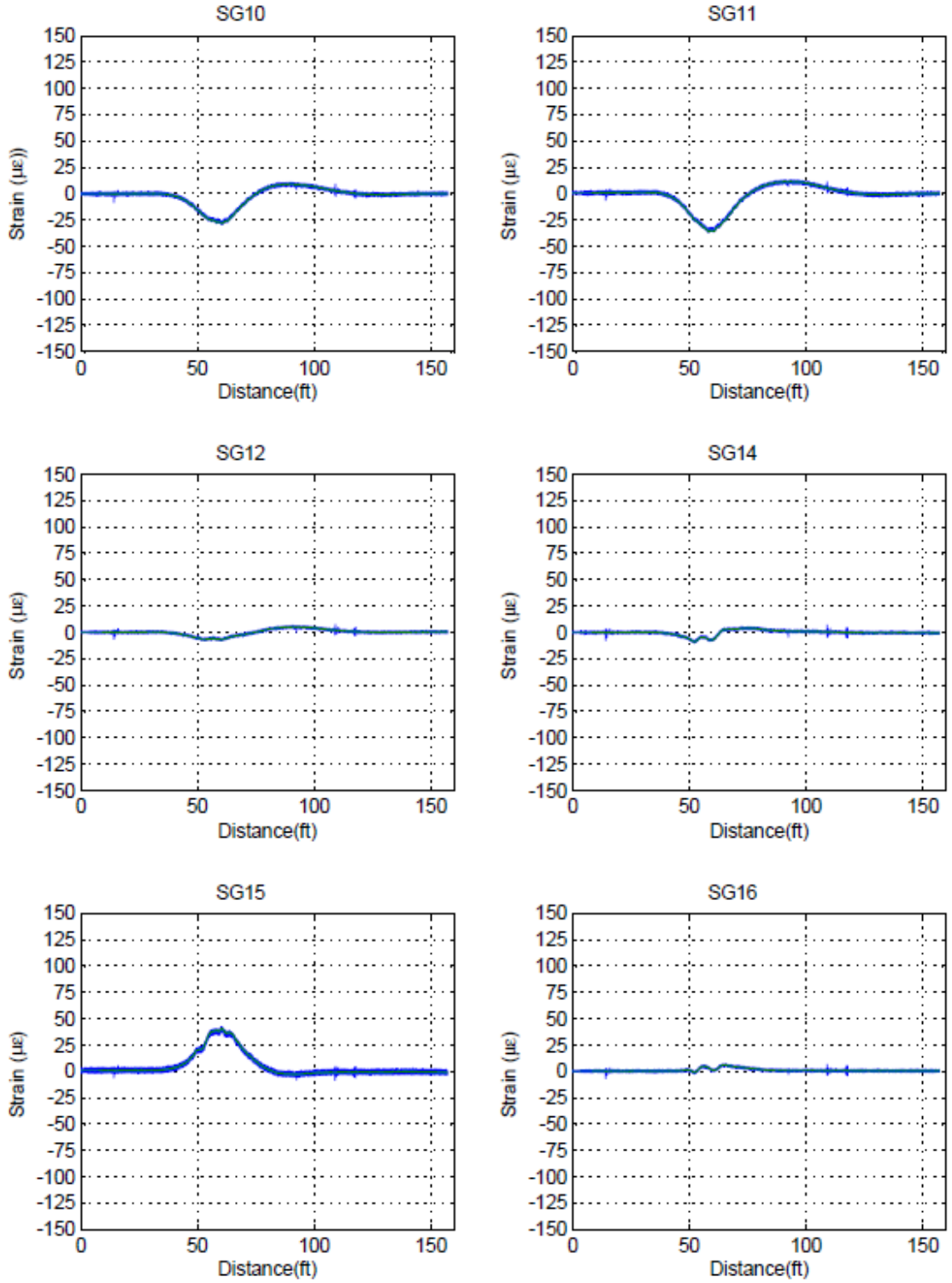

Figure C. 37: East Truck Load Placement 8-16 kph (5-10 mph).

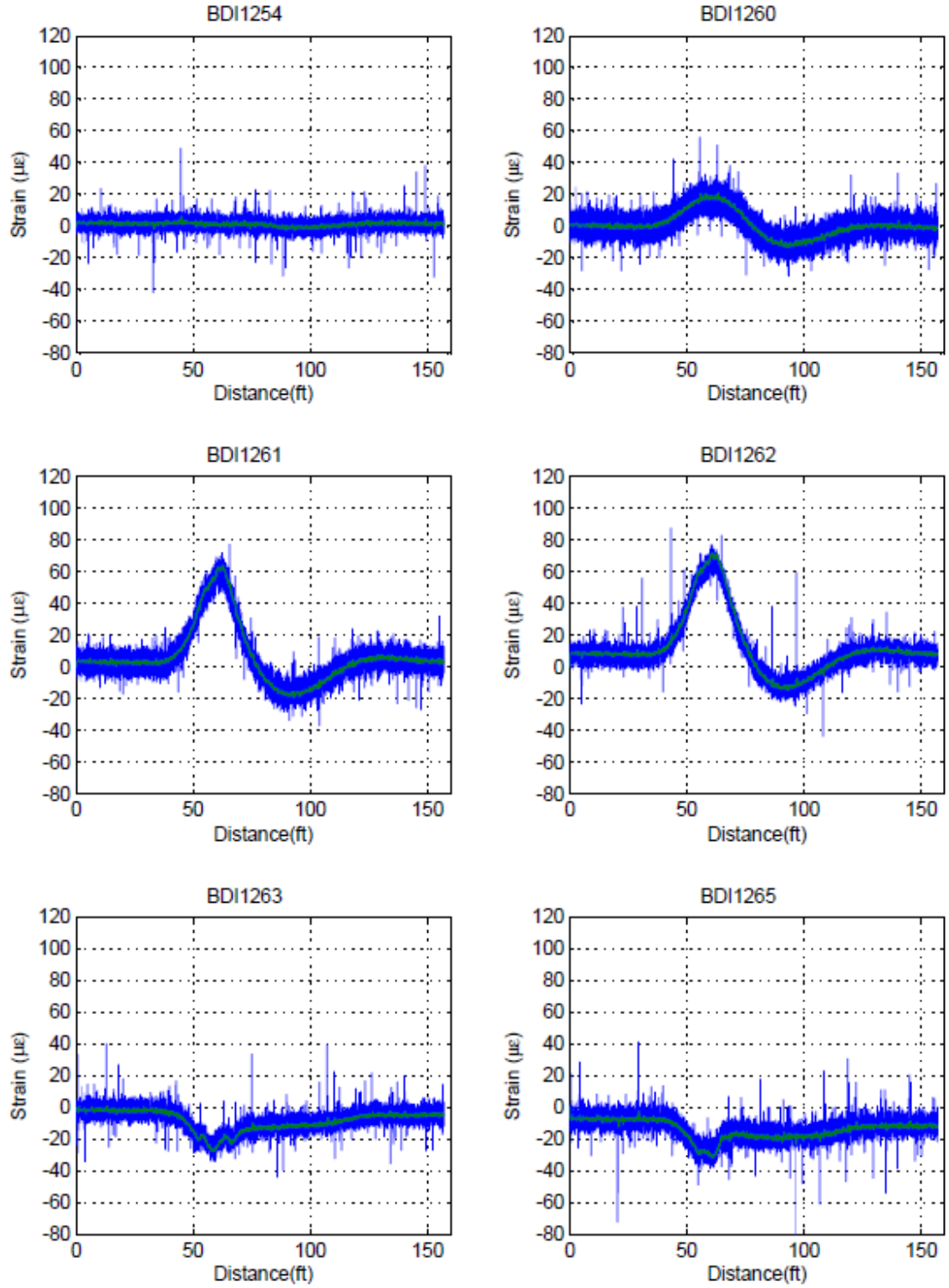

Figure C. 38: East Truck Load Placement 8-16 kph (5-10 mph).

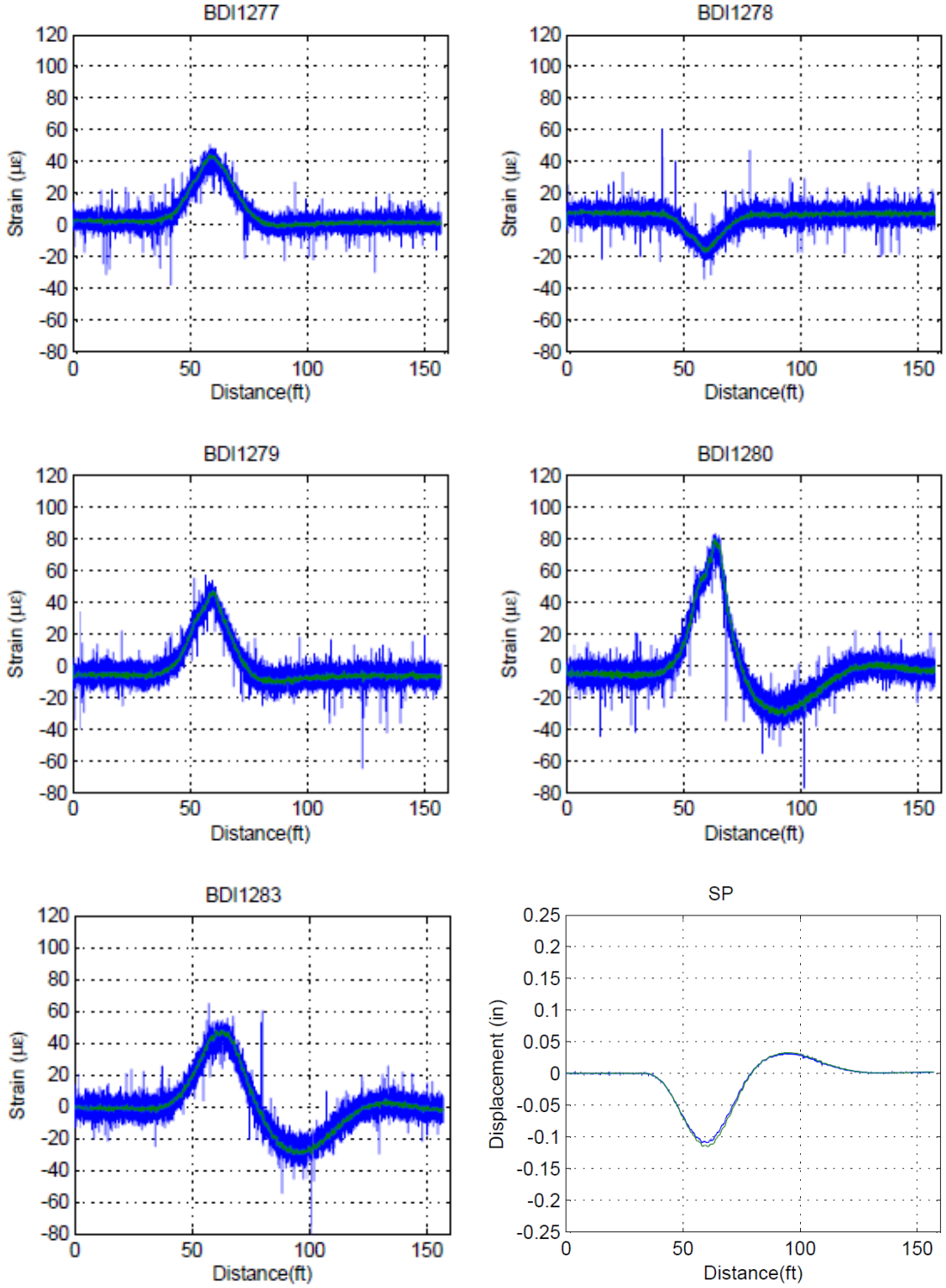

Figure C. 39: East Truck Load Placement 105-121 kph (65-75 mph).

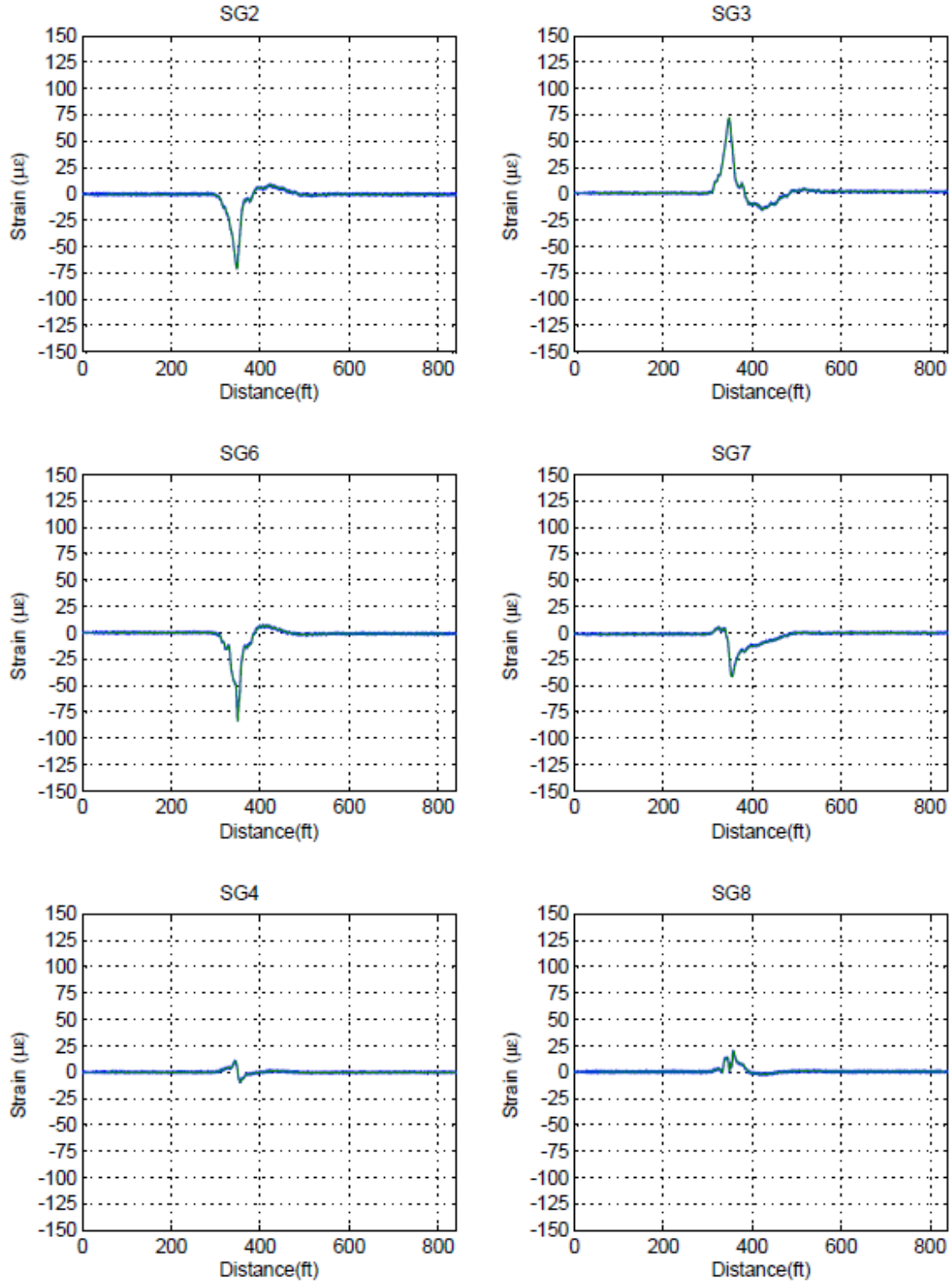

Figure C. 40: East Truck Load Placement 105-121 kph (65-75 mph).

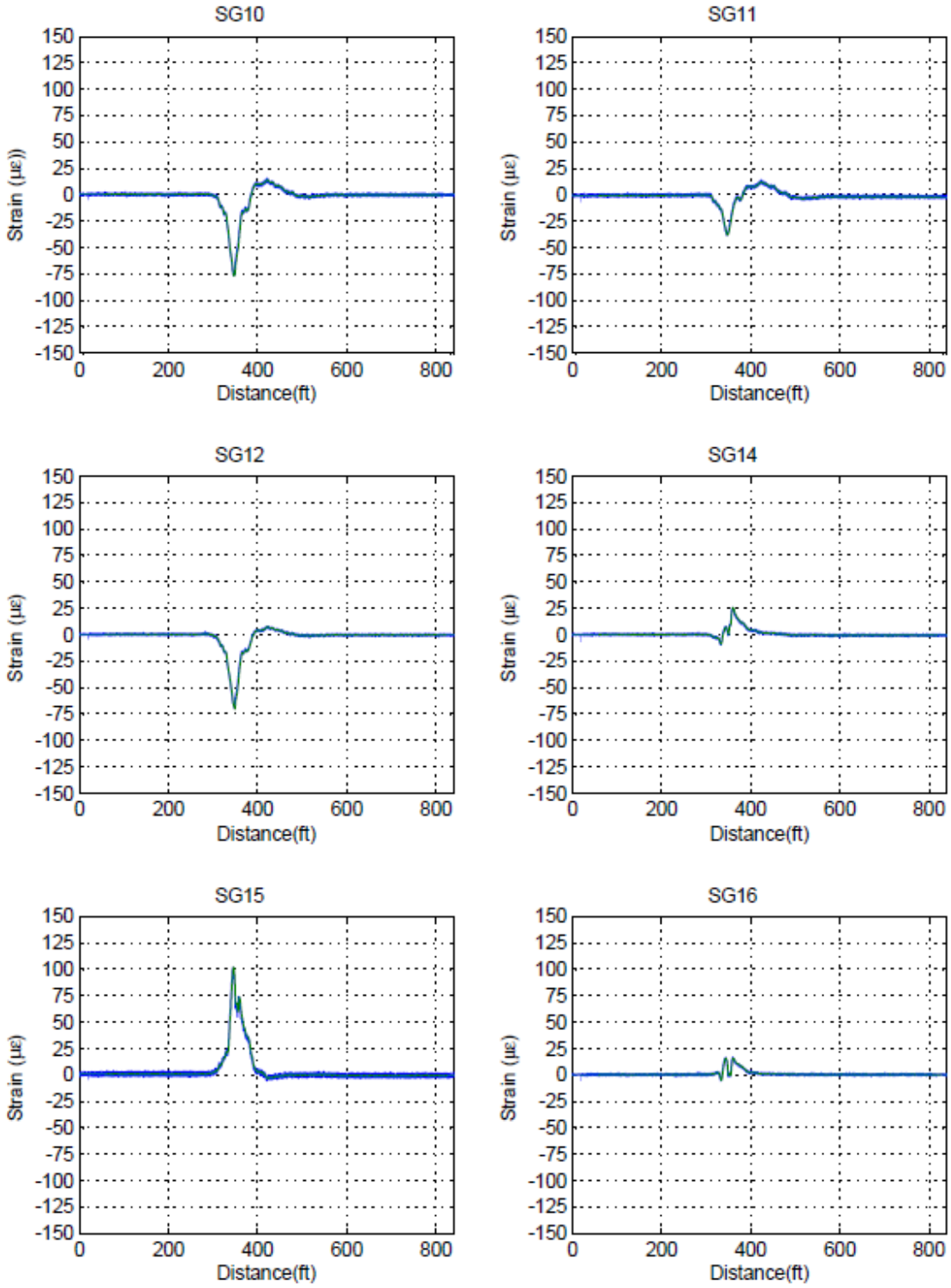

Figure C. 41: East Truck Load Placement 105-121 kph (65-75 mph).

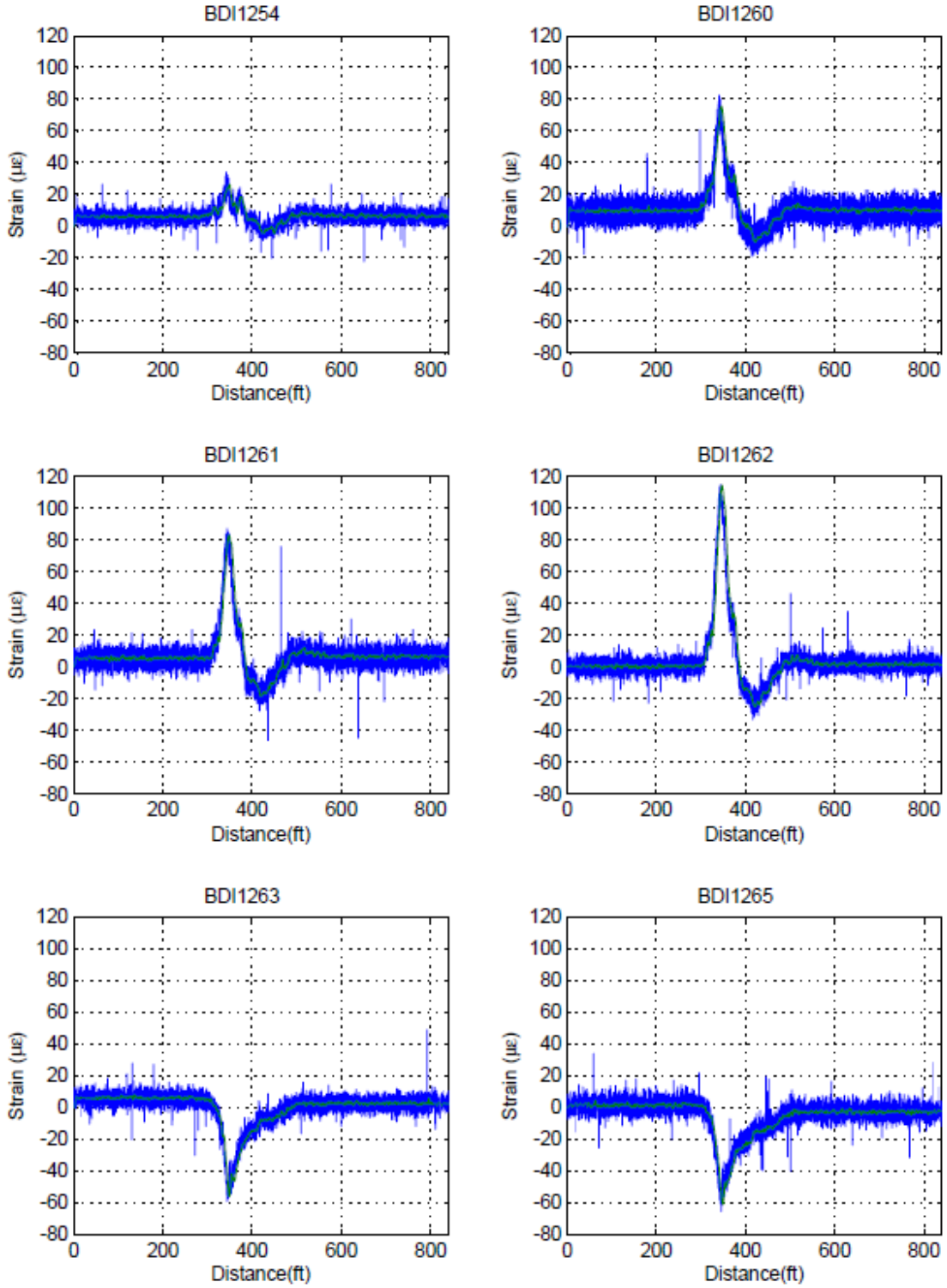

Figure C. 42: East Truck Load Placement 105-121 kph (65-75 mph).

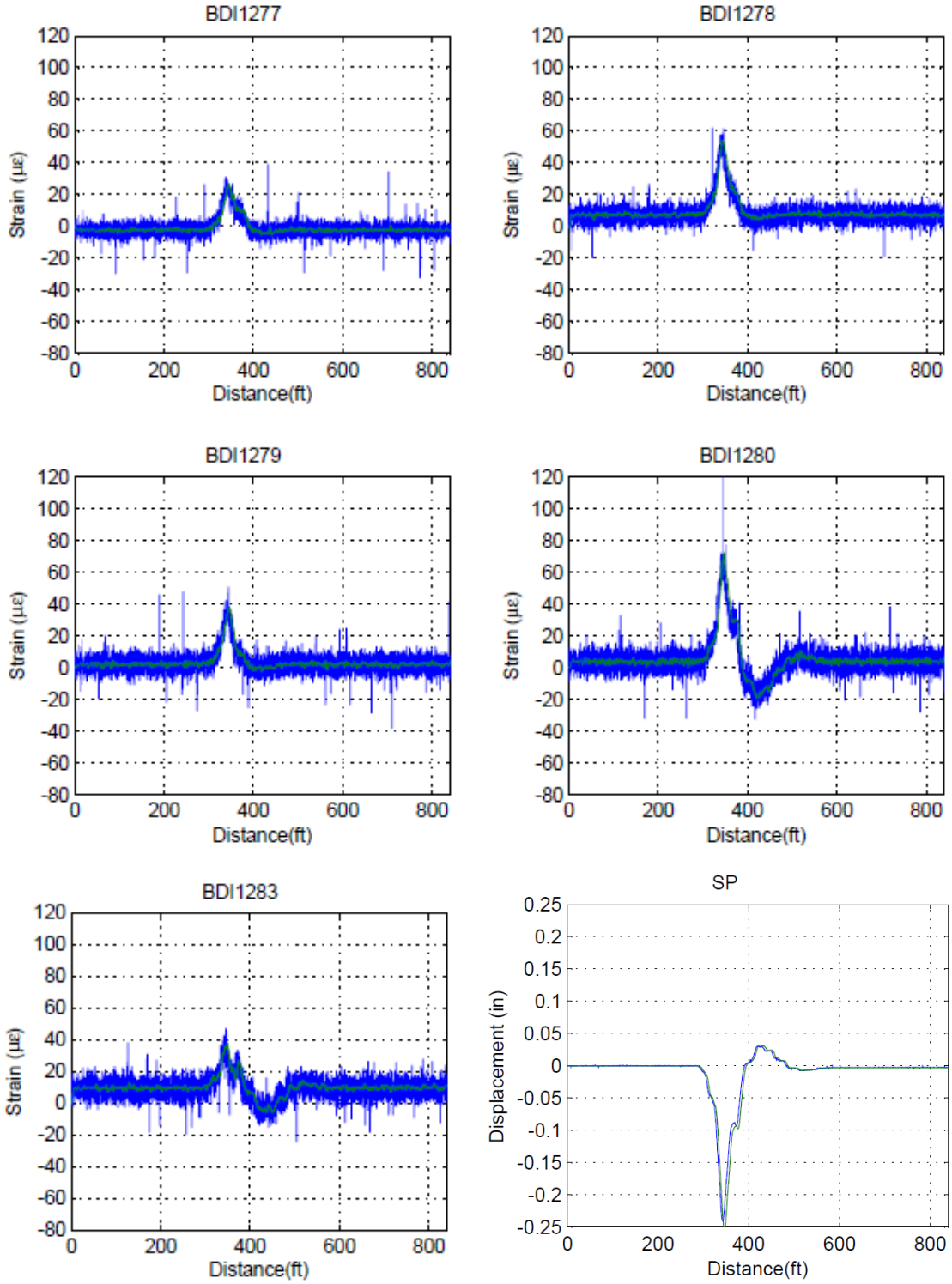

Appendix D: Field Test and Finite Element Analyses Results

Field Test and Complementary Finite Element Analyses

Figure D. 1: West Truck Load Placement Maximum Principal Web Gap Stresses Before and After Retrofit.

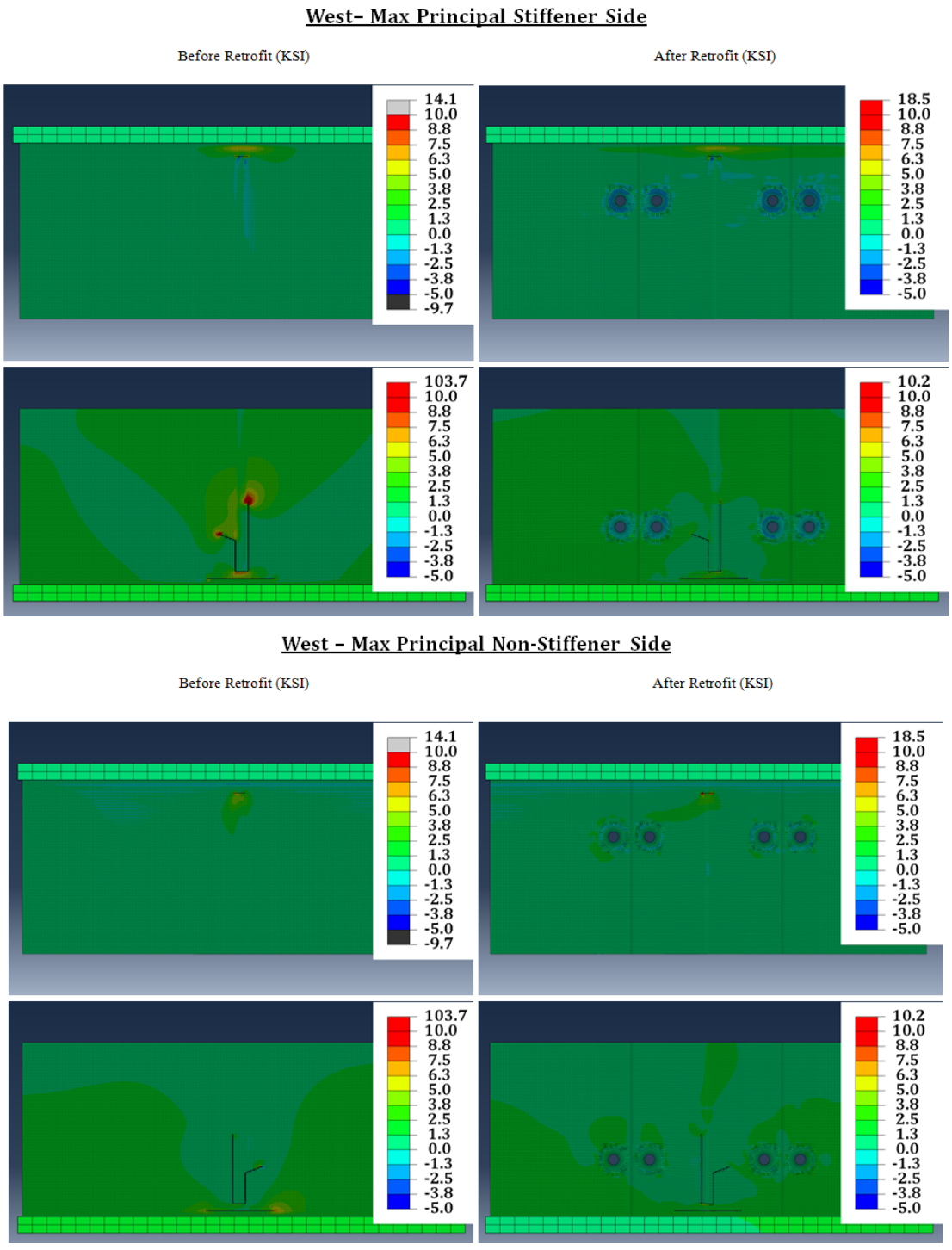

Figure D. 2: West Truck Load Placement Directional Web Gap Stresses Before and After Retrofit.

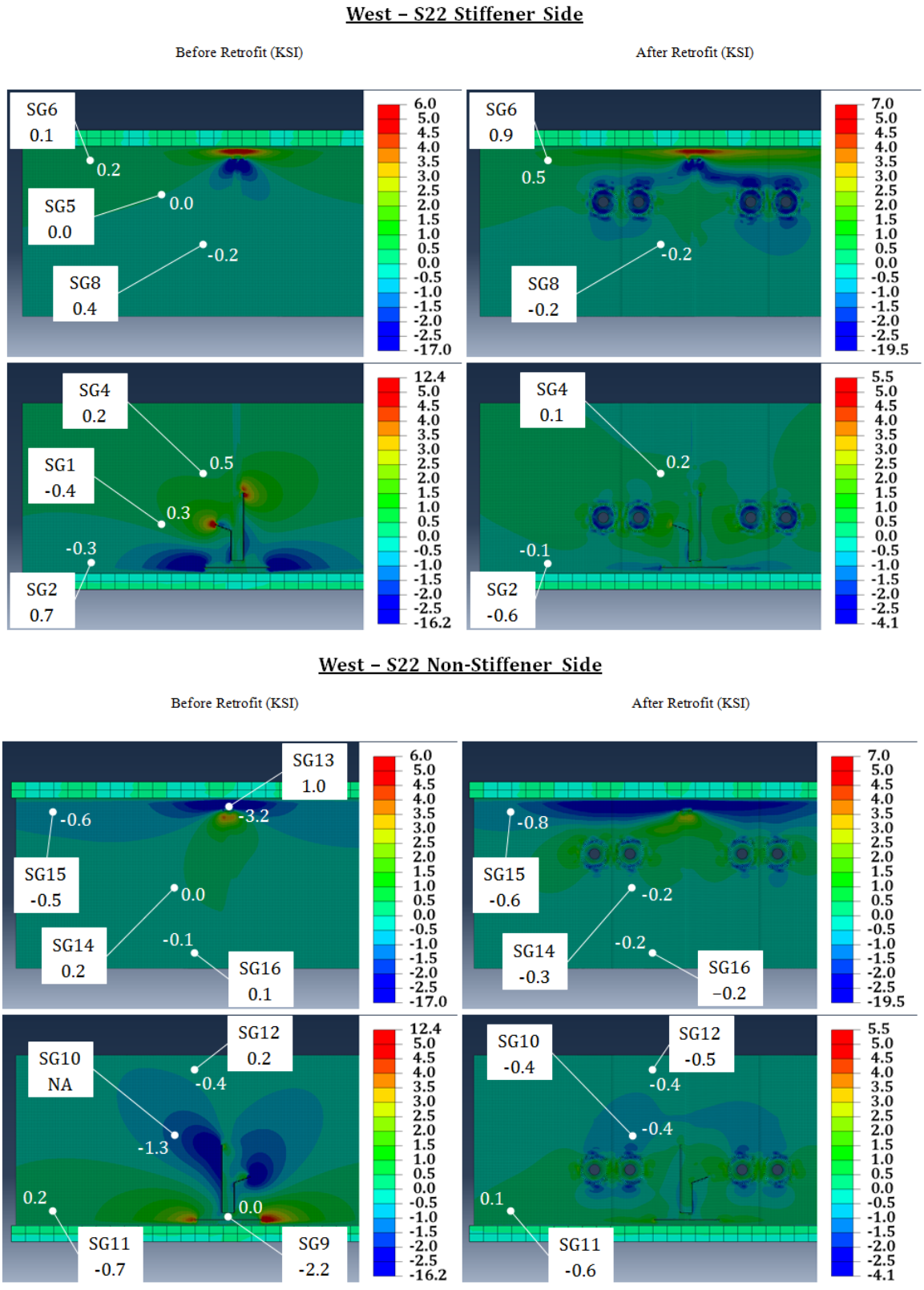

Figure D. 3: West Truck Load Placement Directional Web Gap Stresses Before and After Retrofit.

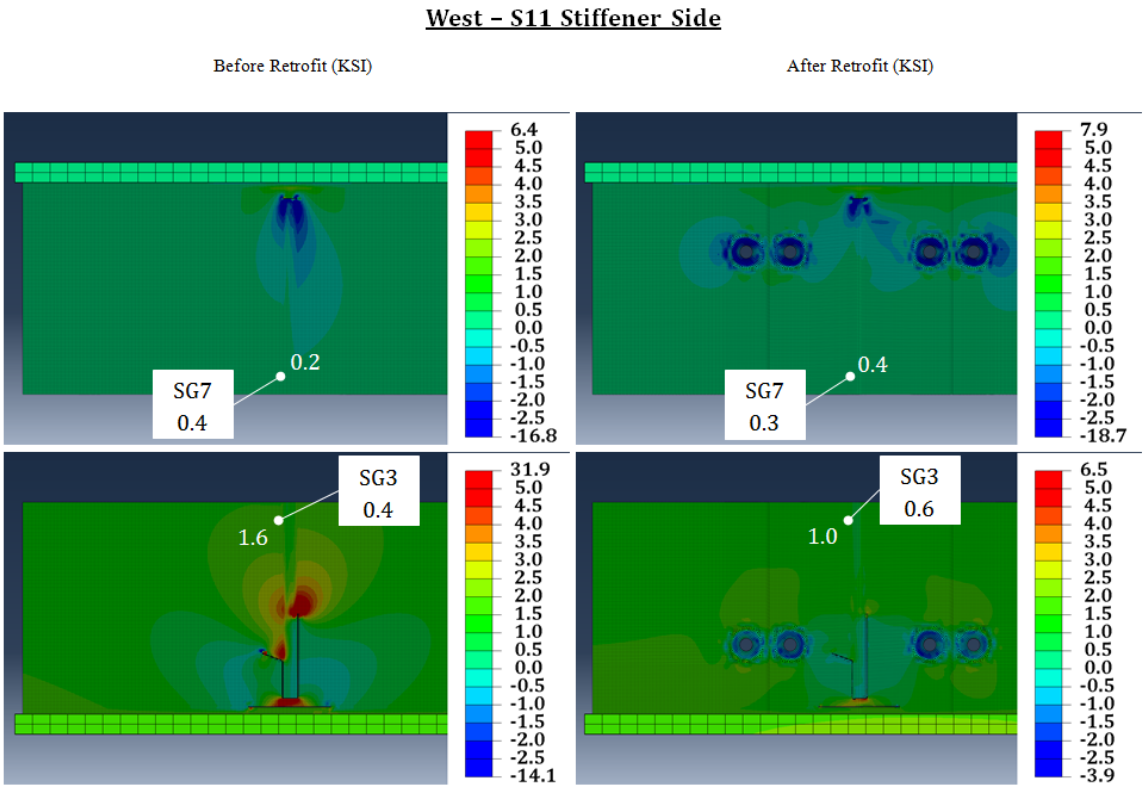

Figure D. 4: Center Truck Load Placement Maximum Principal Web Gap Stresses Before and After Retrofit.

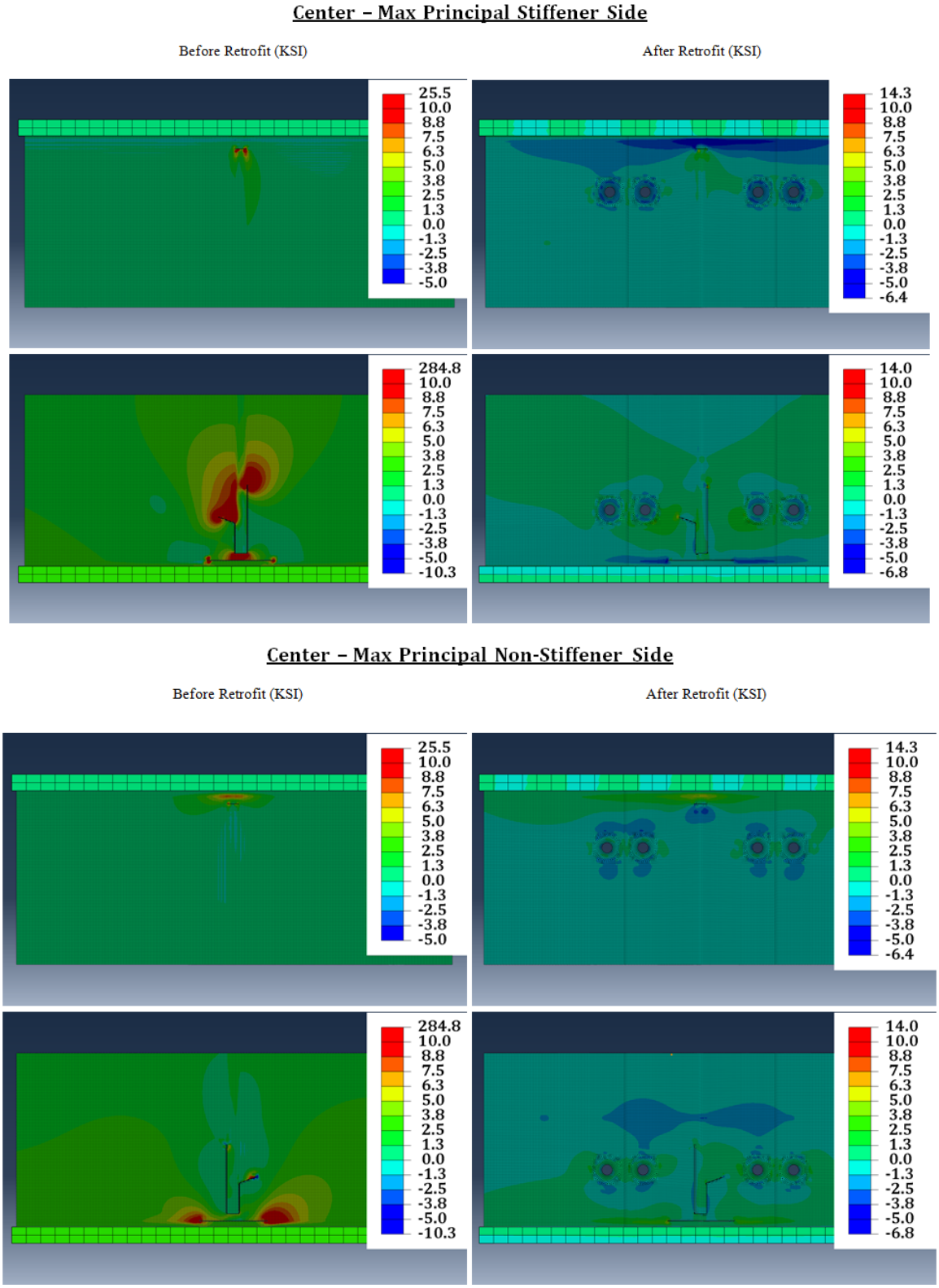

Figure D. 5: Center Truck Load Placement Directional Web Gap Stresses Before and After Retrofit.

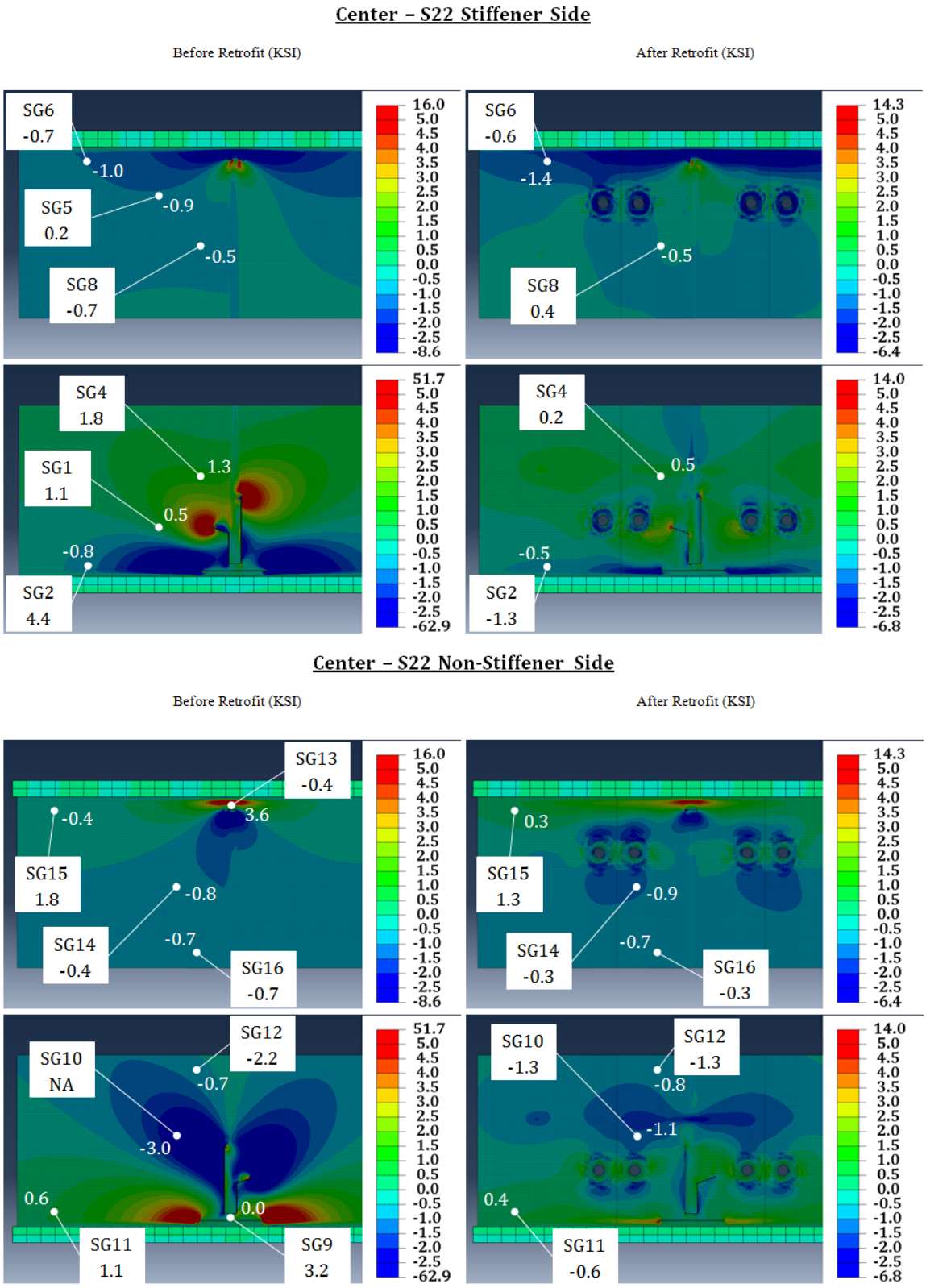

Figure D. 6: Center Truck Load Placement Directional Web Gap Stresses Before and After Retrofit.

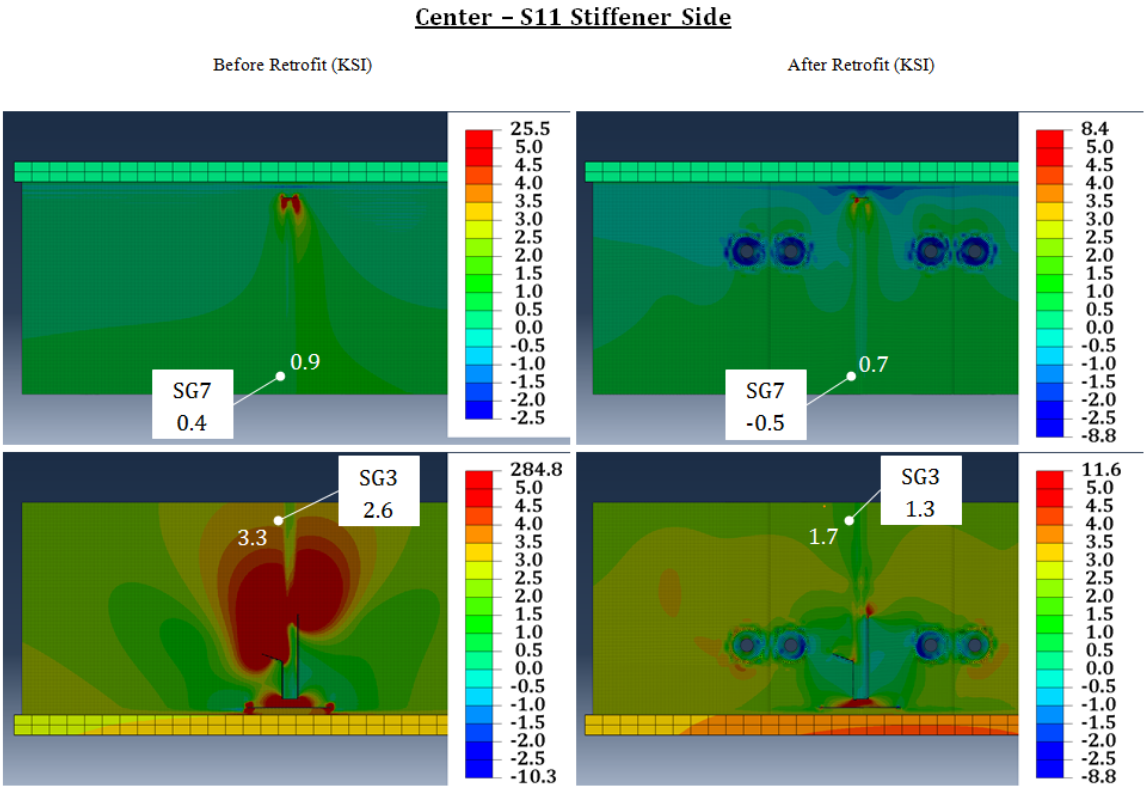

Figure D. 7: East Truck Load Placement Maximum Principal Web Gap Stresses Before and After Retrofit.

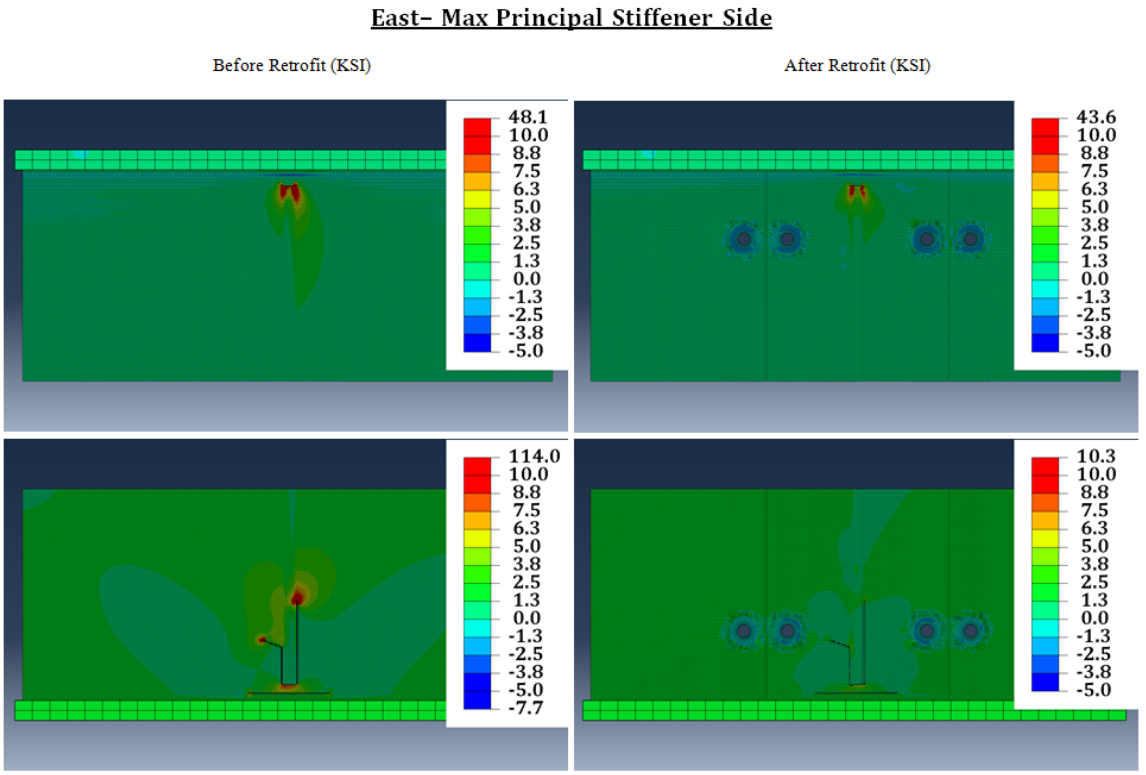

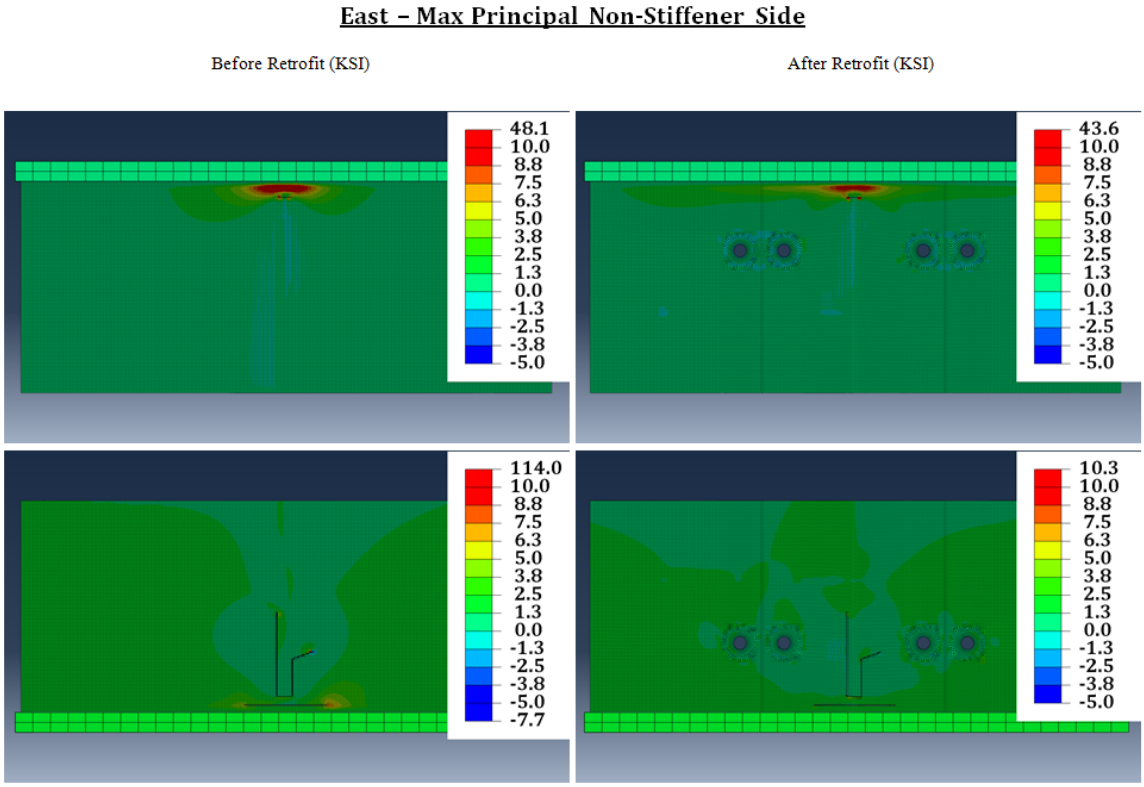

Figure D. 8: East Truck Load Placement Directional Web Gap Stresses Before and After Retrofit.

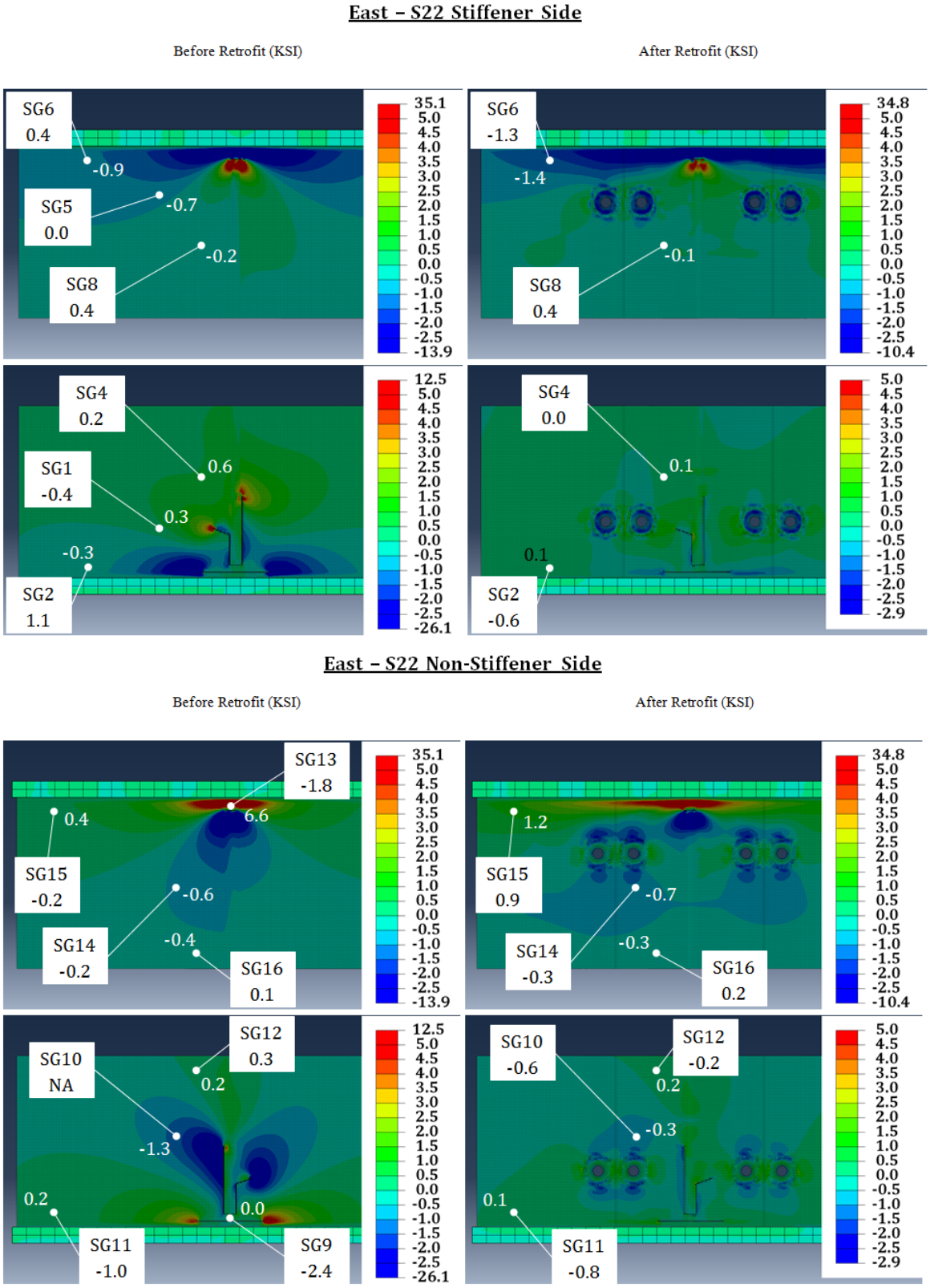

Figure D. 9: East Truck Load Placement Directional Web Gap Stresses Before and After Retrofit.

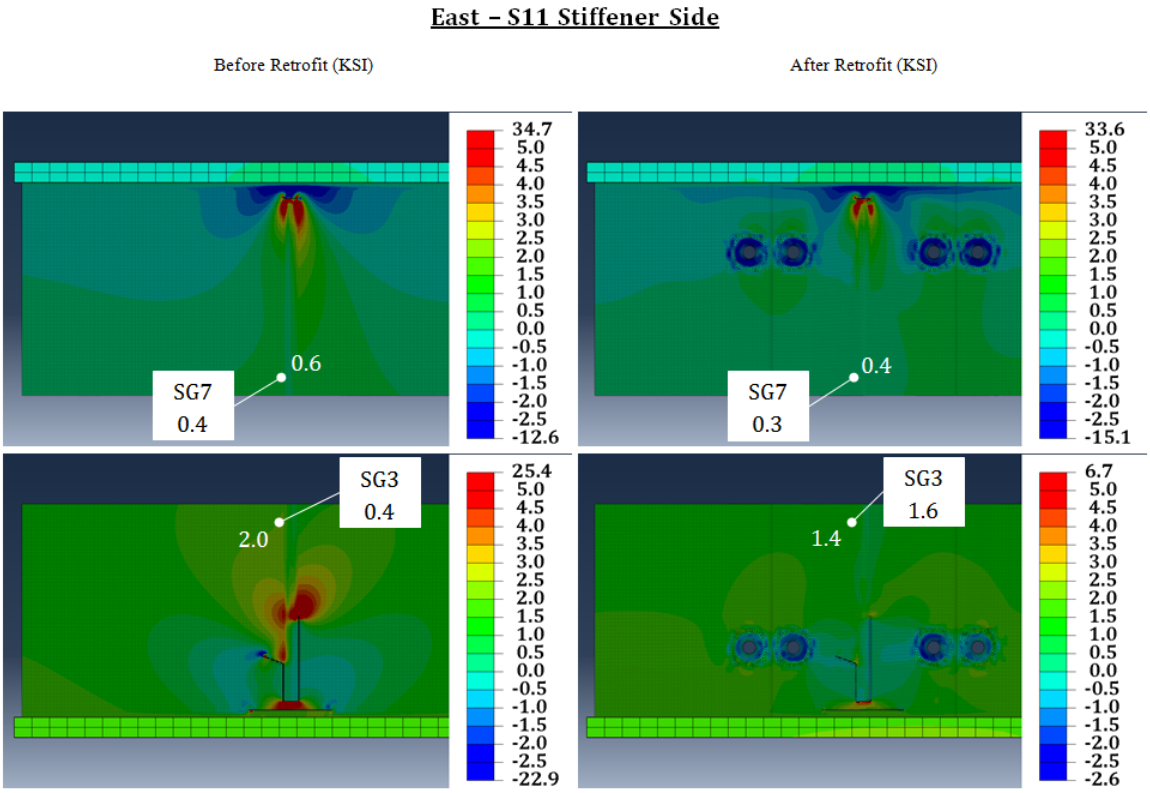

Top Web Gap Behavior Finite Element Analyses

Figure D. 10: Maximum Principal Stresses at Top Web Gap for West Load Truck Placement with Connection Plate-To-Web and Flange-To-Web Weld Cracks Present.

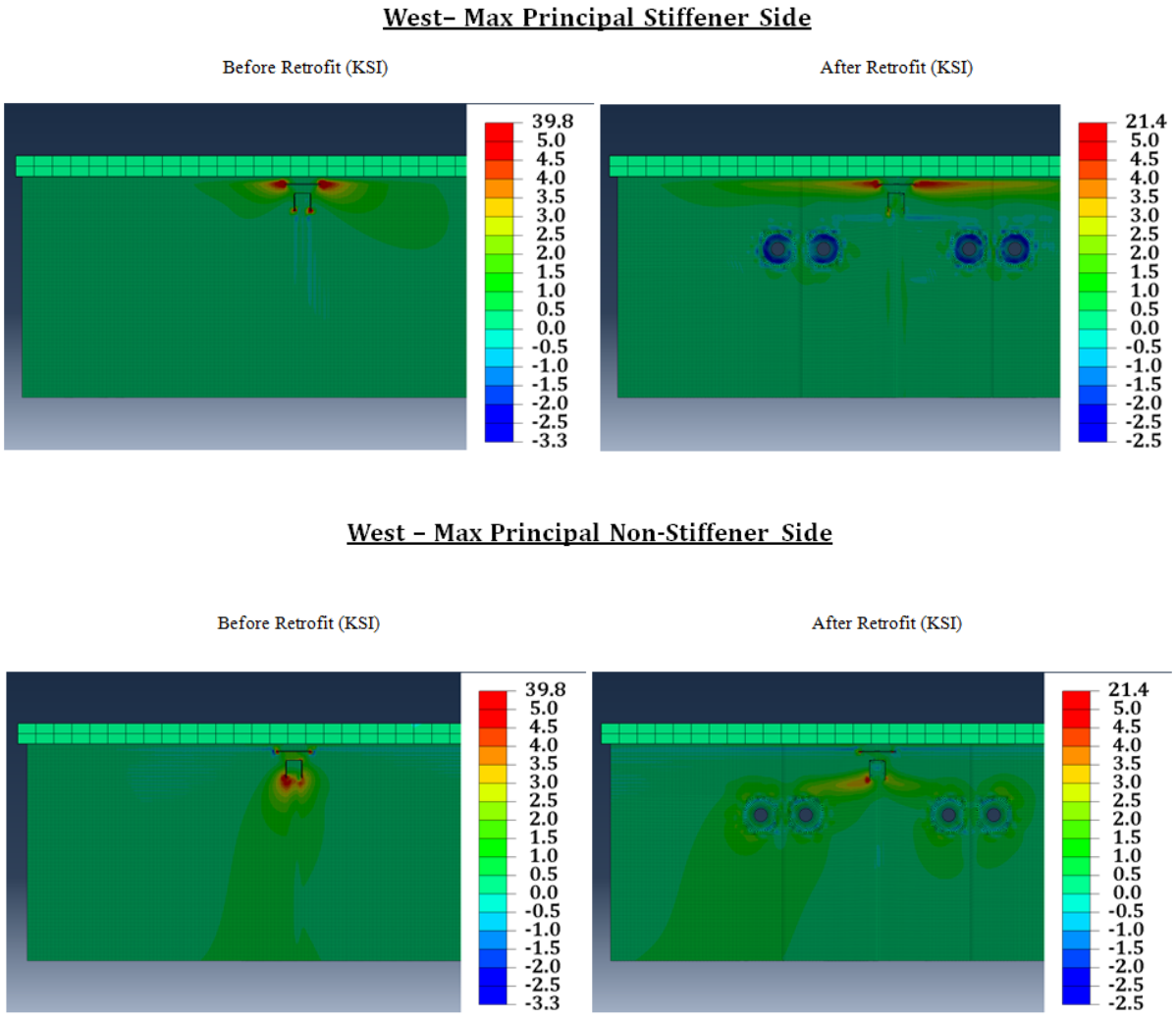

Figure D. 11: Maximum Principal Stresses at Top Web Gap for Center Load Truck Placement with Connection Plate-To-Web and Flange-To-Web Weld Cracks Present.

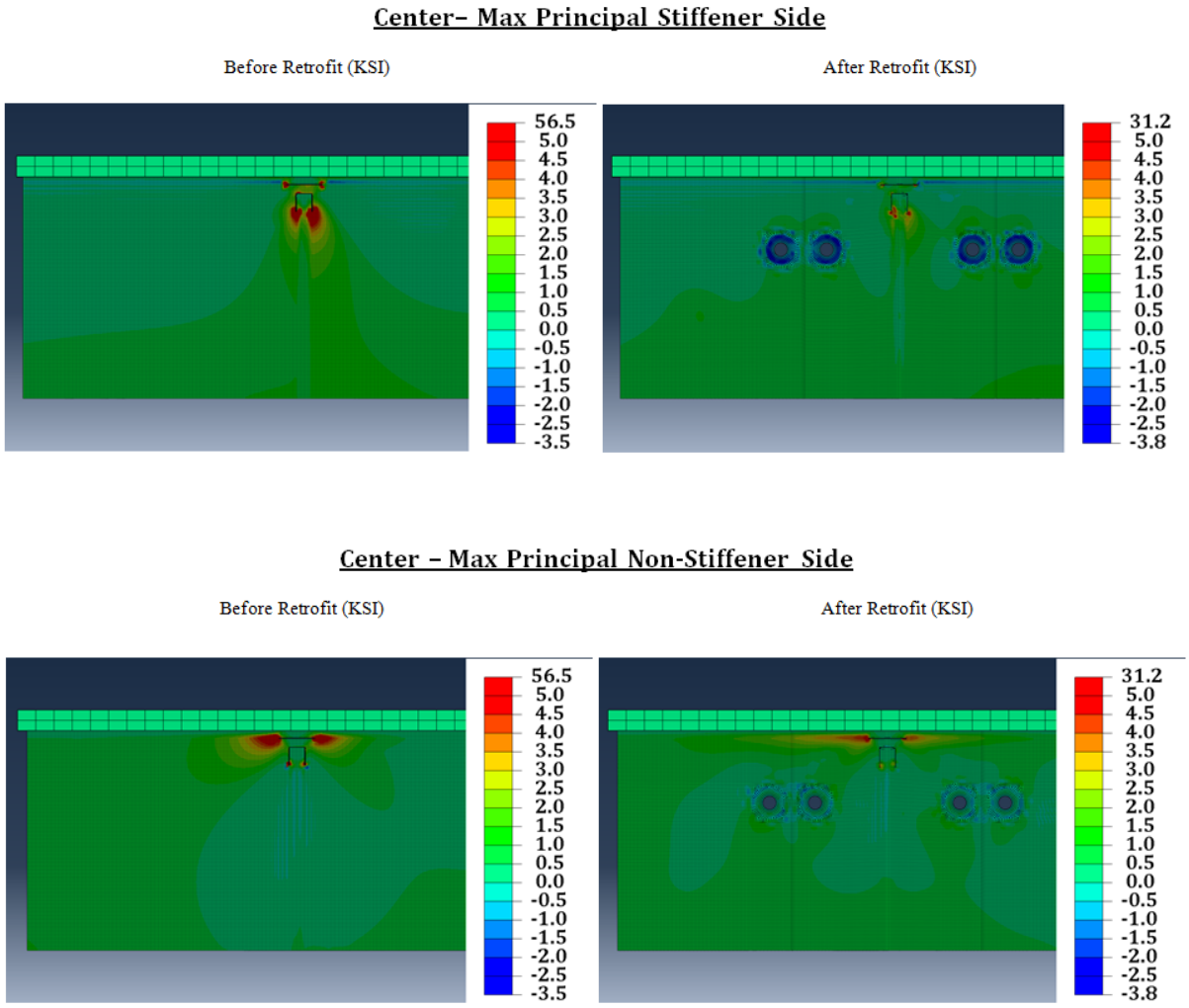

Figure D. 12: Maximum Principal Stresses at Top Web Gap for East Load Truck Placement with Connection Plate-To-Web and Flange-To-Web Weld Cracks Present.

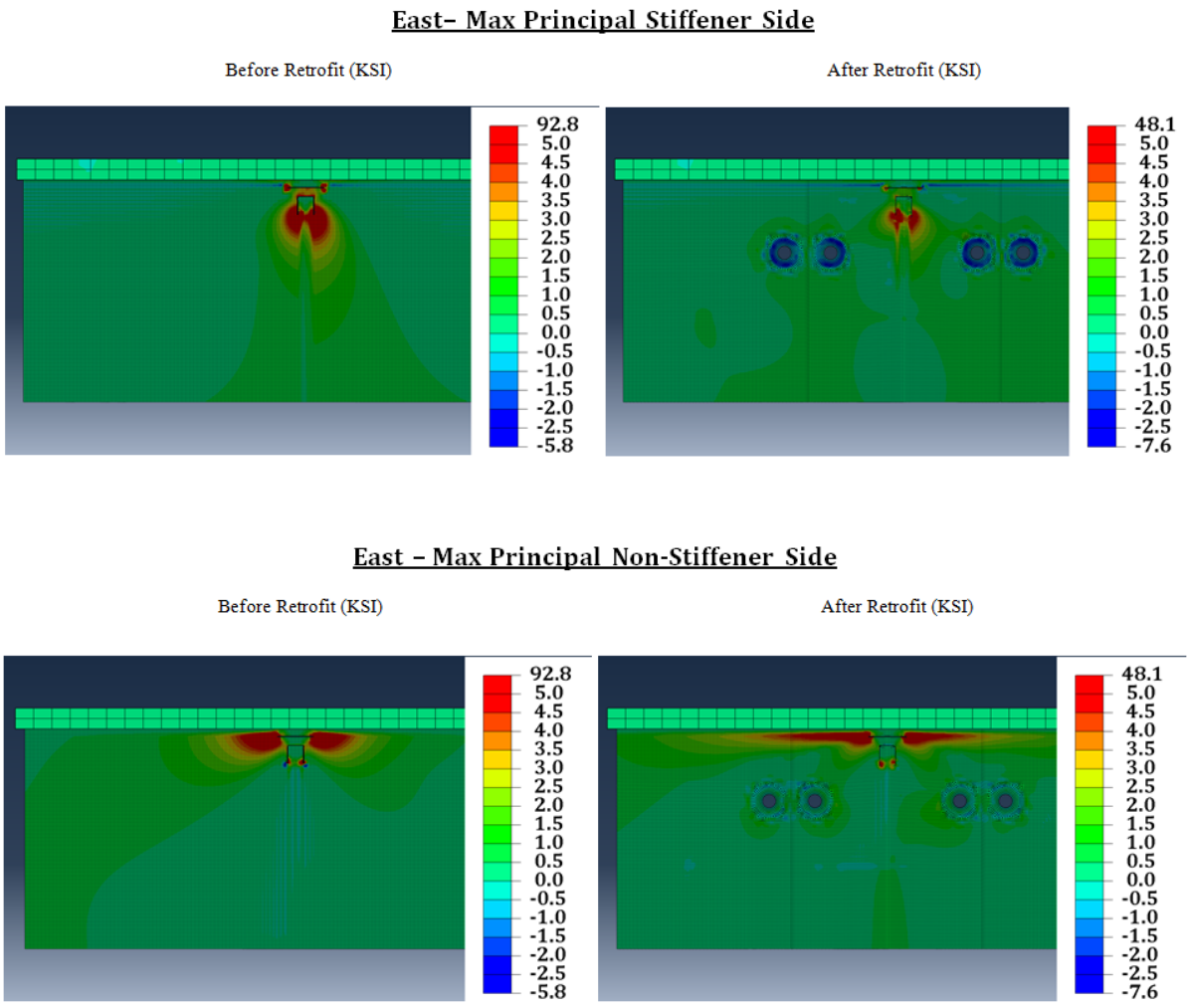

Figure D. 13: Maximum Principal Stresses at Top Web Gap for All Load Truck Placements with Only Connection Plate-To-Web Weld Crack Present.

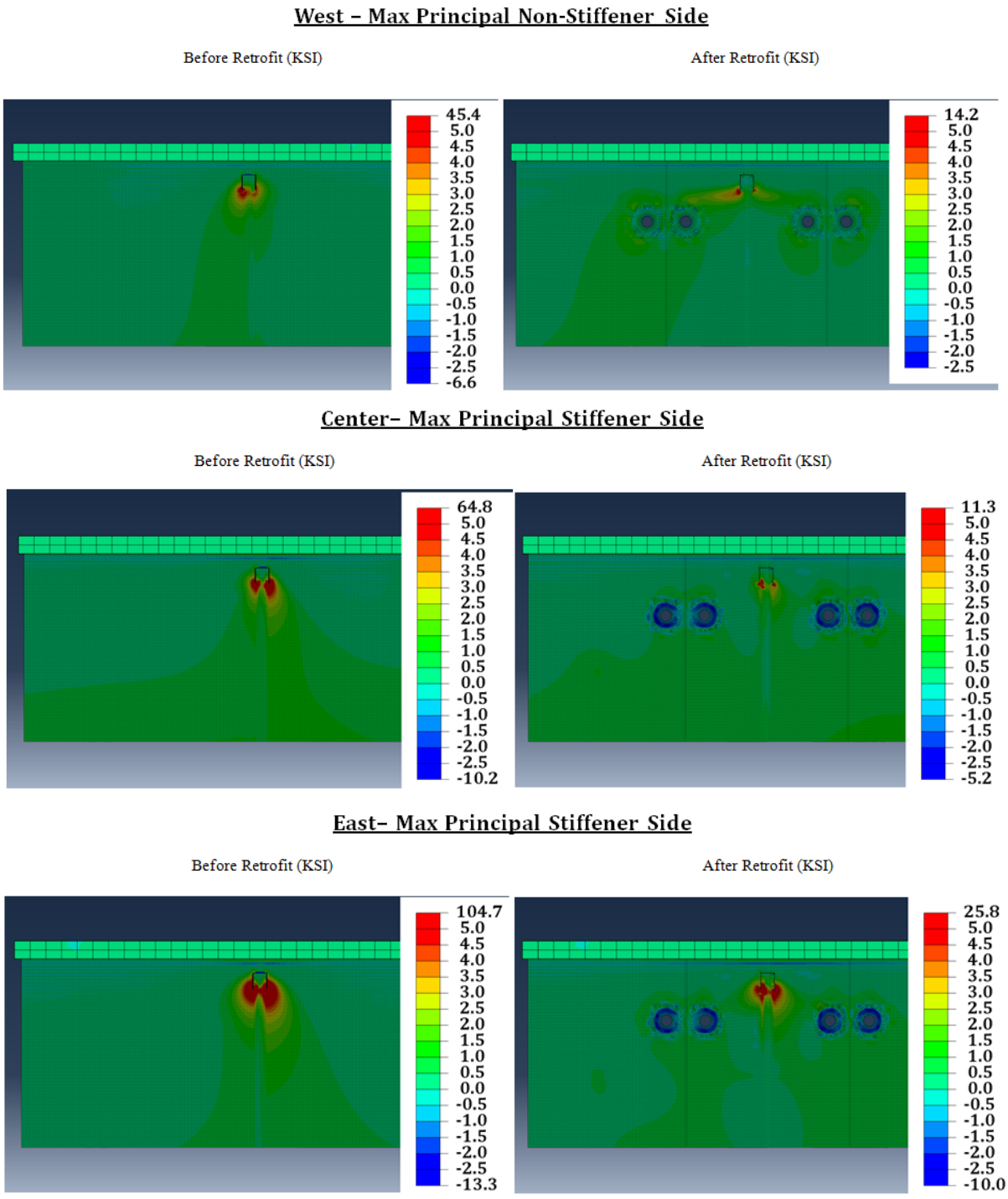

Figure D. 14: Maximum Principal Stresses at Top Web Gap for All Load Truck Placements with Only Flange-To-Web Weld Crack Present.